UNIVERSITY OF OKLAHOMA

GRADUATE COLLEGE

SHRINKAGE, CREEP, AND FATIGUE BEHAVIOR OF CSA CEMENT CONCRETE AND UHPC INCORPORATING INTERNAL CURING

A DISSERTATION

SUBMITTED TO THE GRADUATE FACULY

in partial fulfillment of the requirements for the

Degree of

DOCTOR OF PHILOSOPHY

By MUJTABA AHMADI
Norman, Oklahoma
2026

Downloaded from SHAREOK. Persistent Handle URL: https://hdl.handle.net/11244/342810

SHRINKAGE, CREEP, AND FATIGUE BEHAVIOR

OF CSA CEMENT CONCRETE AND UHPC

INCORPORATING INTERNAL CURING

A DISSERTATION APPROVED FOR THE

SCHOOL OF CIVIL ENGINEERING AND

ENVIRONMENTAL SCIENCE

BY THE COMMITTEE CONSISTING OF

Dr. Royce W. Floyd, Chair

Dr. Jeffery S. Volz

Dr. Shreya Vemuganti

Dr. Matthew Reyes

©Copyright by MUJTABA AHMADI 2026

All Rights Reserved.

Table of Contents

1. Introduction 1
2. Effect of Internal Curing on Shrinkage Behavior of Ultra-High Performance Concrete 7
2.1 Literature Review 7
2.2 Experimental Procedure 10
2.2.1 Materials and Mix Design 10
2.2.2 Shrinkage Testing 13
2.2.3 UHPC with BCSA Cement Replacement 15
2.3 Results 17
2.3.1 Compressive Strength 17
2.3.2 Modulus of Elasticity (MOE) Test (ASTM C469) 18
2.3.3 Setting Time 18
2.3.4 Shrinkage Measurement 20
2.3.5 UHPC with BCSA Replacement 24
2.3.6 Compressive Strength Test Results 25
2.4 Conclusions and Recommendations 26
2.5 References 28
3. Internally Cured UHPC Overlay for Bridge Deck Application 31
3.1 Literature Review 31
3.1.1 UHPC Overlays 31
3.1.2 Installation Strategy 1 (IS1) 42
3.1.3 Installation Strategy 2 (IS2) 43
3.1.4 Installation Strategy 3 (IS3) 44
3.1.5 Surface Preparation 45
3.1.6 UHPC Mixing, Finishing, and Repair 47
3.1.7 Construction Joints 49
3.1.8 Life-Cycle Cost Analysis (LCCA) 50
3.2 UHPC Overlay Specimen Construction and Testing 53
3.2.1 Specimen Design 53
3.2.2 Specimen Construction 55
3.2.3 Casting UHPC Overlay 61

3.2.4 Testing Procedure 64
3.3 Results 66
3.3.1 Fresh Concrete Properties 66
3.3.2 Third Point Bending Test 67
3.3.3 Comparison of Experimental and Calculated Capacity 75
3.4 Conclusions and Recommendations 79
3.5 References 82
4. Shrinkage and Creep Behavior of CSA Cement Concrete Incorporating Internal Curing 85
4.1 Literature Review 85
4.1.1 Calcium Sulfoaluminate (CSA) Cement 85
4.1.2 Internal Curing 93
4.1.3 Shrinkage Measurement 100
4.2 Experimental Procedure 101
4.2.1 Mix Design 101
4.2.2 Specific Gravity and Absorption Tests for the LWS 107
4.3 Results 108
4.3.1 Slump 108
4.3.2 Volumetric Air Content and Unit Weight Tests 110
4.3.3 Compressive Strength Test 113
4.3.4 Modulus of Rupture (MOR) Test 115
4.3.5 Calorimetry Test Results 117
4.3.6 Shrinkage and Creep Measurement 119
4.3.7 Shrinkage Measurement Using ASTM C157 Procedure 122
4.3.8 Shrinkage Measurement Using VWSG 125
4.3.9 Creep Measurement 127
4.3.10 Creep and Shrinkage Results Based on VWSG Measurements 130
4.3.11 Comparison of Shrinkage and Creep Behavior of Each Type of Cement with Different LWS Content 141
4.3.12 Shrinkage Results-ASTM C157 144
4.4 Summary 152
4.5 Conclusions and Recommendations 153
4.6 References 156

.5 The Flexural Fatigue Life of Internally and Externally Cured Expansive BCSA and Type K Cement Concrete for Pavements 160
5.1 Literature review 160
5.1.1 CSA Cement Application 165
5.2 Procedure 166
5.2.1 Experimental Study 166
5.2.2 Fatigue and MOR Test Procedures 169
5.3 Results 171
5.3.1 Fresh concrete tests 171
5.3.2 Hardened Concrete Properties 172
5.3.3 Flexural Fatigue and MOR Test Results 173
5.4 Conclusions and Recommendations 195
5.5 References 198

List of Figures

Figure 2.1: (a) Pan mixer (b) Flow test of UHPC with LWS 12
Figure 2.2: (a) Poorly ground UHPC cylinder, (b) well ground UHPC cylinders 13
Figure 2.3: (a) VWSG placed in the cylindrical mold (b) VWSG with manual readout and (c) UHPC shrinkage specimens attached to data logger 15
Figure 2.4: (a) Ingredients of UHPC, (b) Dry mixing in pan mixer, and (c) Wet mixing for 25 percent replacement mix 16
Figure 2.5: Compressive strength comparison for UHPC with different LWS content 17
Figure 2.6: Secant modulus of elasticity of UHPC 18
Figure 2.7: Semi-adiabatic F-CAL 4000 calorimeter 19
Figure 2.8: Calorimetry test results for UHPC with different amount of LWS 20
Figure 2.9: Shrinkage of UHPC with (a) 0-LWS (b) 1-LWS (c) 2-LWS, and (d) 3-LWS measured over 48 h 22
Figure 2.10: Combined measured total shrinkage of UHPC specimens over time 24
Figure 3.1: UHPC substrate prepared using (a) scarification and (b) hydrodemolition (Graybeal et al., 2018) 39
Figure 3.2: IS1 using a 1.75 in. UHPC overlay (Haber et al., 2022) 43
Figure 3.3: IS2 using a 3.75 in. UHPC overlay (Haber et al., 2022) 43
Figure 3.4: IS3 using a 2.5 in. UHPC overlay with 1.25 in. asphalt layer (Haber et al., 2022) ... 44
Figure 3.5: Construction joint details (a) proposed in SIA 2052 and (b) emerging detail from Switzerland (Garber et al., 2024) 50
Figure 3.6: Typical cross-section for Type II, B, III, C, and IV P.C. Beams – (Oklahoma state bridge design standards, 2009) 53
Figure 3.7: (a) Cross-sectional and (b) elevation view of 8 in. x 8 in. x 30 in. overlay specimens 55
Figure 3.8: Top and bottom reinforcement prepared for placement in the beam specimens 56
Figure 3.9: Overlay beam formwork with the reinforcement and spacers in place 56
Figure 3.10: Representative slump test for the Class AA bridge deck concrete 58
Figure 3.11: Air content test 58
Figure 3.12: Washing the surface of concrete to expose aggregate following the setting time 60
Figure 3.13: Substrate portion of the 8 in. x 8 in. beam specimens with (a) exposed aggregate surface and (b) covered with wet burlap for curing 60
Figure 3.14: First UHPC overlay flow test 63
Figure 3.15: Trial beams after casting UHPC overlay 63
Figure 3.16: Casting UHPC overlay for 8 in. x 8 in. specimens 64
Figure 3.17: Trial overly beam specimens with dry interface after flexural failure with (a) overlay in compression and (b) overlay in tension 68
Figure 3.18: Trial overly beam specimens with wet interface after flexural failure with (a) overlay in compression and (b) overlay in tension 68
Figure 3.19: (a) Broken trial beam tested in UHPC on tension side and (b) close-up of interface between substrate and UHPC overlay 69
Figure 3.20: Load vs. deflection curves for specimens tested with the overlay in compression .. 70

Figure 3.21: Load vs. deflection curves for Specimens tested with the overlay in tension 72
Figure 3.22: Failure of 8 in. x 8 in. x 30 in. No Overlay beam specimens with (a) No. 4 bar at the bottom and No. 3 bar at the top (positive moment) and (b) No. 3 bar at the bottom and No. 4 bar at the top (negative moment) 72
Figure 3.23: Failure of 8 in. x 8 in. x 30 in. UHPC-0LWS overlay beams with (a) overlay in compression and (b) overlay in tension 73
Figure 3.24: Fibers bridging the crack in the UHPC in an overlay tested in tension 73
Figure 3.25: Failure of 8 in. x 8 in. x 30 in. UHPC-1LWS overlay beams with (a) overlay in compression and (b) overlay in tension 74
Figure 3.26: Failure of 8 in. x 8 in. x 30 in. UHPC-2 LWS overlay beams with (a) overlay in compression and (b) overlay in tension 74
Figure 3.27: Failure of 8 in. x 8 in. x 30 in. UHPC-3 LWS overlay beams with (a) overlay in compression and (b) overlay in tension 75
Figure 3.28: Mechanics used for UHPC overlay in Tension 76
Figure 3.29: Additional load vs. deflection curves for UHPC-0 LWS and UHPC- 1 LWS specimens tested with the overlay in tension 78
Figure 4.1: Oxide composition of CSA and other common cementitious materials (% by mass) 86
Figure 4.2: Schematic Model of External vs. Internal Curing (Weiss, 2016) 96
Figure 4.3: Example water (a) absorption capacity and (b) release characteristics of different internal curing agents (Ideker et al., 2013) 99
Figure 4.4: Comparison of Autogenous Shrinkage Measured in Sealed Specimens Using ASTM C157 (Beginning at 24 H) And Corrugated Mold Procedure (Beginning Immediately After Mixing) For A w/c = 0.30 mixture (Sant et al., 2006) 101
Figure 4.5: Slump test for (a) BCSA cement concrete and (b) Type K cement concrete 105
Figure 4.6: The mix ingredients of Type K cement concrete 107
Figure 4.7: Slump variation graph over time for the baseline BCSA concrete mix with different citric acid contents 108
Figure 4.8: Slump variation chart over time for the baseline BCSA concrete mix with different 109
Figure 4.9: Volumetric air content test 111
Figure 4.10: Measured volumetric air content with different amounts of LWS for BCSA cement concrete 112
Figure 4.11: Unit weight of BCSA concrete with different amounts of LWS 113
Figure 4.12: Compressive strength of BCSA-cement concrete with 0 LWS 114
Figure 4.13: Compressive strength of BCSA concrete with varying amount of LWS (0.30% citric acid) 114
Figure 4.14: MOR test setup 116
Figure 4.15: MOR test results for BCSA cement concrete 116
Figure 4.16: MOR test results for Type K cement concrete 117
Figure 4.17: Calorimetry test results for BCSA concrete with different LWS content 118
Figure 4.18: Calorimetry test results for Type K cement concrete mixes with different LWS content 118
Figure 4.19: Compressive strength of the BCSA creep specimens 121

Figure 4.20: Compressive strength of the Type K creep specimens 121
Figure 4.21: (a) Prism molds and (b) Shrinkage measurement using comparator..... 124
Figure 4.22: (a) Wet curing and (b) dry specimens stored in a rack 125
Figure 4.23: (a) Model 4200 GEOKON VWSG, and (b) Manual Readout for VWSG Adjustment and Checking 126
Figure 4.24: Shrinkage Measurement Using VWSGs 127
Figure 4.25: (a) Grinding creep and shrinkage cylinders, and (b) creep test setup 129
Figure 4.26: Early-age shrinkage of Type K-8 LWS mix 131
Figure 4.27: Short-term behavior for (a) Total measured creep plus shrinkage and (b) Net creep of Type K-8 LWS using VWSG procedure..... 132
Figure 4.28: Long-term shrinkage strain of Type K 8-LWS mixture 132
Figure 4.29: Long-term (a) total measured creep plus shrinkage and (b) net creep of Type k cement concrete with 8 LWS using VWSG procedure..... 133
Figure 4.30: Early-age shrinkage of Type K-10 LWS mixture..... 134
Figure 4.31: Short-term (a) total measured creep plus shrinkage and (b) net creep of Type K cement concrete with 10 LWS using VWSG procedure..... 134
Figure 4.32: Long-term shrinkage strain of Type K-10 LWS mixture 135
Figure 4.33: Long-term (a) Total measured creep plus shrinkage and (b) net creep of Type K cement concrete with 10 LWS using VWSG procedure..... 136
Figure 4.34: Early-age shrinkage of BCSA-10 LWS mixture 136
Figure 4.35: Short-term (a) total measured creep plus shrinkage and (b) net creep of BCSA-8 LWS mixture using VWSG procedure..... 137
Figure 4.36: Long-term shrinkage of BCSA-8 LWS mixture after setting time..... 138
Figure 4.37: Long-term (a) Total measured creep plus shrinkage and (b) net creep of BCSA-8 LWS mixture using VWSG procedure..... 138
Figure 4.38: Early-age shrinkage of BCSA-10 LWS mixture after setting time 139
Figure 4.39: Short-term (a) Total measured creep plus shrinkage and (b) net creep of BCSA 10 LWS mixture using VWSG procedure..... 140
Figure 4.40: Long-term shrinkage of BCSA-10 LWS mixture after setting time..... 140
Figure 4.41: Long-term (a) total measured creep plus shrinkage and (b) net creep of BCSA 10 LWS mixture using VWSG procedure..... 141
Figure 4.42: Comparison of (a) Shrinkage and (b) Net creep for Type K cement concrete for 8 and 10 LWS..... 142
Figure 4.43: Comparison of (a) shrinkage and (b) creep for BCSA cement concrete for 8 and 10 LWS 143
Figure 4.44: Shrinkage strain for Type K cement concrete with different LWS content - (dry external curing) 146
Figure 4.45: Average shrinkage measurement of Type K cement concrete using ASTM C157 procedure (dry external curing) 147
Figure 4.46: Strain of Type K specimens (wet external curing) 147
Figure 4.47: Average strain of Type K specimens with both internal curing and wet external curing 148

Figure 4.48: Shrinkage strain for BCSA cement concrete with different LWS content (dry external curing) 149
Figure 4.49: Average shrinkage strain for BCSA cement concrete with different LWS content (dry external curing) 150
Figure 4.50: Shrinkage strain for BCSA cement concrete with different LWS content (both internal curing and external wet curing) 151
Figure 4.51: Average shrinkage strain For BCSA cement concrete with different LWS content (both internal and external curing)..... 151
Figure 5.1: 6 in. x 6 in. x 21 in. specimens along with 4 in. x 8 in. cylinders 168
Figure 5.2: Loading setup for MOR and fatigue tests 170
Figure 5.3: Specimen C1-080 after testing 174
Figure 5.4: Curtailed applied load vs. time graph for specimen PC-080..... 176
Figure 5.5: S-N curve for 6 in. x 6 in. conventional concrete (PC1 and PC2) 181
Figure 5.6: S-N curve for the 6 in. x 6 in. expansive BCSA concrete (C2 and C3) 182
Figure 5.7: S-N curve for the 8 in. x 8 in. expansive BCSA cement concrete (C1) 183
Figure 5.8: S-N curve for the 6 in. x 6 in. Type K cement concrete (K3 and K4)..... 184
Figure 5.9: S-N curve for the 8 in. x 8 in. Type K cement concrete (K1) 184
Figure 5.10: S-N curve for the 6 in. x 6 in. expansive BCSA concrete -8 LWS..... 185
Figure 5.11: S-N curve for the 6 in. x 6 in. expansive BCSA concrete - 10 LWS..... 185
Figure 5.12: S-N curve for the 6 in. x 6 in. Type K cement concrete -8 LWS..... 186
Figure 5.13: S-N curve for the 6 in. x 6 in. Type K cement concrete -10 LWS..... 187
Figure 5.14: Broken specimens of expansive BCSA cement (a) No LWS and (b) 8-LWS 188
Figure 5.15: Broken Specimens of Type K cement concrete (a) No LWS and (b) 8-LWS 188
Figure 5.16: S vs. N curve for different concrete fatigue models..... 191
Figure 5.17: Comparison of fatigue models based on RMSE for different concrete types 194
Figure 5.18: RMSE values for expansive BCSA and Type K specimens with LWS..... 195

List of Tables

Table 2.1. UHPC mix proportion by weight 11
Table 2.2. Absolute and relative values of shrinkage for UHPC as a percentage of the control mix 23
Table 2.3. Rapid set replacement for citric dozes of 0.6% or Less 24
Table 2.4. Rapid set replacement for citric dozes above 0.6% 25
Table 2.5. Compressive Strength of 2 in. x 2 in. x 2 in. cubes of UHPC with 15% BCSA 26
Table 3.1. Estimated initial unit cost (Haber et al., 2022) 51
Table 3.2. Service life estimate (Haber et al., 2022) 52
Table 3.3. Lifecycle cost comparison for overlay methods and new precast concrete deck (Haber, 2022) 52
Table 3.4. ODOT class AA mix proportion 57
Table 3.5. Slump/flow and air content test results 66
Table 3.6. Compressive Strength Test Results for Both Class AA and UHPC 67
Table 3.7. Experimental and theoretical values for beams with overlay in tension 77
Table 3.8. Experimental and Theoretical Values for Beams with Overlay in Compression 79
Table 4.1. Types of CSA binders (Bescher et al., 2018) 88
Table 4.2. Baseline mix proportion of BCSA cement concrete 102
Table 4.3. Baseline mix proportion for Type K plus portland cement concrete 106
Table 4.4. Workability and strength for different dosages of citric acid-baseline BCSA mix 109
Table 4.5. Actual internal curing water provided by LWS for both BCSA and Type K cement concrete mixes 120
Table 4.6. Creep load and age of all the CSA specimens 128
Table 4.7. A summary of elastic strain, creep strain, and creep coefficients 144
Table 5.1. Effect of different types of fibers on the flexural strength and endurance limit of concrete (Rama et al., 1989) 164
Table 5.2. Physical requirements of expansive cement (ASTM C845) 166
Table 5.3. Mix designs 168
Table 5.4. Slump, temperature, and citric acid dosage 172
Table 5.5. Compressive strength of fatigue test specimens 172
Table 5.6. Materials and dimensions of the specimens 174
Table 5.7. Fatigue and MOR test results 177
Table 5.8. Fatigue strength of the 6 in. x 6 in. conventional and CSA cement concrete 189
Table 5.9. Fatigue strength of the 8 in. x 8 in. conventional and CSA cement concrete specimens (N=2×106) 189
Table 5.10. Different fatigue models used for comparison 190
Table 5.11. Experimental vs. analytical fatigue stress S_{max} comparison with RMSE 192

Acknowledgement

Glory to the Almighty God, whose mercy and blessing have guided me throughout my life. He has led me on the path of knowledge and opened opportunities for me to grow and learn.

I would like to express my gratitude to my academic advisor, Dr. Royce W. Floyd, for his guidance and support throughout my PhD. From reviewing my analytical work to actively participating in the preparation of the concrete mixtures, his contribution was instrumental to the completion of this research. Throughout this journey, he has been very patient, provided constructive feedback, and corrected me with kindness. I also had the privilege of taking his courses of Structural Design–Wood, Structural Design-Concrete II, and Prestressed Concrete Design, which greatly strengthened my understanding of structural engineering and further enriched my doctoral experience. Beyond academics and research, I have also learned many valuable life lessons from him, and I feel fortunate to have had him as my advisor.

I am thankful to my PhD committee members, Dr. Jeffery S. Volz, Dr. Shreya- Vemuganti, and Dr. Matthew Reyes for their guidance and valuable feedback throughout this research. Their comments on my general exam, research prospectus, and final dissertation have enriched this work.

My parents, Dadullah Ahmadi and Jamila Akbari, have been the greatest source of strength and support throughout my life. They have always encouraged me to pursue higher education and make the most of every opportunity for growth. Their lifelong sacrifices and investment in my education have made this achievement possible. Despite the limited opportunities available where I was raised, they did everything they could to provide me with the best possible

education. Also, I would like to thank my siblings for standing by my side and providing me with the support whenever I needed it.

My wife, Sayeda Fayaz, and her family were of great help as I was busy with my experimental work and my dissertation writing. They took on many of my household responsibilities, allowing me to focus on my research. Their encouragement and understanding played a key role in the completion of this work.

I want to thank the lab manager of the Donald G. Fears Structural Engineering Lab, Mr. John Bullock, for his assistance with the logistical aspects of my research. His support was invaluable in the timely completion of this work.

The experimental program would not have been possible without the support from the fellow students, who contributed to the specimen preparation and testing. I would like to thank Omar Yadak, Courtney Dawson, Ammar Al Batrani, Jackson Milner, Yunxu Chen, Xander Griffin, Sijan Adhikari, and Ali Akbarpour for their contribution in preparing and testing specimens.

I am grateful to all of my teachers, from my undergraduate studies through the completion of my Ph.D., for the invaluable role they have played in shaping my understanding of engineering concepts. In particular, I would like to thank my undergraduate teacher, Professor Zahid Ahmad Siddiqi, who taught me Mechanics of Materials, Steel Structure Design, and Structural Mechanics. His teaching laid the foundation for my civil engineering knowledge, and I will always be grateful for his guidance and the knowledge he shared with me.

I want to thank my colleagues at WSB, Mr. Ute Ganjanathavat, Mr. Caleb Austin, Mr. Rolland Seaman, and Dr. Stephen Roswurm, for sharing their knowledge and expertise during my training with them.

Finally, I acknowledge all of the research sponsors for their support of this research. I am especially thankful to the Expanded Shale, Clay and Slate Institute (ESCSI) for awarding me the John Ries Scholarship, which provided financial support during my doctoral studies.

Abstract

This dissertation consists of four studies investigating the impact of internal curing on the performance of advanced concrete materials. The first chapter introduces the research by presenting its background, motivation, objective and organization. The second chapter focused on Ultra-High Performance Concrete (UHPC), an advanced cementitious material with superior mechanical properties compared to conventional concrete; however, its high cementitious material content results in significant early-age autogenous shrinkage. This study evaluated internal curing using presoaked lightweight sand (LWS) to improve the performance of UHPC. The quantity of LWS varied to supply 0, 1, 2, and 3 lb of internal curing water per 100 lb of total cementitious material. Early-age shrinkage was measured using vibrating wire strain gauges (VWSGs) embedded in 6 in. × 12 in. UHPC cylinders, while calorimetry testing was conducted to evaluate setting time and hydration heat. The results indicate that autogenous shrinkage significantly decreased with increasing LWS, whereas compressive strength, setting time, and hydration heat were not significantly affected.

Bridge deck deterioration is a primary contributor to poor bridge condition ratings in the United States. The third chapter investigated the effects of internally cured UHPC overlays on the flexural capacity of beams simulating bridge decks. Beam specimens were tested under third-point bending, and fresh and hardened properties of UHPC with varying LWS contents were evaluated. The addition of the overlay enhanced the load-bearing capacity while maintaining composite action with the substrate. Incorporation of LWS reduced shrinkage strain, resulting in lower residual interfacial shear stresses and enhanced load-carrying capacity.

Calcium sulfoaluminate (CSA) cement is a viable alternative binder that can partially or fully replace portland cement because of its rapid strength gain, reduced shrinkage, and lower environmental impact. The fourth chapter investigated the use of internal curing provided by presoaked LWS to improve the shrinkage, creep, and mechanical properties of Belitic Calcium Sulfoaluminate (BCSA) and Type K CSA-based cements. A portion of conventional sand was replaced with LWS, and its influence was evaluated through compressive strength, modulus of rupture (MOR), creep, and shrinkage tests using ASTM C157 and VWSGs. The results were used to identify the optimal amount of LWS for enhanced performance.

Finally, the fatigue behavior of CSA cement concretes, including expansive BCSA and Type K cement, was evaluated in the fifth chapter. A total of 88 beams with dimensions of 6 in. × 6 in. × 21 in. and 14 beams with dimensions of 8 in. × 8 in. × 30 in. were tested under different stress levels and loading frequencies. LWS was used to provide internal curing and reduce shrinkage. The results of the S-N curve indicate that the 8 in. × 8 in. specimens provided more reliable fatigue behavior with higher R^2 values and reduced scatter. The addition of LWS significantly enhanced the fatigue strength of Type K cement concrete, and a higher R^2 value of the S-N curve compared to both portland cement and expansive BCSA mixtures.

Chapter 1

1. Introduction

Internal curing has emerged as a relatively new technology that increases the resistance to early-age cracking and improves the durability of concrete. In 2013, ACI defined internal curing as "a process by which the hydration of cement continues because of the availability of internal water that is not part of the mixing water." In general, internal curing is the process of supplying water from within the concrete using highly absorptive, porous materials such as lightweight sand (LWS), super absorbent polymers (SAP), or rice husk ash. The internal curing agents are typically applied in a pre-wetted condition and release their water when a negative pressure forms in the concrete. This negative pressure develops due to the drop in the internal humidity of the concrete matrix, causing capillary pressure and resulting in the release of water from the internal curing materials for continuous hydration. The effectiveness of internal curing is not only affected by the type of internal curing material. Other factors, such as the amount of free water, the amount of internal curing water, replacement ratio, pore size, and the water absorption and desorption rate of the internal curing material, also influence its performance (Xu et al., 2021).

The concept of using lightweight aggregates in concrete predates the development of internal curing. The application of lightweight concrete dates back to Roman times, as it was desired to decrease the weight of the domes of Pantheons as the height increased (Bremner & Ries, 2009). Artificial lightweight aggregate (LWA) was invented by Stephen J. Hayde, and he later allowed the U.S. government to use his patent for lightweight concrete ship production during the First World War (Bentz et al., 2011). However, the first published recognition of the internal curing

effect of LWA was by Paul Klieger in 1957, in which he mentioned that "lightweight aggregates absorb considerable water during mixing which apparently can transfer to the paste during hydration" (Bentz et al., 2011). Concrete produced using pre-soaked LWA demonstrated excellent long-term durability and reliable in-service performance (Cusson et al., 2008).

In recent years, advanced concrete materials such as high-performance concrete (HPC) and Ultra-High Performance Concrete (UHPC) have been widely used in the construction industry due to their superior mechanical properties, good workability, and enhanced durability. In 1993, Richard et al. (1994) used various cementitious materials with increased fineness to develop reactive powder concrete (RPC) (Shi et al., 2015). RPC is characterized by high cement content, a low water-to-binder ratio, superior mechanical properties, and enhanced ductility. In a subsequent effort, De Larrard introduced the term UHPC to describe a special type of concrete that requires specialized mixing and curing procedures. However, the high content of cementitious materials in HPC and UHPC resulted in significant volume change in the matrix at early ages. In addition, the degree of hydration in HPC and UHPC is greater than that of conventional concrete, which consumes water within the pore structures, leading to capillary tension and autogenous shrinkage (Xu et al., 2021). Due to their dense microstructure, external curing cannot penetrate these types of concrete to replenish the reduction in internal relative humidity; therefore, its effect is limited primarily to the surface layer of the concrete. Consequently, internal curing has become an effective approach for mitigating self-desiccation in high-strength concrete and has been applied since the 1990s (Cusson et al., 2008). Building upon this concept, the present research study aims to evaluate the impact of internal curing using LWS on the fresh and hardened properties of various cementitious mixtures.

The contents of this dissertation are organized into five chapters. Excluding the introduction, each chapter includes literature review, experimental procedures, results, conclusions, and references. This format was adopted to improve clarity and avoid mixing the corresponding methodology and results.

The second chapter describes use of internal curing provided by presoaked LWS to mitigate the autogenous shrinkage of the UHPC. UHPC is an advanced cementitious material with superior mechanical properties like excellent strength, durability, and extremely low porosity, making it suitable for different structural applications. Although UHPC has been used at least since 1990, there is not a universal definition. The range of compressive strength assigned for UHPC varies from 17.4 ksi to 22.7 ksi (120 MPa to 150 MPa) (Zhang et al., 2019). UHPC is a combination of active and inert fillers and is designed based on the particle packing principle to achieve the highest packing density of solid particles with a lower water-binder (w/b) ratio (usually below 0.25) (Zhang et al., 2019). The low amount of water causes minimal porosity which leads to an almost impermeable material. However, high cementitious materials content (600-1000 kg/m^3) results in chemical and autogenous shrinkage causing rapid dissociation of the paste and volume change at an earlier age. This rapid desiccation of the pore water exerts negative suction capillary pressure on the walls of the pores which displays as volumetric shrinkage (Loukili, 1999).

Shrinkage can influence crack formation, redistribution of stress, and loss of prestress forces in concrete structures by impacting the dimensional stability of the element, which can influence the mechanical properties, serviceability, durability and aesthetics of UHPC structures. These effects become especially critical when they lead to excessive deflection and compromise strength and serviceability. Thus, shrinkage is a key consideration in long-term structural design.

To mitigate autogenous shrinkage, LWS was introduced to provide water for internal curing. LWS is a porous material which absorbs water and releases it gradually during cement hydration when included in the concrete matrix in a presoaked condition. This mechanism helps mitigate shrinkage due to pore water depletion during cement hydration. For this study, four sets of specimens were analyzed. Each set of specimens used a different UHPC mixture formulation: UHPC-0LWS (control mix with no internal curing), UHPC-1LWS, UHPC-2LWS, and UHPC-3LWS, with each number before LWS indicating the quantity of supplied internal curing water per 100 lb of total cementitious materials. Fibers were excluded from the mixes to eliminate their contribution to shrinkage resistance. A Flow test was performed for each mix using ASTM C1856/1856M procedures to observe the rheology of the mix and ensure adequate workability. Calorimetry testing was conducted using a semi adiabatic F-CAL 4000 machine to record the heat of hydration of each mix for 48 hours after casting. The reults of this test provide a relation between shrinakge and hydration of the cementitious materials over time which helps to determine the final setting time of the mix and can be related to the onset of shrinkage stress in the specimens. Other companion testing included testing 3 in. x 6 in. concrete cylinders for determining the compressive strength of the mix over time using ASTM C39/C39M and ASTM C1856/1856M procedures.

Shrinkage was measured using 6 in. x 12 in. cylindrical specimens with internally embedded VWSGs. The VWSGs were used to measure the deformation and thermal behavior of specimen over time which was recorded using a dedicated data logger.

Chapter three describes the use of internally cured UHPC for bridge deck overlay. An important application of UHPC is bridge deck rehabilitation. Therefore, the goal of this chapter is to investigate the flexural behavior of simulated slab sections with a UHPC overlay.

As of 2016, approximately 38% of the reinforced concrete highway bridge decks in the U.S. exhibit some level of deterioration and require rehabilitation (Haber et al., 2017). The Federal Highway Administration (FHWA) estimates that approximately $200–$300 billion is required to rehabilitate or replace all structurally deficient bridges nationwide (Aaleti et al., 2013). Bridge deck deterioration is commonly attributed to repeated vehicular loading, delamination, freeze-thaw cycles, cracking, and/or corrosion of internal reinforcement, with a substantial portion of the U.S. bridges requiring urgent deck rehabilitation (Graybeal et al., 2018).

Commonly used overlay materials are high-performance concrete (HPC), latex-modified concrete (LCM), asphalt overlay with waterproofing membrane, and polymer-based materials. While these materials have demonstrated varying levels of success, there are durability, crack susceptibility, and permeability concerns for each of them. Using UHPC as an overlay material has emerged as a promising alternative for bridge deck rehabilitation. Similar to the UHPC internal curing section, four UHPC mixes (UHPC-0LWS, UHPC-1LWS, UHPC-2LWS, and UHPC-3LWS) were used to evaluate the impact of internal curing on the flexural and shear behavior of the overlay specimens. The tests included flow, compressive and flexural test on overlay specimens with and without reinforcement.

The fourth chapter investigates using LWS for improving the shrinkage, creep and mechanical properties of rapid setting and Type K expansive calcium sulfoaluminate (CSA) based cements. LWS helps mitigate shrinkage due to pore water depletion during cement hydration and can also provide additional water needed for the hydration of CSA-based cement. Water deficiency exerts suction pressure on the walls of the pores which causes deformation and can lead to cracks. The amount of replaced LWS was selected to introduce 8 lb and 10 lb of internal curing water and its influence on the material's behavior was evaluated. The common tests used for this purpose were

compressive strength using ASTM C39, creep using ASTM C512, and shrinkage tests based on both ASTM C157 and using 6 in. x 12 in. cylinders with embedded VWSGs. The results were used to identify the mix with optimal amount of LWS that yielded enhanced performance and a comparison of results for mixes with varying amounts of LWS.

The fifth Chapter focuses on the flexural fatigue behavior of concrete made with expansive rapid setting CSA cement and a mixture of Type K cement and portland cement as binders. Flexural fatigue tests were used to evaluate the resistance of the material for repetitive transverse loading. Most of the available data related to fatigue are for conventional/normalweight concrete with portland cement as a binder. The stress ratio (S) vs. number of loads corresponding to failure (N) of each tested specimen, also known as S-N curve, were plotted and the resulting graphs used to determine the stress level corresponding to the fatigue strength for each type of material.

Chapter 2

2. Effect of Internal Curing on Shrinkage Behavior of Ultra-High Performance Concrete

2.1 Literature Review

Concrete shrinkage occurs in two main stages: early-age shrinkage which includes chemical, autogenous, and thermal shrinkage and long-term shrinkage known as drying shrinkage. Chemical shrinkage refers to the reduction in volume of cement and water as they react during hydration. Immediately after mixing water and cement, chemical shrinkage begins which leads to the formation of internal voids. As hydration progresses, pore water is consumed and the degree of saturation decreases. With the change in the saturation state of pores from saturated to unsaturated, the inner concave surface of the pore is subjected to internal pressure which causes autogenous shrinkage (Wu et al., 2017). Autogenous shrinkage refers to the reduction in dimensions under constant temperature conditions and in absence of moisture exchange with the environment. This phenomenon is particularly significant for mixes with lower water to binder ratio.

Autogenous shrinkage typically develops within the first month after casting, as it is linked to the cement hydration. Approximately 60-90% of the autogenous shrinkage occurs within the first 28 days (Shurbert-Hetzel et al., 2023).

Drying shrinkage refers to the volumetric reduction in concrete due to water evaporation from capillary pores into the surrounding environment. Unlike autogenous shrinkage, which occurs primarily at the early age in UHPC, drying shrinkage develops over a longer period.

In conventional concrete the governing type of shrinkage is drying shrinkage due to higher water-to-binder ratio. In contrast, UHPC, with its lower water content, lacks sufficient pore water

pressure to develop drying shrinkage, therefore, the significant part of total shrinkage in UHPC is due to autogenous shrinkage. Shrinkage can influence crack formation, redistribution of stress, and loss of prestress forces in the concrete structures which can influence the mechanical properties, serviceability, durability and aesthetics of UHPC elements. These effects become especially critical when they lead to excessive deflection or compromise strength and serviceability. Thus, shrinkage is a key consideration for long-term structural design.

Based on a study by Zhang et al., (2019), UHPC shrinkage is divided into four stages. In the first stage the internal temperature of the mix is higher than the room temperature due to mixing, and mechanical energy of the mixer and the mix tries to equilibrate its temperature to the room temperature. The second stage starts once the mix cools down to the room temperature and contraction due to mix cooling ceases. Thus, the shrinkage observed during the first two stages is primarily due to thermal contraction. The third stage is characterized by a rise in temperature due to accelerated hydration. During this period, rapid consumption of pore water leads to self-desiccation, generating significant autogenous shrinkage. This short stage accounts for approximately 58% of the total shrinkage strain within the first 7 days. Finally, in stage four, the rate of shrinkage reduces due to decrease in hydration and increased stiffness of the matrix. The temperature and heat flow of the mix decreases which results in a more stable stage.

To mitigate autogenous shrinkage, presoaked lightweight sand (LWS) has been used to provide water for internal curing. According to ACI, internal curing is defined as “Supplying water throughout a freshly placed cementitious mixture using reservoirs, via pre-wetted lightweight aggregates, that readily release water as needed for the hydration or to replace moisture lost through evaporation or self-desiccation” (Ideker et al., 2013). The water intended for internal curing disperses inside the concrete after it hardens and improves the hydration process. The

materials used for internal curing can be divided into two main types: materials containing physically absorbed water (e.g., super absorbent polymer-SAP) and porous materials (e.g., lightweight aggregate-LWA). The water is sucked from the reservoirs by the cement paste during curing due to capillary pressure and is transported to the surrounding concrete. Hence there is more hydration in the cement surrounding LWA in the interfacial transition zone which creates a stronger bond between the cement and LWA (Weiss, 2016). The advantages of internal curing are increased hydration, strength development, reduced early-age shrinkage and low cracking risk, low permeability, high durability, and saving water used for external curing. Several studies have focused on internal curing specifically for UHPC. Work by Liu et al. (2019) examined methods of internal curing for UHPC made with silica fume and fly ash and found that LWS was effective for mitigating autonomous shrinkage. Su et al. (2026) examined internal curing using fine coral aggregates in UHPC using silica fume, fly ash, seawater, and sea sand and also found reduced autogenous shrinkage when internal curing was provided. Justs et al., (2015) investigated the use of SAP for internal curing of UHPC and reported than internal curing using SAP can significantly decrease self-desiccation and autogenous shrinkage of UHPC. However, SAP reduces the workability of the mixture due to water uptake from the mixing water, making less water available in the matrix (Snoech et al., 2014).

This study evaluated the impact of internal curing on shrinkage and hydration behavior of a locally developed UHPC mixture. This study contributes to the existing literature in that the mix design examined in this work utilized slag cement as the primary supplementary cementitious material, which provides additional data for a more robust understanding of UHPC behavior. For this study, four sets of specimens were analyzed: UHPC-0 LWS (control mix), UHPC1-LWS, UHPC 2-LWS, and UHPC-3 LWS, with each number before LWS indicating the quantity of

supplied internal curing water per 100 lb of total cementitious materials. Fibers were excluded from the mixes to eliminate their contribution for resisting shrinkage. A semi adiabatic F-CAL 4000 calorimeter was used to record the heat of hydration of each mix over the first 48 hours after casting. These results provide a relation between shrinkage and hydration of the cementitious materials over time which helps to determine the setting time of the mix and can be related to the onset of shrinkage stress in the specimens. Additionally, 3 in. x 6 in. concrete cylinders were tested to determine the compressive strength of the mix over time.

2.2 Experimental Procedure

2.2.1 Materials and Mix Design

To evaluate the effect of internal curing on UHPC a volume of masonry sand was replaced with LWS for introducing a desired quantity of internal curing water into the mix. The LWS used for this project was expanded shale with a measured absorption of 36.5%, specific gravity of 1.35, and gradation with 88.9% passing a No.4 sieve. A desorption test was not performed for the LWS used in this study. Care was taken to prepare the lightweight sand using the same procedure each time in order to obtain consistent moisture content. The LWS was pre-soaked in water for 48 hours before mixing and subsequently drained for 15 minutes in a perforated bucket with geotextile placed on its bottom. After 15 minutes the LWS was stirred with a rod and was left to drain for five more minutes, and the same procedure was repeated for another 5 minutes to ensure consistent surface moisture removal between batches. The quantity of LWS used in this study was designed to provide 1 lb, 2 lb, and 3 lb of internal curing water per 100 lb of total cementitious materials. However, these target values slightly differed from the actual moisture contents of the LWS. Since the moisture content samples for each mix were collected just before the mixing, the true moisture content was not known until after batching. Therefore, the actual

moisture content values were back calculated following the mix. The initially assumed moisture content was based on the average from numerous trial batches. Whereas the actual measured moisture content for the UHPC-1LWS, UHPC-2LWS, and UHPC-3LWS mixes provided 0.926 lb, 1.85 lb, and 2.88 lb per 100 lb of cementitious materials, respectively.

The first mix was a baseline J3 UHPC mix, originally developed at the University of Oklahoma (Looney et al. 2019). The mixing procedure started with weighing all the dry materials (cement, sand, slag, silica fume) to the proportion given in Table 2.1 and dumping them into the mixer using the sequence discussed by Looney et al. (2019). The LWS was added to the mix after adding half of the water containing high range water reducing admixture (HRWR) to the dry materials and was mixed for 1 minute. Adding LWS too early with dry material could cause release of stored moisture which undermines the primary purpose of providing internal curing water once the external water is consumed during hydration. As mentioned earlier, the fibers were excluded.

Table 2.1. UHPC mix proportion by weight

Constituent	**Mix Proportion**
Type I Cement	0.6
Silica Fume	0.1
Slag Cement	0.3
Masonry Sand (1:1 agg/cm) in oven dry condition	1.0
w/b	0.2
Steel Fibers	2% by Volume
HRWR	18-28 oz/cwt

A pan mixer (vertical-shaft mixer) was used to prepare UHPC mixes as shown in Figure 2.1(a). For each batch, the flow of the mix was measured using ASTM C1856 as shown in Figure 2.1(b). If the diameter of the flow was less than 8 in. additional HRWR was added to achieve a flow

between 8 in. to 10 in. Additionally, nine 3 in. x 6 in. cylinders were cast for determining the compressive strength at 3, 7, and 28 days of age. The fresh UHPC was transported in buckets and carefully poured into cylindrical molds containing the strain gauges. To avoid disturbing the strain gauges from the impact of the fresh mix, the concrete was not poured directly over the gauges. After casting, the specimens were covered with plastic sheets to avoid probable moisture loss. All specimens were cast in a temperature-controlled room with 68 ˚F temperature and approximately 50% relative humidity and were maintained in this environment for the rest of the shrinkage monitoring. Specimens were demolded three days after casting and were rested on a wooden board with a wooden plate on their tops to give a volume to surface area ratio similar to creep specimens tested as part of an adjacent study.



(a) (b)

Figure 2.1: (a) Pan mixer (b) Flow test of UHPC with LWS



(a) (b)

Figure 2.2: (a) Poorly ground UHPC cylinder, (b) well ground UHPC cylinders

It was observed that the inclusion of LWS introduced some relatively coarser particles which floated to the surface of mix and generated a perforated surface on approximately 0.25 in. of the top surface, as shown in Figure 2.2(a). Additionally, the presence of LWS might have entrapped small air pockets which might contribute to the localized surface pores. To eliminate the potential influence of pores to the compressive strength of UHPC the top was ground until the visible pores were removed. For the field application, it is recommended that the bridge deck be cast approximately 0.5 in. thicker and the top 0.5 inches be removed by surface grinding the section to ensure a dense and uniform surface layer.

2.2.2 Shrinkage Testing

Shrinkage of UHPC was measured using vibrating wire strain gauges embedded vertically in 6 in. x 12 in. cylindrical specimens, as shown in Figure 2.3(a). Four different mixes were prepared for shrinkage evaluation and for each mix, two 6 in. x 12 in. cylinders were used for shrinkage measurement.

The vibrating wire strain gauges (VWSG) used were GEOKON model 4200 having 6 in. length and capable of measuring simultaneous temperature and strain. The initial reading of the strain gauge was adjusted to get the reading from the manual readout (Figure 2.3(b)) to around 2600 micro-strain which would provide adequate range for anticipated shrinkage. The recorded strains were corrected to account for temperature-induced effects, and the data was collected at predefined intervals by a data logger and periodically downloaded for analysis. The data collection interval was set to 5 minutes for the first few days to better record the early-age shrinkage behavior and later set to 15 minutes for the rest of the test. Figure 2.3 (c) shows the UHPC cylindrical specimens used for shrinkage measurement.

The shrinkage strain was calculated using Eq. (2.1)

$$\text{Microstrain} = (R_1-R_0) \times B+(T_1-T_0) \times (C_1-C_0) \quad (2.1)$$

Where:

R_0=Initial reading

R_1=Current reading

B=Batch gauge factor which is used as 0.975

T_0=Initial temperature

T_1=Current temperature

C_1=Coefficient of expansion of steel: 12.2 micro-strains / ˚C

C_2=Coefficient of expansion of concrete: 10 micro-strains / ˚C

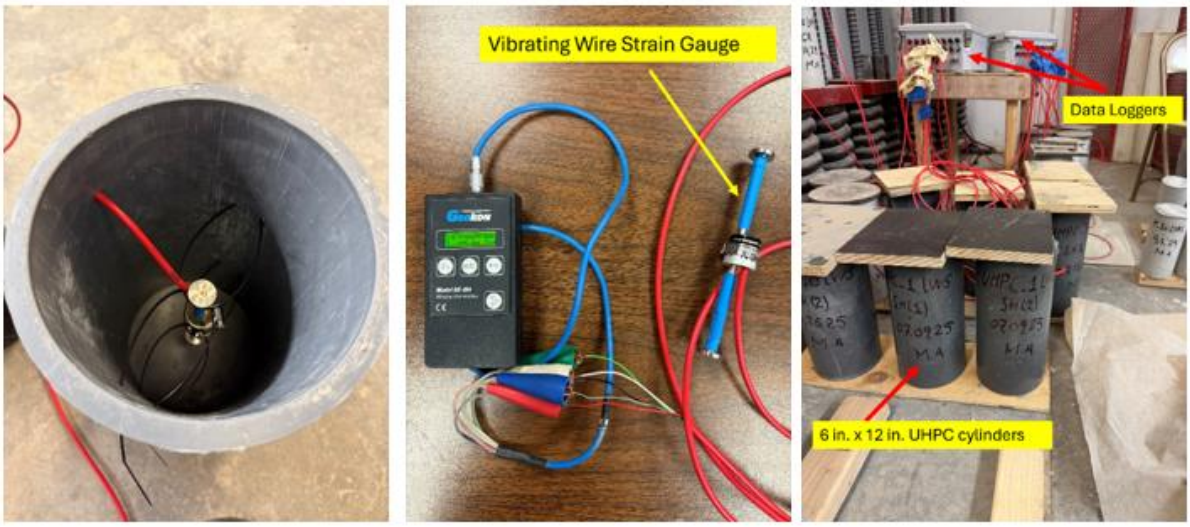


Figure 2.3: (a) VWSG placed in the cylindrical mold (b) VWSG with manual readout and (c) UHPC shrinkage specimens attached to data logger

2.2.3 UHPC with BCSA Cement Replacement

Similar to internal curing, partial replacing of portland cement in UHPC with Belitic Calcium sulfoaluminate (BCSA) Cement, a lower shrinkage cement, has the potential to reduce the autogenous shrinkage and carbon footprint of UHPC. Therefore, a series of trial mixes was prepared to evaluate the effect of BCSA cement replacement on workability and compressive strength of the UHPC. Figure 2.4 shows the dry and wet mixing of the UHPC in a pan mixer.



Figure 2.4: (a) Ingredients of UHPC, (b) Dry mixing in pan mixer, and (c) Wet mixing for 25 percent replacement mix

The first goal was to achieve a workable mix. For this purpose, the percentage replacement amount of BCSA was varied while keeping the citric acid set retarder dosage as the highest allowable by the manufacturer which was 0.6% of weight of cementitious materials. After all the trial mixes, 15% replacement selected as a possible cement replacement amount. However, the workability was still a challenge. To overcome the poor workability due to rapid setting of UHPC, the citric acid dosage was increased to as high as 7% of total cementitious material weight and the corresponding flow and compressive strength was observed. The results are presented in the results section.

2.3 Results

2.3.1 Compressive Strength

Compressive strength results presented in Figure 2.5 indicate that addition of LWS did not significantly affect the compressive strength development of the UHPC over time. Among all LWS combinations, the UHPC-2LWS mix exhibited equal or higher compressive strength compared to the reference mix (UHPC-0LWS) at all testing ages. However, increasing LWS content to 3-LWS led to a reduction in compressive strength. Therefore, UHPC-2LWS can be considered the optimal LWS dosage for achieving the highest compressive strength. It should be noted that while compressive strengths were on the low end of those qualifying for UHPC, previous studies of the baseline mix design indicate high flexural strength and durability (Floyd et al., 2024). However, only compressive strength was examined in this study.

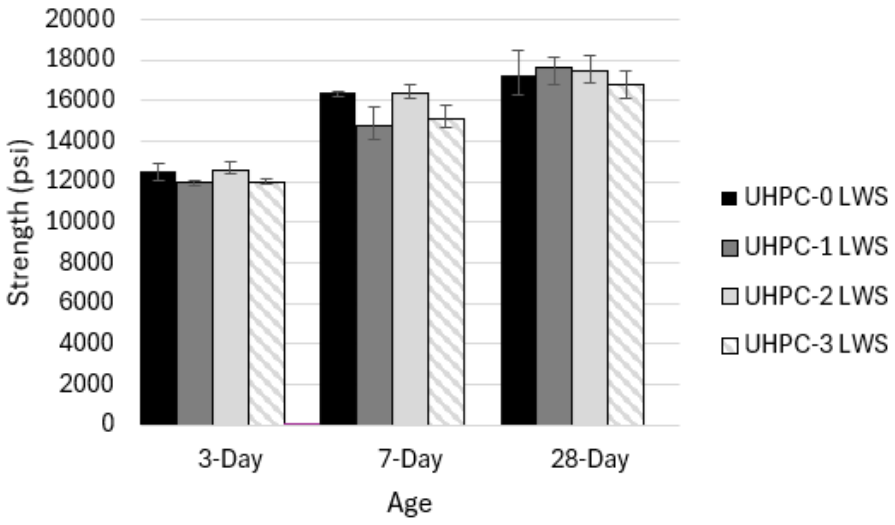


Figure 2.5: Compressive strength comparison for UHPC with different LWS content

2.3.2 Modulus of Elasticity (MOE) Test (ASTM C469)

MOE test was conducted to evaluate the impact of LWS on the stiffness of UHPC mix. The results, as shown in Figure 2.6, indicate that addition of LWS did not cause a significant change in the MOE of the UHPC. The increase in MOE with respect to the base mix with addition of 1 LWS and 2 LWS were 3.6% and 5.3% and a decrease of -0.17% for 3 LWS mixture.

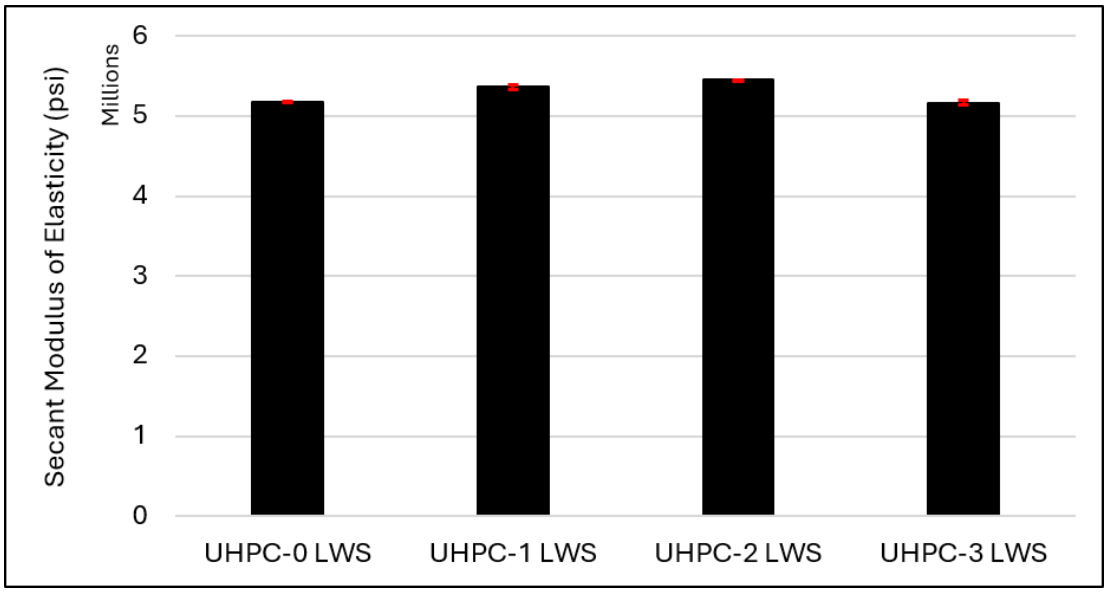


Figure 2.6: Secant modulus of elasticity of UHPC

2.3.3 Setting Time

Setting time of UHPC was determined using a semi adiabatic F-CAL 4000 calorimeter. In this test, a 4 in. x 8 in. cylinderical specimen was placed in the machine which continuously measured the heat evolution of the specimen over time, as shown in Figure 2.7. Data were collected for 48 h after which the specimen was removed from the machine.



Figure 2.7: Semi-adiabatic F-CAL 4000 calorimeter

A temperature-time curve was generated from the calorimetry data as presented in Figure 2.8, and the time corresponding to one-third of the maximum temperature rise was taken as setting time of the concrete (Calmetrix, 2025). The test results indicate that the setting time for the UHPC-0LWS and UHPC-1LWS mixes was 7.9 hours while for the UHPC-2LWS and UHPC-3 LWS mixes it was 7.1 hours. The shorter setting time for the latter mixes may be attributed to the presence of internal curing water, which accelerates the hydration process.

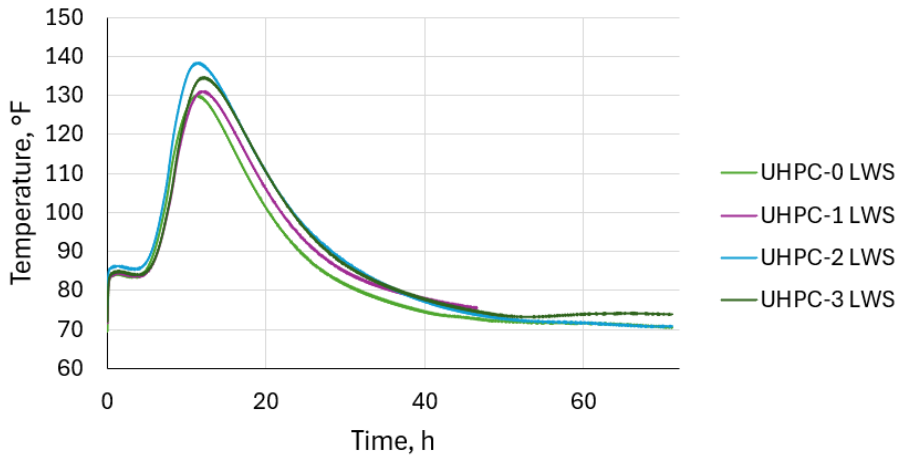


Figure 2.8: Calorimetry test results for UHPC with different amount of LWS

2.3.4 Shrinkage Measurement

In this study UHPC shrinkage was analyzed in two main stages. Shrinkage before final setting time covers the early age shrinkage behavior and shrinkage after final setting focuses on long term shrinkage behavior.

2.3.4.1 Early Age Shrinkage Behavior

At early age UHPC shrinkage is governed by self-desiccation and hydration of cementitious products. The early age shrinkage of UHPC-0LWS follows a multi-stage pattern. During stage I (0-4 h) the mix underwent an initial shrinkage immediately after casting which was the onset of chemical shrinkage and thermal equilibrium. Stage II (4-6 h) corresponds to the dormant period where hydration slows temporarily and the shrinkage curve levels off. In stage III (6-7.9 h) the shrinkage curve follows a steep increase in shrinkage magnitude with time which is mainly due to a rise in heat of hydration and lack of internal curing moisture availability. This generates strong capillary tension, producing significant contractions. The end of stage III (7.9 h) coincides

with the setting time of the mix. Finally, during stage IV, the rate of heat generation declines, and the concrete shrinkage gradually stabilizes.

Addition of 1 lb internal curing water per 100 lb of binder resulted in a slower shrinkage rate in Figure 2.9(b) than the control mix Figure 2.9(a). The decrease in early age shrinkage can be specifically observed in stage III of Figure 2.9(d). For UHPC-3LWS, the shrinkage within first 50 hours was minimal, and the strain curve was smoother and more stable. Since the shrinkage occuring before setting time does not induce stress within the mix the corresponding strain can be excluded from shrinkage stress calculations by subtracting the pre-setting shrinkage from the total shrinkage measured beginning at casting. In summary, the addition of LWS is primarily effective in controlling the shrinkage during stage III (just after setting time) where heat of hydration increases the demand for water. In the UHPC-0LWS mix, the absence of internal curing water causes the available mixing water to be consumed rapidly by hydration. Due to insufficient water, a negative capillary pressure develops within the pore structure, leading the material to shrink. In contrast, mixes containing LWS mitigate this effect, as the LWS particles release their absorbed water to sustain hydration and reduce shrinkage during stage III.

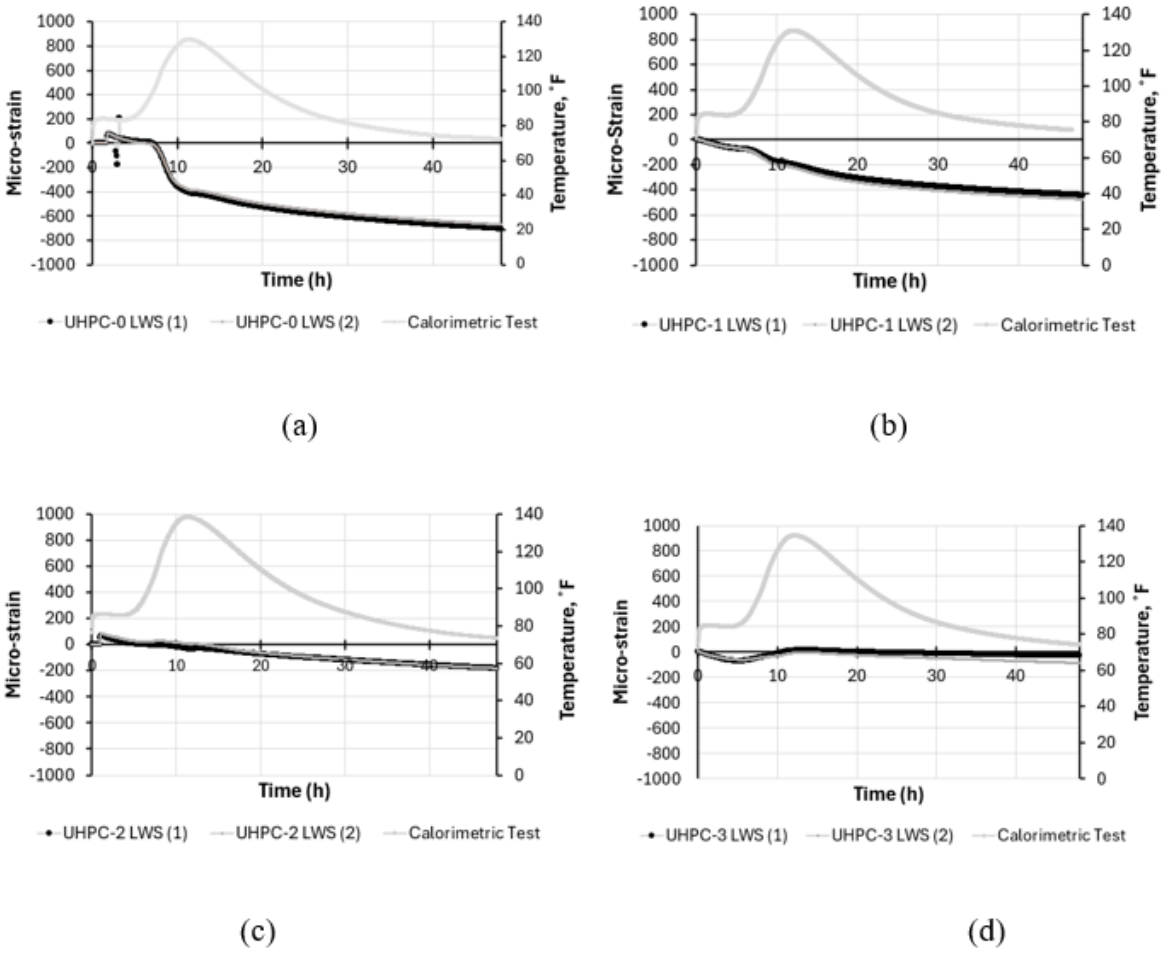


Figure 2.9: Shrinkage of UHPC with (a) 0-LWS (b) 1-LWS (c) 2-LWS, and (d) 3-LWS measured over 48 h

Since the heat due to cement hydration stabilizes after approximately 48 hours, the shrinkage of all mixes within this period has been compared and is shown in the plots in Figure 2.9. Reduction in shrinkage can be observed at the end of 48 hours after mixing, and the reduction becomes greater with increasing LWS content.

2.3.4.2 Long-Term Shrinkage

In this study long term shrinkage is considered to begin after the final setting time of UHPC which is 7.9 h for the mixes 0-LWS and 1-LWS, and 7.1 h for the mixes with 2-LWS and 3-LWS as determined by calorimetry. The shrinakge rate is initially high at the onset of long-term shrinkage and gradually decreases with time. Table 2.2 presents the relative and absolute values of shrinkage compared to the 0-LWS base mix during different time intervals. In the first column of Table 2.2, 2 days is considered as the time for heat of hydration to normalize and stabilize. Shrinkage decreases with increasing amounts of LWS, reducing the 2-day shrinkage by up to 8% of the shrinkage of base mix (0-LWS). The relative shrinkage between 2-50 days is equal or lower for the mixes containing LWS, and the overall (absolute) shrinkage after 50 days decreases progressively with the higher LWS content. For instance, the total shrinkage of UHPC-3 LWS mix is only 52% of that of UHPC-0 LWS mix.

Table 2.2. Absolute and relative values of shrinkage for UHPC as a percentage of the control mix

Specimen	**Relative 0-2 DAY (%)**	**Relative 2-50 Day (%)**	**Absolute 50 Day (%)**
UHPC-0 LWS	100	100	100
UHPC-1 LWS	66	102	77
UHPC-2 LWS	26	74	61
UHPC-3 LWS	8	65	52

The percentage reduction in early age shrinkage indicates that the influence of LWS on shrinkage is most significant at early ages. As time progresses, the shrinkage curve between different mixes becomes almost parallel, suggesting that the effect of internal curing gradually diminishes with time, as shown in Figure 2.10.

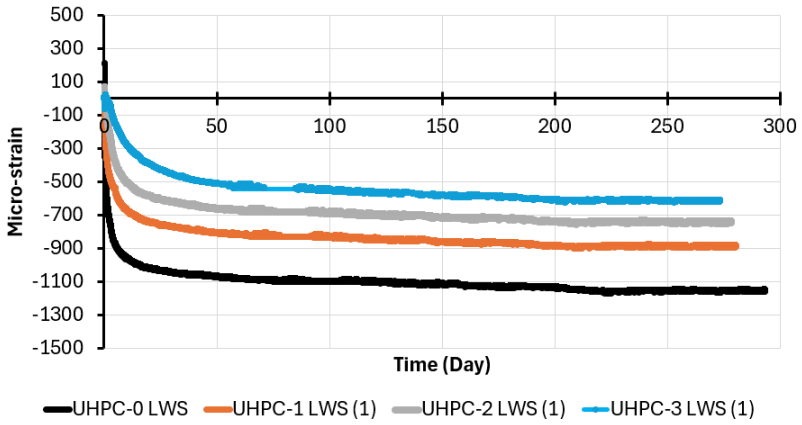


Figure 2.10: Combined measured total shrinkage of UHPC specimens over time

2.3.5 UHPC with BCSA Replacement

2.3.5.1 Flow Test

For UHPC with citric acid dosage below 0.6%, the flow droped almost to half of its initial value 5 minutes after the initial flow test despite reduction in the BCSA replacement to as low as 2% of the portland cement. The quick loss of workability makes it challenging for field application and entails the risk of premature stiffening in the mixer and placement tools prior to casting. Table 2.3 represents the intial flow and flow after 5 minutes for the mix with 0.6% citric acid.

Table 2.3. Rapid set replacement for citric dozes of 0.6% or Less

Batch #	% Replacement	Citric Doze (%)	HRWR (Glenium)	Initial Flow (in.)	Five Minutes Flow (in.)
1	25	0.6	27	7.0	3.0
2	20	0.6	28	9.4	3.75
3	15	0.6	29	10	5.0
4	10	0.6	29	10	6.25
5	5	0.6	30	10	6.25
6	2	0.6	30	10	5.5
9	0	0	24	10	10
10	0	0	24	10	10

Increase in citric acid dosage relatively enhanced the workability for the first five minutes followed by gradual drop in the flow. After 20 minutes the flow was almost half the initial value providing a short window for its application. Table 2.4 shows the workability of UHPC having BCSA cement with higher than 0.6% citric acid dosage.

Table 2.4. Rapid set replacement for citric dozes above 0.6%

Batch #	% Replacement	Citric Doze (%)	HRWR (Glenium)	Initial Flow (in.)	Five Minutes Flow (in.)	10 min. flow (in.)	15 min. flow (in.)	20 min. flow (in.)
1	15	5.0	34	NW*	NW	15	5.0	34
2	15	5.0	42	7.0	5.5	15	5.0	42
3	15	5.0	34	NW	NW	NW	NW	NW
4	15	5.0	42	7.0	5.5	NW	NW	NW
5	15	5	46	9.50	7.50	6.50	5.00	4.00
6	15	6	47	8.50	6.25	5.75	5.00	4.25
7	15	7	48	6.75	6.25	5.25	4.50	4.00

NW=Not Workable

2.3.6 Compressive Strength Test Results

Compressive Strength test on cubes indicates a lower value for the UHPC with 15% replacement during all the ages. Table 2.5 expresses the change in compressive strength of UHPC cubes with change in citric acid dosage.

Table 2.5. Compressive Strength of 2 in. x 2 in. x 2 in. cubes of UHPC with 15% BCSA

Specimen	15% repl., 5% citric acid	15% repl., 6% citric acid	15% repl., 7% citric acid	UHPC base mix
3-day strength (psi)	1820	2243	2209	11119
	2172	2350	2417	10890
	2221	2270	2269	10576
	Avg: 2070	**Avg: 2290**	**Avg:2300**	**Avg: 10860**
7-day strength (psi)	5844	4037	3053	13298
	5368	3971	3186	13788
	5343	4046	3256	11442
	Avg: 5520	**Avg:4018**	**Avg: 3160**	**Avg: 12840**
28-day strength (psi)	9252	6221	7245	13884
	7779	9449	6707	13913
	9096	8555	7069	12094
	Avg: 8710	**Avg: 9070**	**Avg: 7010**	**Avg: 13300**

The results indicate that compressive strength of UHPC with BCSA and citric acid is much lower than the base mix without BCSA, indicating that BCSA replacement have an adverse impact on both fresh and hardned UHPC properties.

2.4 Conclusions and Recommendations

The study described in this paper examined the impact of different quantities of internal curing water provided by presoaked lightweight sand on the shrinkage behavior of UHPC. The following conclusions and recommendations are based on the results of the experimental testing.

- The incorporation of LWS did not have any negative impact on the compressive strength of UHPC.

- Calorimetry test results indicate that addition of LWS had no significant effect on the heat of hydration and setting time of the mix. The final setting time was 7.1 h for both the UHPC-0 LWS and UHPC-1LWS and 7.9 h for UHPC- 2LWS and UHPC-3LWS mixes, respectively.
- Increasing internal curing water from 1 lb to 3 lb per 100 lb of total cementitious material reduced the early age and long-term shrinkage rate and magnitude.
- Between 0-2 days, the greatest shrinkage reduction was observed in UHPC-3LWS mix, which exhibited a decrease up to 8% compared to the control mix.
- The relative shrinkage between 2-50 days was 102%, 74%, and 65% of the control mix for UHPC-1LWS, UHPC-2LWS and UHPC-3LWS mixes, respectively, indicating decrease in shrinkage with increase in LWS.
- The absolute shrinkage at 50 days shows a reduction with increase in LWS amount with the UHPC-1LWS, UHPC-2LWS and UHPC-3LWS having 77%, 61% and 52% that of the control mix, respectively.
- One limitation of this study was the exclusion of steel fibers from the mixes tested. It is anticipated that all measured shrinkage would be less if fibers had been included.
- Replacing a portion of portland cement with BCSA reduced the workability and compressive strength of UHPC which may limit its practical application.
- In this study, LWS was added after the first half of the mixing water. Future studies should evaluate the effect of adding LWS after the complete addition of the mixing water.

2.5 References

1. Bentz, D. P., & Weiss, W. J. (2011). *Internal curing: A 2010 state-of-the-art review* (NISTIR 7765). National Institute of Standards and Technology. https://doi.org/10.6028/NIST.IR.7765.

2. Bremner, T. W., & Ries, J. (2009). *Stephen J. Hayde: Father of the lightweight concrete industry*. Concrete International, 31(8), 35–38.

3. Cusson, D., & Hoogeveen, T. (2008). *Internal curing of high-performance concrete with pre-soaked fine lightweight aggregate for prevention of autogenous shrinkage cracking*. *Cement and Concrete Research, 38*(6), 757–765. https://doi.org/10.1016/j.cemconres.2008.02.001

4. Floyd, R. W., Volz, J. S., Zaman, M., Dyachkova, Y., Roswurm, S., Choate, J., Looney, T., Campos, R., and Walker, C. (2024). *Development of Non-Proprietary UHPC Mix*. Report No. ABC-UTC-2016-C2-OU01, Accelerated Bridge Construction University Transportation Center, Florida International University, Miami, FL, 150 pp.

5. Ideker, J. H. (2013). *Internal Curing of High-Performance Concrete for Bridge Decks*. Research Report, Oregon Department of Transportation.

6. Justs, J., Wyrzykowski, M., Bajare, D., & Lura, P. (2015). *Internal curing by superabsorbent polymers in ultra-high performance concrete*. Cement and Concrete Research, 76, 82–90. https://doi.org/10.1016/j.cemconres.2015.05.005.

7. Liu, J., Shi, C., and Khayat, K. H. (2019). "Comparison of Shrinkage-Reducing Methodologies of UHPC." *Second International Interactive Symposium on Ultra-High Performance Concrete*, Des Moines, IA.

8. Liu, K., Long, Y., Chen, L., Ling, X., Yu, R., Shui, Z., Fei, S., Yu, W., Li, C., and Ge, K. (2022). "Mechanisms of Autogenous Shrinkage for Ultra-High Performance Concrete (UHPC) Prepared with Pre-Wet Porous Fine Aggregate (PFA)." *Journal of Building Engineering*, 54, 104622.

9. Looney, T., et al. (2019). "Development and Characterization of Ultra-High Performance Concrete with Slag Cement for Use as Bridge Joint Material." *British Journal of Civil and Architecture Engineering*, 1(2), 1–14.

10. Loukili, A., Khelidj, A., Richard, P., and Baroghel-Bouny, V. (1999). "Hydration Kinetics, Change of Relative Humidity, and Autogenous Shrinkage of Ultra-High-Strength Concrete." *Cement and Concrete Research*, 29(4), 577–584.

11. Shi, C., Wu, Z., Xiao, J., Wang, D., Huang, Z., & Fang, Z. (2015). *A review on ultra high performance concrete: Part I. Raw materials and mixture design.* Construction and Building Materials, 101*,* 741–751.

12. Shurbert-Hetzel, C., et al. (2023). "Data-Enabled Comparison of Six Prediction Models for Concrete Shrinkage and Creep." *Case Studies in Construction Materials*, 19, e02406.

13. **Snoeck, D., et al. (2014).** *Effect of high amounts of superabsorbent polymers and additional water on the workability, microstructure and strength of mortars with a water-to-cement ratio of 0.50.* Construction and Building Materials, 72, 148–157. DOI: https://doi.org/10.1016/j.conbuildmat.2014.09.012

14. Su, W., et al. (2026). "Internal Curing of Fine Coral Aggregates Incorporated in Ultrahigh-Performance Seawater Sea Sand Concrete." *Journal of Materials in Civil Engineering*, 38(4).

15. Wu, L., Farzadnia, N., Shi, C., Zhang, Z., and Wang, H. (2017). "Autogenous Shrinkage of High Performance Concrete: A Review." *Construction and Building Materials*, 149, 62–75.

16. Weiss, J. (2016). *Internal Curing for Concrete Pavements*. Tech Brief No. FHWA-HIF-16-006, Federal Highway Administration, Washington, DC.

17. Xu, F., Lin, X., & Zhou, A. (2021). *Performance of internal curing materials in high-performance concrete: A review*. Construction and Building Materials, 311, 125250. https://doi.org/10.1016/j.conbuildmat.2021.125250

18. Zhang, X., Zhao, S., Liu, Z., and Wang, F. (2019). "Autogenous Shrinkage Behavior of Ultra-High Performance Concrete." *Construction and Building Materials*, 226, 459–468.

19. Calmetrix. (2025). *Application videos for F-Cal*. https://www.calmetrix.com/application-videos-for-f-cal (accessed June 21, 2026).

Chapter 3

3. Internally Cured UHPC Overlay for Bridge Deck Application

3.1 Literature Review

3.1.1 UHPC Overlays

UHPC has attracted interest from several state Department of Transportation (DOTs) and FHWA for use in bridge deck overlays. For successful implementation, the existing substrate must be in good condition. Full deck replacement is recommended if cracks extend throughout the entire deck. Therefore, a thorough bridge deck assessment is required before overlay placement.

Assessment methods may include visual inspection or use of ground penetrating radar to identify the condition of reinforcement corrosion, determine the concrete cover and existing overlay thickness, and locate reinforcement. Core sampling may be performed to evaluate existing deck condition and chloride level, which helps in determining the suitability of UHPC application.

At the time of this writing, available UHPC performance data is less than two decades old, indicating that no data related to the long-term in-service performance of UHPC is available. Consequently, the estimate of UHPC overlay design life is largely based on laboratory testing and existing data from field applications.

UHPC is a suitable option for overlay applications for the following reasons:

- UPHC has a low permeability, which increases the freeze-thaw resistance of the bridge deck and improves the long-term durability.
- UHPC has good abrasion resistance, which minimizes surface wear and the likelihood of rutting.

- A well-designed UHPC can reduce shrinkage compared to conventional concrete, which helps mitigate shrinkage-related cracks.
- Traditional concrete overlays typically range from 2.5 in. to 6 in. in thickness, resulting in dead loads of 30 psf to 75 psf, respectively. In contrast, UHPC overlays are much thinner, generally between 1 in. to 2 in., corresponding to a significantly lower dead load of 13 psf to 26 psf. According to Garber et al., (2024), the final overlay thickness shall be not less than 1.0 in. or 1.5 times the maximum fiber length, whichever is greater, and shall provide a minimum clear cover of 0.625 in. over the reinforcement. Some states add 0.5 in. construction tolerance, increasing the nominal overlay thickness to 1.5 in. At the upper end, overlay thickness can reach several inches and be tied into the upper reinforcement mat, resulting in a significant increase in deck structural capacity. In certain applications, an extra thickness between ¼ in. and 3/8 in. is provided to remove the surface cracks and defects that may occur during construction (Garber et al., 2024).
- UHPC develops a strong bond with existing concrete substrates. Various surface preparation techniques like scarification and hydro demolition are typically used to expose aggregate and create a roughened surface finish for a better mechanical interlock. Test results indicate that the hydrodemolition technique provides superior bond strength compared to scarification (Graybeal et al., 2018). This improvement is due to the fact that mechanical surface preparation methods may induce micro-cracking in the substrate concrete, which can adversely affect the bond strength.
- UHPC overlay over UHPC substrate resulted in a higher bond strength compared to the conventional concrete substrate.

Previous studies have shown that applying a 1.25 in. to 4 in. of overlay can increase structural stiffness, reduce crack width and spacing, and enhance the load bearing capacity of the member (Haber et al., 2017). Further, UHPC can behave as a composite section if properly bonded to the substrate concrete.

Researchers at the Michigan Technological University examined applying UHPC as an overlay material considering the time dependent behavior such as shrinkage, and service level stresses. A parametric study was also carried out using two- and three-dimensional finite element model analysis to evaluate the influence of different girder spacing on UHPC overlay performance. The results indicated that increasing the thickness of UHPC overlays leads to higher shear and debonding stresses, while the tensile forces associated with crack initiation decrease (Haber et al., 2017). The cause was mainly attributed to the change in the neutral axis position. The study identifies stresses caused by shrinkage and live loading as the controlling factor in UHPC overlay design. In addition, it was concluded that UHPC overlay may not be compatible for bridge decks thicker than the 10 in. as the shift of the neutral axis can result in a high tensile stress within the UHPC layer (Haber et al., 2017).

In an experimental study by Khayat (2018), a total of 16 slabs measuring 6.56 ft x 4.92 ft x 5.9 in. were cast to evaluate the effect of surface preparation, overlay type and thickness, and fiber content on the performance of UHPC overlays placed on a conventional concrete substrate. All slabs were reinforced with two mats of No. 4 reinforcing bars spaced at 9.8 in., positioned at depths of 0.98 in. from the top surface and 2 in. from the bottom surface. After demolding at 24 h, the specimens were moist cured for 14 days and were covered with wet burlap. The specimens were dry cured for 12 months prior to overlay application. Surface preparation was performed by spraying a chemical retarder onto the surface concrete using a low-pressure sprayer. After 24 h,

the surface was washed and scrubbed with a brush to remove the weakened particles and expose the aggregate. The specimens were then left outside for 12 months before overlay placement. Instrumentations were installed to measure the strain, relative humidity and temperature between normal concrete and UHPC layers. The results indicate that using 1.0 in. thick UHPC overlay was the most cost-effective option. The results indicate that using 1.0 in. thick UHPC overlay was the most cost-effective option. Visual and microscopic examinations revealed no evidence of cracking and interfacial debonding between the slabs and overlays 200 days after casting.

In a study conducted by Starke et al., (2024), five slab specimens were subjected to three-point bending to investigate the contribution of overlay with different thicknesses, base concrete strength, and positive and negative bending moment. The experimental program included: one control slab with a total thickness of 6.25 in. made with conventional concrete of 4 ksi; two slabs with varying UHPC overlay thickness (1.5 in. and slightly more than 1.5 in.) tested under positive bending, one specimen combining UHPC with a weaker substrate concrete of 2 ksi strength, and one slab with a UHPC overlay layer slightly more than 1.5 in. tested in the negative bending. The initial flexural cracks of the control specimen were observed at a load of 4 kips at mid span. After the cracks formed, the reinforcing steel started resisting the load until yielding occurred. The specimen reached a maximum load of 21.5 kips corresponding to a midspan deflection of 1.3 in. Ultimate failure was by crushing the deck concrete at midspan region.

For the slab incorporating a UHPC overlay and tested under positive bending, cracking initially developed in the form of flexural cracks, followed by shear cracking that ultimately governed the failure. With increase in load the shear cracks extended toward the interface between UHPC and substrate leading to partial debonding. The specimen achieved an ultimate load of 29.4 kips, exceeding that of the control specimen. After debonding, the load carrying behavior was similar

to the control slab. For the specimen with slightly thicker UHPC overlay tested under the same condition, the ultimate load increased to 32.5 kips and the final failure was due to shear cracks propagating upwards and reaching the UHPC at the top. The overlay slabs had an ultimate load37% and 51% higher than the control specimen without overlay, respectively. It is notable that despite shear dominant failure, the specimens had a ductile behavior as a result of yielding of reinforcing steel (Starke et al., 2024).

For the slab constructed with a weak substrate concrete with a compressive strength of 2.7 ksi, the failure mechanism was similar to the specimens with typical concrete strength tested under positive bending. However, the ultimate load was limited to 22.9 kips with a midspan displacement of 2.6 in. In this specimen the shear cracks propagation was abrupt with rapid propagation after crack initiation.

The slab with a UHPC overlay tested under negative bending exhibited different behavior than the previously tested overlay specimens. Due to the high stiffness and tensile strength of the UHPC layer, the initial crack formed at a load of 20 kips which is much higher than the cracking load of approximately 4 kips for other slabs. The peak load was 29.8 kips at a displacement of 0.55 in., after which the load dropped to 18 kips. Beyond this point the slab behaved similarly to the control specimens.

For slabs with UHPC in compression (positive bending), an increase in compressive strength generally does not lead to a substantial increase in moment capacity. However, higher compressive strength can reduce the depth of the compression block, which increases the moment arm between compression and tensile forces and enhances the moment capacity. In these tests, the control specimen failed by concrete crushing. In contrast, for the specimens with UHPC

overlay, concrete crushing was delayed due to the high compressive strength of the UHPC which shifted the ultimate failure mode to shear failure in the substrate concrete.

The specimen with regular-strength substrate concrete was 28.2% stronger than the corresponding specimen with weaker substrate. In addition, the control slabs exhibited a similar performance to the overlayed slab with weak substrate despite noticeable differences in their compressive strength and depth (4.1 ksi and 6.28 in. for the control specimen versus 2.1 ksi and 5.73 in. for the overlay specimen with weak substrate). The difference in their ultimate load was only 6.7% which indicates that a UHPC applied over a weak substrate can achieve a similar performance to a deck made with stronger conventional concrete.

In a study by Aaleti et al., (2013), three 7.87 in (200-mm) thick, 23.6 in (0.6 m) wide, and 108.2 in. (2.75 m) long deck specimens, each with 1.5 in. (38 mm) thick UHPC overlay, were tested to failure. For all three flexure tests, the surface texture was the only variable, and the specimens were subjected to a combination of flexure and shear loading until failure. The surface texture roughness ranged from 0.08 in. (2mm) to 0.24 in. (6 mm). Based on the slant shear test, a minimum of 0.08 in. (2 mm) roughness was deemed sufficient for developing bond strength between UHPC and normal concrete surfaces under combined shear and compression loading.

All slab specimens were tested under combined flexure and shear loading. The measured compressive strength of the normal concrete substrate and the UHPC overlay were 4.6 ksi (32 MPa) and 15.5 ksi (107 MPa), respectively. Specimen reinforcement conformed to the current Iowa DOT bridge deck standards, and the overlay thickness was selected as 1.5 in. The specimens were loaded using a single concentrated point load at midspan, corresponding to a three-point bending configuration. The span length was set to 6 ft (1.83 m) to maximize the shear demand at the interface and represent the minimum girder spacing in a typical Iowa bridge.

Under service load, several hairline cracks developed directly beneath the load. All specimens ultimately failed in shear within the normal concrete region of the composite section. Interface slip was monitored using an Optotrak motion capture system, and no relative displacement was observed at the interface until the initiation of shear failure in the specimen. The shear crack in the normal concrete did not penetrate the overlay; instead, the crack deflected horizontally along the interface, leading to delamination. For specimens with deeper surface roughness, the delamination started at a higher deflection (Aaleti et al., 2013).

The following sections provide a summary of UHPC overlay field application for different bridges.

3.1.1.1 Morge Bridge

One of the earliest UHPC bridge deck overlays was constructed in 2004 in Châteauneuf Conthey, Switzerland, on a bridge spanning the Morge River (Haber et al., 2022). The system consisted of a 1.18 in. thick UHPC layer topped with an asphalt wearing surface. Inspections conducted 10 years after placement indicated that the overlay was in good condition, with chloride testing showing only 0.1 in. penetration into the UHPC overlay. Additional field investigations, including a study by Moffatt et al., (2022), reported that chloride ingress was only 0.12 in. below the surface exposed to salt water. After 13 years of exposure, reinforcement protected with 0.4 in. of UHPC cover exhibited no sign of corrosion. Complementary lab studies further demonstrated that UHPC exhibits virtually no deterioration under freeze and thaw cycles (Haber et al., 2022).

3.1.1.2 The Mud Creek Bridge

The first application of UHPC as a bridge overlay in the U.S. was completed in May 2016 on a reinforced concrete slab bridge (Laporte road bridge) in Brandon, Iowa (Graybeal et al., 2018; Haber et al., 2017). The bridge is 102 ft long and 30 ft wide and is a continuous concrete slab

bridge with two lanes and 5% superelevation (Starke et al., 2024). The bridge exhibited deterioration along the northern curbline and at each end of the expansion joints (Haber et al., 2017). The distress could be due to freeze-thaw cycles which was further worsened by possible chloride ingress which resulted in poor concrete, cover spalling, and corrosion of top mat reinforcement. To fix the problem, a UHPC overlay was proposed. It was decided that the concrete removal from the existing bridge should not pass the top mat reinforcement and the deck surface should be pre-wetted to increase the bond with the existing substrate. Due to superelevation, typical use of self-consolidating UHPC was not practical therefore, a thixotropic mix was developed by Lafarge Holcim by introducing thickening admixtures.

Before field application, researchers from Iowa State University carried out experimental programs to assess the performance of the material under practical conditions. The tests included prismatic slant shear and flexural testing of specimens prepared with different degrees of surface roughness. The slant shear test results indicate that a 0.125 in. surface roughness produced the highest bond strength between the UHPC and the conventional concrete. The flexural strength test results indicate that a surface roughness of 0.25 in. produced the highest bond strength with the failure occurring in the normal concrete (Starke et al., 2024).

Before placement of the UHPC overlay, the top 0.25 in. of the deck surface was removed and the existing deck surface was prepared using a truck-mounted diamond grinder to enhance the bond, as shown in Figure 3.1 (Starke et al., 2024; Graybeal et al., 2018). The UHPC was mixed onsite and placed directly onto the prepared surface with a loading and batching time of approximately 20 minutes (Starke et al., 2024; Graybeal et al., 2018). A 1.5 in. thick thixotropic UHPC overlay was placed and compacted over the base concrete (Starke et al., 2024). Following placement, the overlay surface was coated with wax-based curing compound and covered with a plastic sheet to

avoid moisture loss during curing (Graybeal et al., 2018). On fourth day after casting, the overlay surface was ground and grooved after the UHPC had reached a compressive strength of 12.3 ksi.

According to Haber (2017), bond pull off tests and visual observation results indicate that a good bond was achieved even where the substrate was not roughened. However, this is not a recommended practice by the author. Microstructural analysis shows a higher accumulation of the paste which contributed to an increase in the tensile strength of the interface. In addition, steel fibers were found to be largely absent in the interface region. Discontinuities at the interface, including air voids and debris, were found in the contact surface of the scarified specimens between UHPC and substrate.

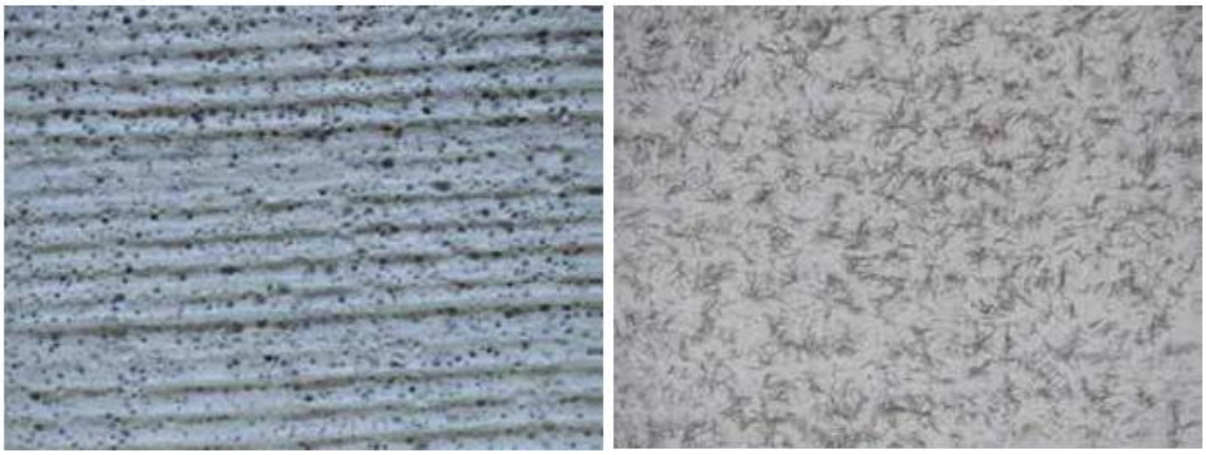


Figure 3.1: UHPC substrate prepared using (a) scarification and (b) hydrodemolition (Graybeal et al., 2018)

3.1.1.3 Bridge 7032 in Socorro, New Mexico

Located in Socorro, New Mexico, Bridge 7032 is a four span structure constructed with concrete box girders extending approximately 300 ft in length and 54 ft in width. The bridge has two

traffic lanes separated by a median. Field inspections identified full-depth transverse cracks at the negative moment region over the column bents, while no sign of delamination was observed (Starke et al., 2024.

The proposed repair was removing the existing deck, casting a high-performance deck (HPD) layer, followed by casting 1 in. thick UHPC overlay (Starke et al., 2024). Construction started with four mock-up placements over the course of one year to make the contractor familiar with the workflow.

Construction of the new deck began with removing deteriorated concrete and adding a new HPD. Surface texturing was achieved using a line rake to produce grooves with a minimum depth of 0.25 in. Following curing, the surface was treated with ceramic bead blasting and maintained in a saturated condition until the UHPC placement. During the initial placement of UHPC, early age cracking developed as a result of inadequate moisture protection due to not covering the surface with plastic sheets after surface finishing. To prevent this issue in the subsequent placements, curing compound and plastic sheeting were applied immediately after the surface was finished.

The bond between the substrate and UHPC was evaluated at ten locations suspected to have delamination using direct tension pull-off tests, hammer sounding, chain drags, and thermal imaging. The measured average bond strength was 239 psi which is slightly lower than 250 psi, the limit assigned by ACI, whereas 4 of the cores exhibited failure within the epoxy layer rather than the concrete interface (Starke et al., 2024).

3.1.1.4 Delaware Memorial Bridge

In another experimental study by Haber et al., (2022), a UHPC overlay was implemented over the Delaware Memorial Bridge (DMB), which is a long-span suspension bridge connecting

Delaware and New Jersey. This bridge's total length is 3650 ft and has a main span of 2150 ft. The first structure opened to traffic in 1951, followed by the construction of a parallel bridge in 1968. After completion of the second bridge, the first bridge with a 51 ft width was reconfigured to carry one-directional traffic. By 2019, the deck of the first bridge had reached approximately 50 years of service. Subsequent condition assessment indicated that the routine, small-scale deck patching was no longer effective in protecting the deck surface and was not a sustainable long-term solution. Analysis further suggested that complete deck replacement could be required in 5 to 15 years. In response, the Delaware River and Bay Authority (DRBA) conducted a number of life cycle cost analyses (LCCA) to identify the optimal alternative for the full deck replacement. It was determined that the DMB did not possess sufficient reserve structural capacity to accommodate the additional overlay dead load at the top of the deck. Therefore, the selected overlay strategy was implemented as a partial deck replacement. For the deck overlay application of this project, three repair materials were evaluated: Latex-modified concrete (LMC), high early strength LMC (LMC-VE), and UHPC. Ultimately, DRBA selected UHPC as a repair material and LMC was used for comparison with UHPC (Haber et al., 2022). Below is a brief description of LCM and LCM-VE presented by Haber et al., 2022.

Latex-Modified Concrete (LMC): LMC has been used in the state of Virginia for more than five decades. The addition of latex to concrete enhances flexural performance and decreases its permeability. LMC bonds well with the substrate if the surface is prepared well before placement. However, LMC applications present several challenges, including the requirement for experienced contractors, specialized equipment, and sensitivity to environmental conditions during construction

LMC-VE: LMC-VE is a variation of conventional LMC designed to rapidly gain compressive strength. The accelerated strength gain is due to the addition of rapid-setting hydraulic cement in place of ordinary Type I/II portland cement. This material has been used in Virginia since 1997. The primary advantage of LCM-VE is its ability to gain strength in a short time frame, reducing the construction duration and allowing for reopening the structure to traffic as early as 3 hours after placement. Although the initial cost of LMC-VE is higher than that of conventional LMC, the overall project cost is offset by reducing the construction time and minimizing traffic control. The primary challenge with LMC-VE is due to rapid strength development and high curing heat, which increases the risk of plastic shrinkage cracking, making moist curing essential for successful placement.

For the same research project by Haber et al., (2022), three different overlay installation strategies were evaluated, each included partial removal followed by replacement with UHPC. The deck of the first DMB structure overlayed in this project consists of upper and lower steel reinforcement mat connected by transverse reinforcement with an average concrete cover of 2.2 in.

3.1.2 Installation Strategy 1 (IS1)

IS1 would involve the removal of the top 1.75 in. of the deck concrete, leaving approximately 0.4 in. of concrete cover above the top of the reinforcement mat. This concrete would subsequently be replaced with UHPC. The detail of this configuration is illustrated in Figure 3.2.

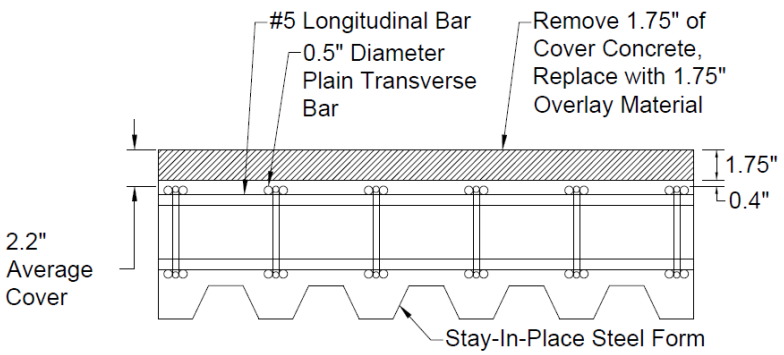


Figure 3.2: IS1 using a 1.75 in. UHPC overlay (Haber et al., 2022)

3.1.3 Installation Strategy 2 (IS2)

In IS2, the concrete would be removed to a depth of 0.5 in. below the top mat of rebar. This corresponds to a total concrete removal of 3.75 in., which would subsequently be replaced with UHPC. The primary advantage of this strategy is that the increased removal depth would facilitate the elimination of chloride-containing concrete and provide better protection for the reinforcing steel. The details are illustrated in Figure 3.3.

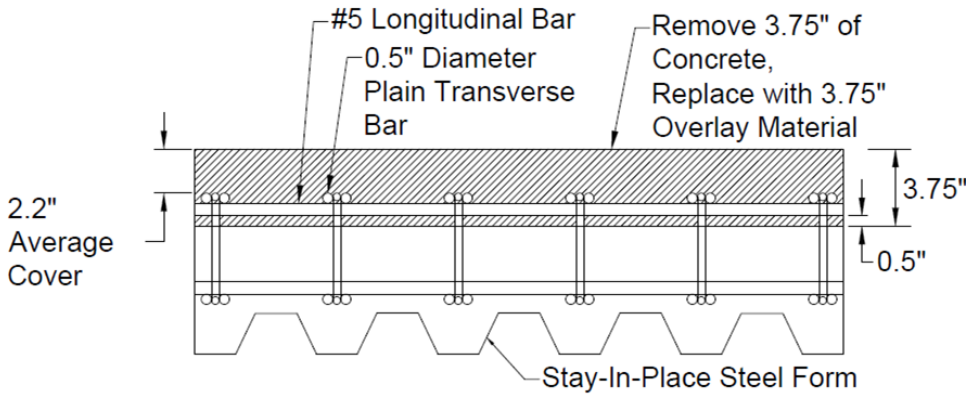


Figure 3.3: IS2 using a 3.75 in. UHPC overlay (Haber et al., 2022)

3.1.4 Installation Strategy 3 (IS3)

IS3 would include the same depth removal as IS2. However, the removal material is replaced with a composite system consisting of 2.5 in. of UHPC and 1.25 in. of asphalt topping. This approach would reduce the overall cost of the overlay. The details are illustrated in Figure 3.4.

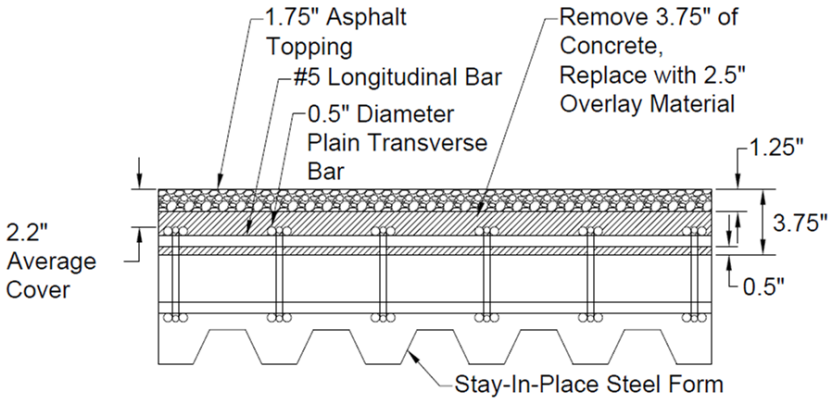


Figure 3.4: IS3 using a 2.5 in. UHPC overlay with 1.25 in. asphalt layer (Haber et al., 2022)

Payment for the UHPC overlay construction may be based on either the volume of the UHPC or the unit surface area. Because contractors may modify the construction practice to maximize monetary return, all the terms, limits, and acceptance criteria associated with both volumetric and surface area-based payment methods must be clearly defined. For example, if the payment method is based on surface area, a contractor may be incentivized to remove less concrete than specified, resulting in an insufficient UHPC overlay. However, when payment is based on volume, excessive concrete removal may occur, leading to a thicker-than-necessary overlay. Neither outcome is desirable. To avoid malpractice, the owner should require verification of removal depth through deck sampling and inspection. Additionally, the owner might consider providing a contingency volumetric estimate to account for unanticipated variation in required UHPC volume.

3.1.5 Surface Preparation

Garber et al. (2024) summarized some of the experiences of four different entities with their recent UHPC installations.

Proper surface demolition and preparation are critical in achieving adequate bond between UHPC and the substrate concrete. One commonly used surface preparation method is hydromilling, also known as hydrodemolition, which removes weak or deteriorated concrete from the substrate. However, there are several challenges with the hydrodemolition process:

- Discharge generated from hydrodemolition must be properly collected and may require a permit from environmental agencies. The resulting slurry is typically removed using pumps and tank trucks, which requires additional planning and coordination.
- The concrete beneath the upper reinforcement mat is often difficult to remove, which complicates surface preparation when the depth of the overlay extends below the top mat of reinforcement.
- Achieving a uniform substrate removal is difficult due to variation in concrete strength and substrate condition across the deck. Low-strength concrete will be removed to a higher depth if the pressure and traverse speed are not adjusted. In very weak areas, it can lead to the formation of a blow through, defined as a localized hole through the deck. Therefore, water pressure and traverse rate should be carefully adjusted to avoid non-uniform surface preparation. The use of a multi-jet head can improve demolition uniformity but may increase construction cost.

The depth of hydrodemolition is counted from the base of the mortar, not from the surface of the exposed aggregates (Garber et al., 2024). The resulting concrete roughness should be at least 0.25 in. defined as the average distance between peaks and valleys of the prepared surface

(Newtson et al., 2018). The actual roughness is usually greater than 0.25 in. when hydrodemolition is used and depends on many factors, including the coarse aggregate size. Excessive surface roughness may result in air being trapped between the UHPC overlay and the substrate. Depending on the replacement and consolidation method, the air may vent to the surface or remain confined within the overlay. Various types of air voids have been observed in the UHPC overlay. Minor voids typically do not need repair or any corrective action; however, large voids with depth of several inches, and diameter approaching ½ in. can extend to the level of the upper reinforcement mat, and typically require filling and repair (Garber et al., 2024). In some cases, such voids remain concealed until surface grinding exposes them. To minimize later disputes, the owner should specify the acceptance and rejection of the geometry of the void size. Field experiments have shown that placing a thicker overlay than designed and removing the material through grinding can reduce the occurrence of surface defects (Garber et al., 2024). In one documented case, the overlay was placed approximately 3/8 in. thicker than the specified value. The top 1/8 in. was removed by grinding. A profilograph was then used to identify the high and low points and then another ¼ in. was removed to achieve the desired profile. Based on experience of another contractor a ¼ in. overfilled UHPC overlay will enable greater removal of surface imperfections during grinding.

Conventional surface preparation is often performed using milling, which is highly preferred by contractors over hydrodemolition. However, milling may induce microcracking along the exposed substrate surface (Newtson et al., 2018)., and the thickness of this weak layer is generally thought to be ½ in. deep (Garber et al., 2024). In some projects, milling is used to remove the majority of the required depth, and hydrodemolition is used to remove the last ½ in. of the total depth. The advantage of this combined surface preparation procedure is to reduce the

amount of materials being removed using milling, limit the need for multiple passes using hydrodemolition, and produce a relatively uniform surface profile. Instead of grinding and grooving, an asphalt overlay can also be used to provide a wearing surface at the top of the overlay; however, this approach limits the visual inspection of the UHPC surface (Garber et al., 2024).

When a UHPC overlay is placed over a newly cast bridge deck, a set retarding chemical can be applied at the top of the deck surface, which delays setting concrete in a shallow zone. Once the concrete has hardened, the surface layer can be removed by washing without the need for mechanical or force-based surface preparation (Garber et al., 2024).

Concerns are sometimes raised regarding steel fibers exposed as a result of the overlay grinding. Field observations indicate that the fibers undergo corrosion, and the corrosion ceases at the surface and does not propagate inside the UHPC(Garber et al., 2024).

3.1.6 UHPC Mixing, Finishing, and Repair

UHPC constituent materials should be stored in dry conditions away from moisture. Prolonged storage of materials for four months or more may lead to material degradation that adversely affects both fresh and hardened concrete properties.

Fibers should be introduced uniformly and gradually to the mix to cause proper dispersion and prevent the formation of fiber balls. In some cases, achieving adequate fiber distribution can take up to 20 minutes following fiber addition. For field application, the concrete mixing should be adjusted such that it yields a placement rate designed to avoid any interruption that could lead to discontinuity.

The mixing procedure may need to be modified throughout the day of a placement to account for temperature variation. On hot days, a portion of the mixing water may be replaced with ice to lower the mix temperature. For large volumes of work and long placement durations, the mixer should be cleaned periodically, which should be accounted for during project planning. Conditions such as direct sunlight, low humidity, and wind can accelerate moisture loss, leading to reduced workability and increased risk of plastic shrinkage cracks. Given the lower water-cementitious materials ratio of UHPC, moisture exchange with the substrate concrete should be controlled. To limit the water absorption from the overlay, the substrate should be in a saturated surface dry condition prior to placement of UHPC. In practice, this is usually achieved by spraying water on the substrate and protecting it with a temporary covering to retain moisture. Preconditioning is performed several hours before the cast. For example, for a morning cast, it is usually done overnight. Any water remaining on the surface is removed before UHPC placement, often using a leaf blower. Formwork materials should be nonabsorbent to prevent moisture loss from the UHPC mixture. Plywood with a resin coating is particularly effective for this purpose.

Curing becomes more critical when the humidity is low, combined with sustained wind, as these conditions accelerate the moisture loss from the UHPC surface. Effective curing of UHPC requires timely protection of the freshly placed overlay. It is recommended that the curing compound be applied shortly after placement of UHPC. This can be performed a short distance behind the placement operation or a time period not exceeding 5 minutes after placement. Subsequently, plastic sheets should be used to cover the surface of the UHPC. Care should be taken so that the plastic sheet does not come into direct contact with the UHPC surface; otherwise, it will leave wrinkles at the surface, which may lead to cracks later.

Common issues involving UHPC overlay application include filling the air voids, cracking that may require epoxy injection, deficiencies related to curing, and removal and replacement of fiber balls. Minor voids can be repaired using fiber-free UHPC, also known as UHPC slurry. In cases where fiber balling occurs, the fiber ball or the affected area can be selectively removed using a grinder or hydrodemolition and subsequently repaired with new UHPC.

3.1.7 Construction Joints

Construction joints represent the localized discontinuity within UHPC overlays and are therefore more susceptible to distress than the rest of the overlay. As a result, they require careful consideration to avoid future problems. There are two common configurations of construction joints used for overlays. The first configuration, which is currently prevalent in the U.S., involves a localized increase in thickness at the joint and a portion of the initial placement extending underneath the subsequent overlay segment, as shown in Figure 3.5(a). Based on the experience of some contractors, joint placement can be difficult to construct, particularly if the UHPC needs to be placed below the top reinforcement mat. Achieving good consolidation around reinforcement can be challenging when using a thixotropic UHPC mixture. The second configuration of the joint, which has been increasingly used in Switzerland, offers improved constructability compared to the first configuration. In this method, a more flowable UHPC with a thickness greater than that of the overlay is first cast at the joint location between the adjacent casting segments, as shown in Figure 3.5(b). This second configuration joint is relatively new, and no data are available on its long-term performance; however, it is expected to offer similar performance to the first configuration.

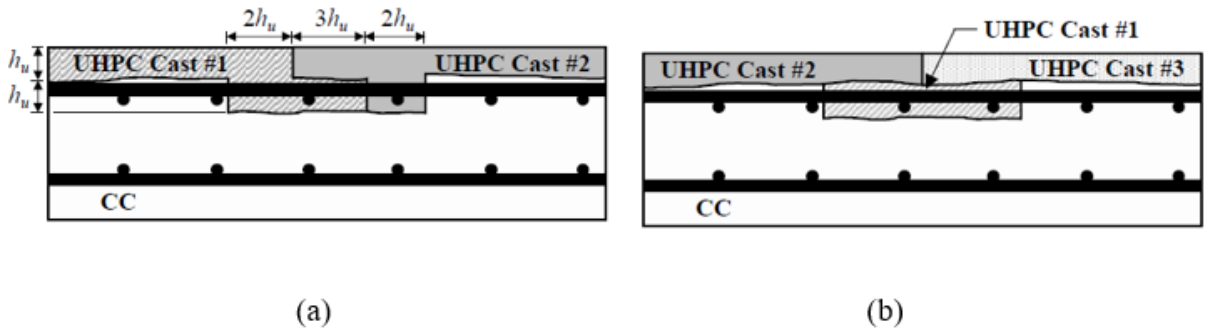


Figure 3.5: Construction joint details (a) proposed in SIA 2052 and (b) emerging detail from Switzerland (Garber et al., 2024)

3.1.8 Life-Cycle Cost Analysis (LCCA)

UHPC overlays have been shown to offer lower life-cycle costs than conventional overlay options or full deck replacement (Garber et al., 2024). UHPC will provide superior durability with reduced maintenance demand and is applicable across a wide range of environmental conditions.

There are two primary challenges with using UHPC as an overlay material. The first is the limited availability of long-term in-service performance data, and the second is the relatively high initial material cost compared with conventional overlay systems. Commercially available UHPC can cost 30 times more than the conventional concrete (Starke et al., 2024). To address the concerns related to high initial cost, LCCA is used in the research by Haber (2022) to compare cost for different bridge deck overlay alternatives. The cost analysis compared UHPC overlay with various thicknesses with alternative rehabilitation strategies, including other overlay systems and full deck replacement.

The total cost associated with the overlay includes materials, labor, hydrodemolition, and traffic control. For the DMB project discussed earlier, the unit cost of hydrodemolition was assumed to

be \$15/ $ft^{2,}$ which was based on the data from a previous project and will decrease with an increase in the surface area (Haber et al., 2022). Installation strategy IS1 was selected for the DMB project, and the cost data was compiled from the nine UHPC projects constructed between 2016 and 2020 in the states of Iowa, Delaware, New York, and New Jersey.

For comparison purposes, pilot overlay projects were also conducted using strategies IS2 and IS3, with results summarized in Table 3.1. These pilot projects were carried out on both the DMB and Commodore Barry Bridge, located south of Philadelphia International Airport. Experience from these applications indicates that removal of concrete below the top mat reinforcement presents constructability challenges, often requiring additional effort, which results in increased costs. A comparative summary of the construction cost associated with different installation strategies is provided in Table 3.1, with all estimates including material, labor, hydrodemolition, and traffic control.

Table 3.1. Estimated initial unit cost (Haber et al., 2022)

Installation Strategy	Brief Description	UHPC (Cost/ft^2)	LMC (Cost/ft^2)
IS1	1.75 in. partial depth replacement	\$55	\$23
IS2	3.75 in. partial depth replacement	\$127	\$39
IS3	2.5 in. partial depth replacement with 1.25 in. asphalt topping	\$109	Not considered for analysis

Based on this research conducted by Moffatt et al., the service life of IS1 using UHPC was estimated to be 30 years, while the service life of IS2 and IS3 was assigned 50 years and 45 years, respectively. For comparison, the service life of LMC was estimated to be approximately 12 years for IS1 and 25 years for IS2, respectively, as described in Table 3.2.

Table 3.2. Service life estimate (Haber et al., 2022)

Installation Strategy	UHPC	LMC
IS1	30 yr	12 yr
IS2	50 yr	25 yr
IS3	45 yr	_

Since the initial cost of some of the overlay materials presented in Table 3.1 were relatively comparable to each other there was a need for long-term cost analysis.

Table 3.3. Lifecycle cost comparison for overlay methods and new precast concrete deck (Haber, 2022)

Material/Deck Type	UHPC	UHPC	UHPC	LMC	LMC	New Precast Concrete Deck
Overlay installation strategy	Method 1	Method 2	Method 3	Method 1	Method 2	—
Estimated service life = L_S	30 yr	50 yr	45 yr	12 yr	25 yr	75 yr
Total initial cost = C_{TI}[c] (Yr 0 costs)	$40.3M	$80.0M	$70.0M	$22.7M	$31.5M	$171.8M
Yr 5 costs	$0	$0	$0	$0	$0	$0
Yr 10 costs	$0	$0	$1.6M[b]	$0	$0	$0
Yr 12 costs	$0	$0	$0	$141.6M[a]	$0	$0
Yr 20 costs	$0	$0	$1.4M[b]	$0	$0	$0
Yr 25 costs	$0	$0	$0	$0	$116.6M[a]	$0
Yr 30 costs	$108.3M[a]	$0	$1.2M[b]	$0	$0	$0
Yr 35 costs	$0	$0	$0	$0	$0	$0
Yr 40 costs	$0	$0	$1.0M[b]	$0	$0	$0
Yr 45 costs	$0	$0	$86.7M[a]	$0	$0	$0
Yr 50 costs	$0	$0	$0	$0	$0	$0
Total future cost (C_{TF})	$108.3M	$0	$91.9M	$141.6M	$116.6M	$0
RV	$59.8M	$0	$76.2M	$40.3M	$54.4M	$26.1M
C_{NP}	$88.7M	$80.0M	$85.8M	$124.0M	$93.7M	$145.7M

Notes:
All monetary values are expressed as present value.
—Not applicable.
[a]Estimated service life reached. Existing overlay and deck removed, new precast concrete deck with stainless steel rebar installed.
[b]Asphalt removal and replacement.
[c]C_{TI} is the sum of C_D and C_S.

Table 3.3 summarizes the LCCA results for the various overlay alternatives considered by Haber (2022). Among the options considered, IS2 offers the most cost-effective option since it does not require any additional cost over its 50 year life span. IS1 has the highest life cycle cost due to its

shorter design life of 30 years and IS3 requires asphalt overlay renewal every ten years which adds to the total cost of overlay. The new precast deck has the highest cost while the cast-in-place deck was excluded from the comparison due to its extended construction duration (Haber, 2022).

3.2 UHPC Overlay Specimen Construction and Testing

3.2.1 Specimen Design

The experimental program began with design of the test specimens. This process involved selecting the size and reinforcement of the beams to best represent a typical bridge deck in Oklahoma. The representative bridge deck cross-section shown in Figure 3.6 was selected from the Bridge Standards available on the Oklahoma State Bridge Design Standards (2009)) website.

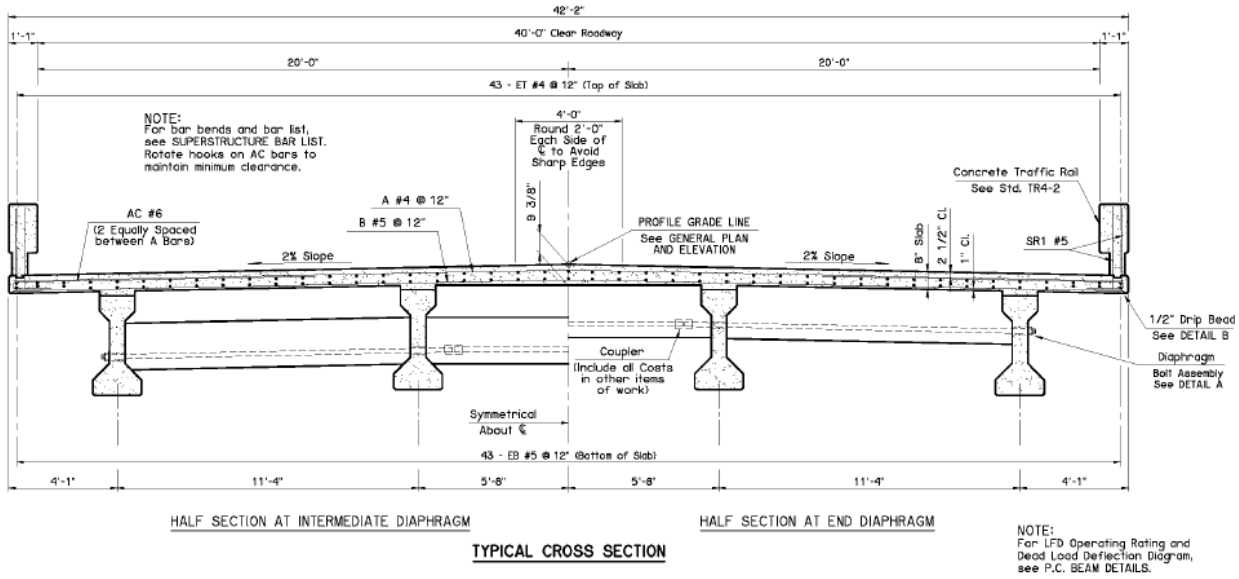


Figure 3.6: Typical cross-section for Type II, B, III, C, and IV P.C. Beams – (Oklahoma state bridge design standards, 2009)

The thickness of beam specimens used in this research was selected as 8 in., corresponding to the thickness of the bridge deck specified in the standard drawings (Figure 3.6). The beam

reinforcement was proportioned to achieve the same reinforcement ratio as the actual bridge deck. The clear concrete cover was selected as 2.5 in. at the top and 1 in. at the bottom to match the bridge deck section. One No. 3 reinforcing bar was placed at the top, and one No. 4 reinforcing bar was placed at the bottom of each beam, both provided with 90˚ hooks on each end for adequate anchorage within the short span. The specimens were cast in two sections: first the substrate followed by the UHPC overlay. The substrate portion of the specimen had dimensions of 7 in. x 8 in. x 30 in and was cast with an exposed aggregate surface. The height of the specimen (7 in.) was cast one inch less than the anticipated final depth to accommodate a 1 in. thick UHPC overlay, which would result in the 8 in. overall depth of the bridge deck. The length of the specimens was selected based on the available size of the formwork in the lab, which had a maximum length of 30 in. Calculations confirmed that the available length was adequate to provide the required development length for both compression and tension reinforcement. Figure 3.7 illustrates the 8 in. x 8 in. x 30 in. beam detailing. The length of the specimens is significantly shorter than the spacing between the girders in the actual bridge deck, which may influence the failure mechanisms of the specimens. This effect is further discussed in the results section.

To ensure adequate bond between the UHPC overlay and concrete substrate for the proposed surface preparation methods, two unreinforced trial beams with dimensions of 5.0 in. x 6.0 in. x 21.0 in. were built. The specimen depth was cast 1.0 in. less than that of a standard 6 in. x 6 in. modulus of rupture beam to allow the subsequent placement of a 1.0 in. thick UHPC overlay.

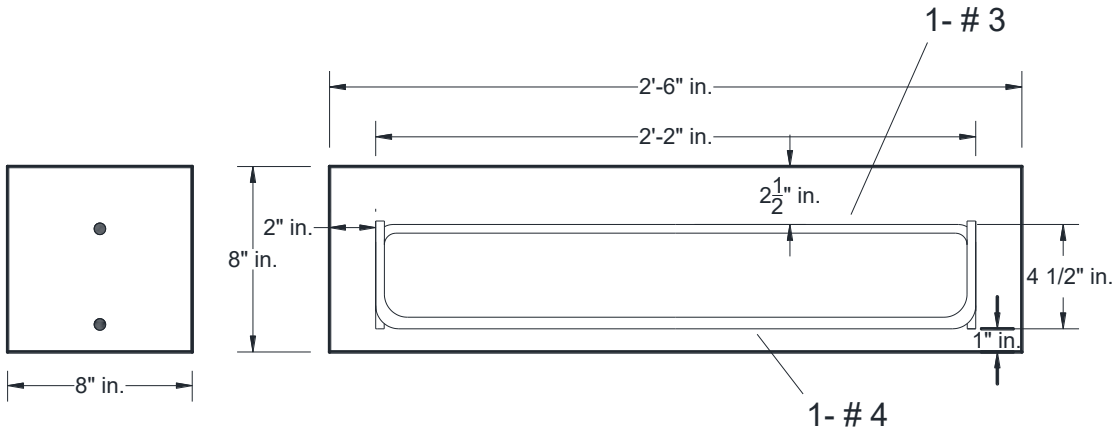


Figure 3.7: (a) Cross-sectional and (b) elevation view of 8 in. x 8 in. x 30 in. overlay specimens

3.2.2 Specimen Construction

Following the design of the specimens, construction of the overlay beams started by cutting and bending the reinforcement to the dimensions shown in Figure 3.7. The reinforcing bars were tied together, maintaining 4.5 in. vertical spacing from outside to outside of the bars (Figure 3.8). The metallic forms were then assembled, and the spacer chairs providing a 1.0 in. clear cover from the bottom were placed beneath the longitudinal reinforcement. To ensure stability and maintain the vertical alignment of the reinforcement during casting, temporary wooden spacers were placed at the sides of the forms around the rebars and were removed with the completion of casting. The reinforcement was additionally tied at the top by wires to the top board spanning across the forms, as shown in Figure 3.9.

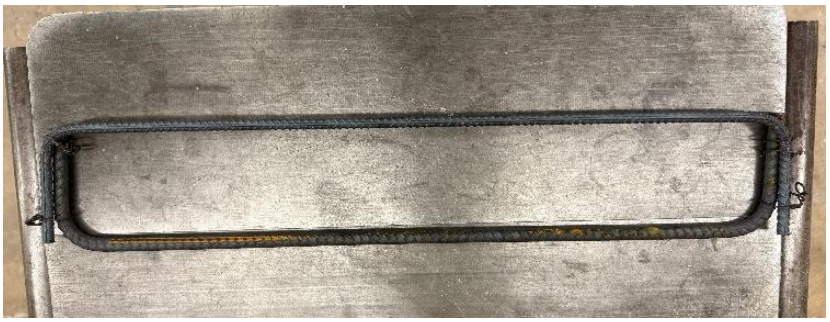


Figure 3.8: Top and bottom reinforcement prepared for placement in the beam specimens



Figure 3.9: Overlay beam formwork with the reinforcement and spacers in place

An ODOT Class AA bridge deck concrete mix was used for the substrate portion of the specimens over which UHPC overlay was applied. The class AA mix design is presented in Table 3.4 and the sequence of mixing is as follows:

1. Add the air entrainer evenly to the pre-weighed sand,
2. Dump the coarse aggregate and sand into the mixer and allow to mix for 1-2 minutes,

3. Add half of the mixing water,
4. Mix for at least two minutes,
5. Add the cement to the mixer,
6. Mix half of the high range water reducing admixture (HRWR) into the remaining half of the mixing water, and add the mixture gradually into the mix,
7. Add the remaining HRWR gradually and observe the consistency,
8. Allow to mix for at least three minutes,
9. Add additional HRWR as necessary to get the desired slump mixing at least one minute after each addition.

Table 3.4. ODOT class AA mix proportion

Material	Quantity
Cement (lb/yd^3)	588
¾ in. Crushed Limestone (lb/yd^3)	1841
Concrete Sand (lb/yd^3)	1280
Water (lb/yd^3)	223
w/cm	0.38
HRWR (oz/cwt)	6.0
Air Entraining Agent (oz/cwt)	0.9

A slump test was conducted using the procedure discussed in ASTM C143 and a representative slump is shown in Figure 3.10. In addition, the air content was measured using the procedure specified in ASTM 231 (Figure 3.11).



Figure 3.10: Representative slump test for the Class AA bridge deck concrete



Figure 3.11: Air content test

The concrete was cast in five separate batches to prepare a total of 4 unreinforced 6 in. x 6 in. trial beams and 12 reinforced 8 in. x 8 in. beams and consolidated using manual and mechanical vibration. After consolidation, the specimen's surface was finished using a trowel and was sprayed with Coca-Cola® to delay the setting of the top surface. The specimens were placed in the lab at ambient temperature and were covered with plastic sheets to avoid moisture loss. Following the final setting time of the mixture, which was found to be 7 hours using a companion calorimetry test, the top surface was washed using a water jet to remove the top layer of cement paste and expose the coarse aggregate at the top surface, as illustrated in Figure 3.12. The exposed aggregate was intended to roughen the surface and provide a mechanical interlock with the UHPC overlay once cast. The average measured peak-to-valley roughness of the prepared surface was approximately ¼ in. After three days, the concrete cylinders were demolded for the compressive strength test, and all the specimens were covered with wet burlap for a week to ensure curing of the top surface, as shown in Figure 3.13.



Figure 3.12: Washing the surface of concrete to expose aggregate following the setting time



Figure 3.13: Substrate portion of the 8 in. x 8 in. beam specimens with (a) exposed aggregate surface and (b) covered with wet burlap for curing

During the first trial, it was noted that the surface was very soft during washing at 4.5 hours after casting, which resulted to more surface disturbance due to the water pressure. The concrete setting time is essential to ensure that the concrete below the surface is set before washing. Therefore, a calorimetric test was conducted based on ASTM C1753/1753M and using a semi-adiabatic CALMETRIX P-CAL 4000 apparatus to measure the heat of hydration over time. Calorimetry is the measure of heat lost or gained during a chemical reaction, such as cement hydration. The thermal profile is plotted on a time scale from the time of adding the water to the cementitious materials. The temperature was continuously recorded in 1-minute intervals, which is according to the timer interval specified in ASTM C1753. According to ASTM C1753/1753M, this test is not intended to provide quantitative results that can be compared across different labs with different test equipment but is intended for comparison of early age hydration performance of different combinations of materials that are stored under the same conditions. In order to achieve a constant initial mix temperature, ASTM recommends the material be stored in 73.5+-3.5 F and for this reason, the materials were stored in a controlled room with a standard temperature of 68 °F before casting. All the 4 in. x 8 in. cylindrical forms used for the calorimetry test were equally filled with concrete to keep the difference in mass of the specimens below 5%. The time of cement addition was noted to the nearest minute and was inserted into the program as the starting time for hydration.

Cylinder specimens with dimensions of 4 in. x 8 in. were cast with each mix and compressive strength tests were performed at 3, 7, and 28 days to evaluate the rate of strength gain over time.

3.2.3 Casting UHPC Overlay

Once the exposed aggregate surface was prepared, the next step was to apply the UHPC overlay. For the trial 6 in. x 6 in. specimens the overlay was cast around 10 days after casting substrate,

whereas for the 8 in. x 8 in. specimens overlay was cast around 2 months after casting the substrate. To ensure a proper bond between substrate and UHPC overlay, four trial unreinforced specimens were prepared. The interface of two out of four trial beams was kept dry, and for the remaining two, the base surface was sprayed with water before pouring the UHPC to avoid absorption of water from the UHPC by the base concrete. Surface moisture was used to observe the impact of interface moisture on bond strength. The UHPC used for the overlay of trial specimens was the same J3 mix discussed in Chapter 1. The only difference between the trial UHPC J3 mix and the other UHPC used in the overlay specimens was the fibers used in the trial UHPC mix were from a different supplier, but with similar properties.

The UHPC was prepared following the J3 mixing procedure, and the amount of HRWR used for the trial mix was 20 oz/cwt. A vertical-axis rotary mixer was used for the mixing of 0.48 ft^3 of UHPC. Due to lower volume, the rotational direction of mixing blades was continuously changed to ensure the ingredients were thoroughly mixed.

For the trial mixes, the fibers used were from a different supplier but had similar properties to those used for the primary overlay specimens and no LWS was used. A flow test was conducted to evaluate the workability of the mix as shown in Figure 3.14. A total of 18 3 in. x 6 in. cylinders were cast to measure the compressive strength development over time. The UHPC used in this project was a flowable mixture and was placed without external vibration. Figure 3.15 shows the completed overlays for the trial beams.



Figure 3.14: First UHPC overlay flow test

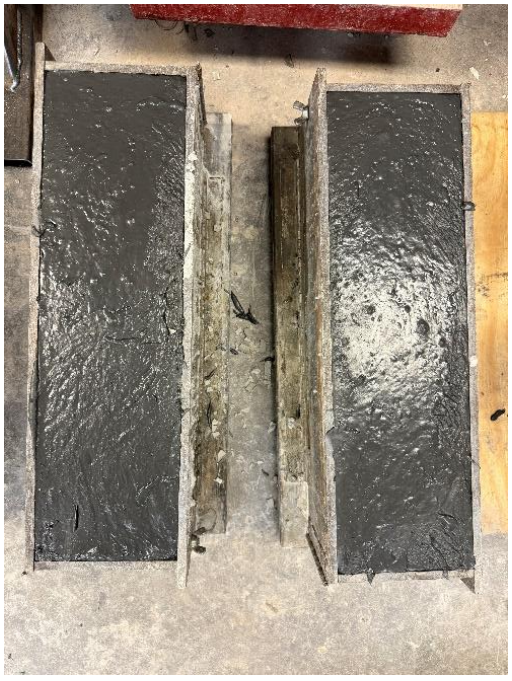


Figure 3.15: Trial beams after casting UHPC overlay

Four different UHPC overlays were tested in this research and are designated 0LWS, 1LWS, 2 LWS, and 3LWS. In these designators the number before LWS indicates the amount of lightweight sand (LWS) that supplies that amount of internal curing water per 100 pounds of total cementitious materials in UHPC. For example, 1LWS indicates 1 lb of internal curing water per 100 lb of cementitious materials. Each mix has a different shrinkage, which may impact the residual interfacial stresses between the overlay and substrate. Therefore, the surface of the substrate specimens was sprayed with water before casting the UHPC. Following mixing, the UHPC was transported to the forms using buckets for overlay casting, as shown in Figure 3.16. Flow was measured and 12 3 in. x 6 in. cylinders were cast to test the compressive strength on 3, 7, and 28 days and on the day of flexural testing. Two 8 in. x 8 in. x 30 in. beams cast entirely with Class AA bridge deck concrete, and no overlay were also tested as baseline beams for results comparison.



Figure 3.16: Casting UHPC overlay for 8 in. x 8 in. specimens

3.2.4 Testing Procedure

All the specimens were tested using a third point loading bending testing setup. The two concentric applied loads, each acting at 8 in. from supports, induced pure flexural stress at the

middle third span and a combination of shear and flexural stresses at the ends. The tests started with two sets of unreinforced 6 in. x 6 in. x 21 in. trial beams. The load was applied using a pre-calibrated load control testing machine, and the corresponding load values were recorded. The testing goal was to ensure that exposed aggregate interface roughness was adequate for developing a strong bond between UHPC and substrate concrete at the failure load, and to determine the impact of interface moisture on bond strength. Since the beams were unreinforced the deflection value for the trial specimens was not measured.

The reinforced 8 in. x 8 in. x 30 in. overlay specimens were also tested in flexure using a third point loading. Two Linear Variable Differential Transformer (LVDTs) were used to record the deflection on both sides of the beam at midspan, and their average value was used to plot the load deflection curve. A 100-kip capacity load cell was used to record the load. All the sensors were connected to a single data acquisition system, which recorded the deflection for each applied load. Due to the presence of reinforcement, the ultimate load and ductility of the members were much higher than unreinforced trial beams. To avoid stress concentration due to the uneven surface of UHPC at the contact surface between UHPC and rollers, Hydrostone gypsum cement was poured below the rollers, and a 1/8 in. thick steel plate was positioned at the top of the fresh Hydrostone to create a level surface for the rollers. Each steel plate was levelled both along the length of the beam and in the transverse direction to ensure the levelness of the Hydrostone and steel plate. Each specimen was loaded continuously to failure. The summary of test is discussed in results.

3.3 Results

3.3.1 Fresh Concrete Properties

Table 3.5 presents the slump and flow test results for the Class AA substrate concrete and the UHPC mixtures. Class AA concrete achieved the target workability and exhibited satisfactory consolidation. The targeted flow range for the J3 UHPC mix was 8 in. to 10 in., and all the UHPC mixes had flows within this expected range. The specified air content for the Class AA concrete specified by ODOT is 6.5% ± 1.5%; however, the air content values range from 3.0% to 5.2% which are below the specified value.

Table 3.5. Slump/flow and air content test results

Material	Trial AA Mix	AA-Batch #1	AA-Batch #2	UHPC-0 LWS	UHPC-1 LWS	UHPC-2 LWS	UHPC-3 LWS
Slump/Flow(in.)	7.7	7.5	7.5	9.5	9.5	10.0	10.0
Air content (%)	3.0	4.2	5.2	NA	NA	NA	NA

The compressive strength test results presented in Table 3.6 show that all Class AA concrete batches achieved consistent compressive strength values. For UHPC mixtures incorporating LWS, the compressive strength for 3 and 7 days exceeded the UHPC with no LWS; however, at the later age, the strength converged toward those of the baseline UHPC. Among the UHPC mixes containing LWS, the 2-LWS mixture exhibited the highest compressive strength.

Table 3.6. Compressive Strength Test Results for Both Class AA and UHPC

Material	Trial AA Mix	AA-Batch #1	AA-Batch #2	UHPC-0 LWS	UHPC-1 LWS	UHPC-2 LWS	UHPC-3 LWS
3-day strength (psi)	6950	5740	6518	13300	13550	13990	14000
7-day strength (psi)	7760	7500	7220	14650	16220	16540	14700
28-day strength (psi)	8560	8970	8960	19345	16250	17070	15340
Test-day strength (psi)	NA	9000	8980	20760	19610	19840	18880

3.3.2 Third Point Bending Test

3.3.2.1 Trial Overlay Beams

Two trial UHPC overlay specimens were cast over a dry interface, while the remaining two were cast with a pre-wetted interface. For each interface condition, one specimen was tested with the UHPC overlay in compression, while the other was tested with the UHPC overlay in tension. The results indicated that specimens with either the dry or wet interface exhibited comparable load capacities, with the wet interface resisting almost 2000 lb higher total applied load than those with a dry interface. In all cases, cracking initiated within the middle one-third of the span, regardless of whether UHPC was subjected to tension or compression, as shown in Figures 3.17 and 3.18.



Figure 3.17: Trial overly beam specimens with dry interface after flexural failure with (a) overlay in compression and (b) overlay in tension



Figure 3.18: Trial overly beam specimens with wet interface after flexural failure with (a) overlay in compression and (b) overlay in tension

The specimens maintained composite action throughout the test and no evidence of delamination or debonding was observed, as confirmed by visual inspection of the fractured specimens shown in Figure 3.19.



(a) (b)

Figure 3.19: (a) Broken trial beam tested in UHPC on tension side and (b) close-up of interface between substrate and UHPC overlay

3.3.2.2 Reinforced Beams with UHPC Overlay in Compression

Failure of the beams tested with the overlay placed at the top (in compression) initiated as vertical flexure cracks at midspan. With increasing load, these vertical cracks propagated upward through the section and eventually penetrated the UHPC layer, while some cracks extended horizontally along the interface. At higher load levels, diagonal shear cracks developed leading to reduction in the available development length of the tension reinforcement and in some cases bond failure, which resulted to a splitting crack at the end cross section. The minimum spacing between bridge girders are around 6 ft, which is much higher than the 24 in. span of bending test, making flexure the dominant failure behavior in bridge decks. Throughout testing, no delamination or interfacial debonding was observed between the UHPC overlay and the substrate. The load vs. deflection response shown in Figure 3.20 indicates that UHPC-1LWS specimens achieved the highest ultimate strength among all specimens, followed by the UHPC-2 LWS and UHPC-3LWS mixtures. Overall, beams with UHPC including LWS exhibited a higher

ultimate load than both specimens with no overlay and UHPC-0LWS specimens. This trend suggests that internal curing contributed to improved ultimate load capacity of the overlay beams. The observed enhancement in behavior may be partially attributed to the reduction in shrinkage strain in the UHPC overlay due to incorporation of LWS. Reduction in shrinkage strain decreases the residual shear stress at the UHPC-substrate interface which may contribute to the increased ultimate strength in compression.

For the UHPC-0LWS and UHPC-1LWS specimens, the initial deflection was not captured by the LVDTs. The reason could be due to negligible initial deflections or instrumentation limitation which did not record the data close to the end limits of the LVDT's needle stroke. Additionally, the beam with No Overlay was initially tested in a different loading configuration and the load exceeded the capacity of the load cell; therefore, the loading stopped and the specimen was considered to have failed due to the presence of existing cracks.

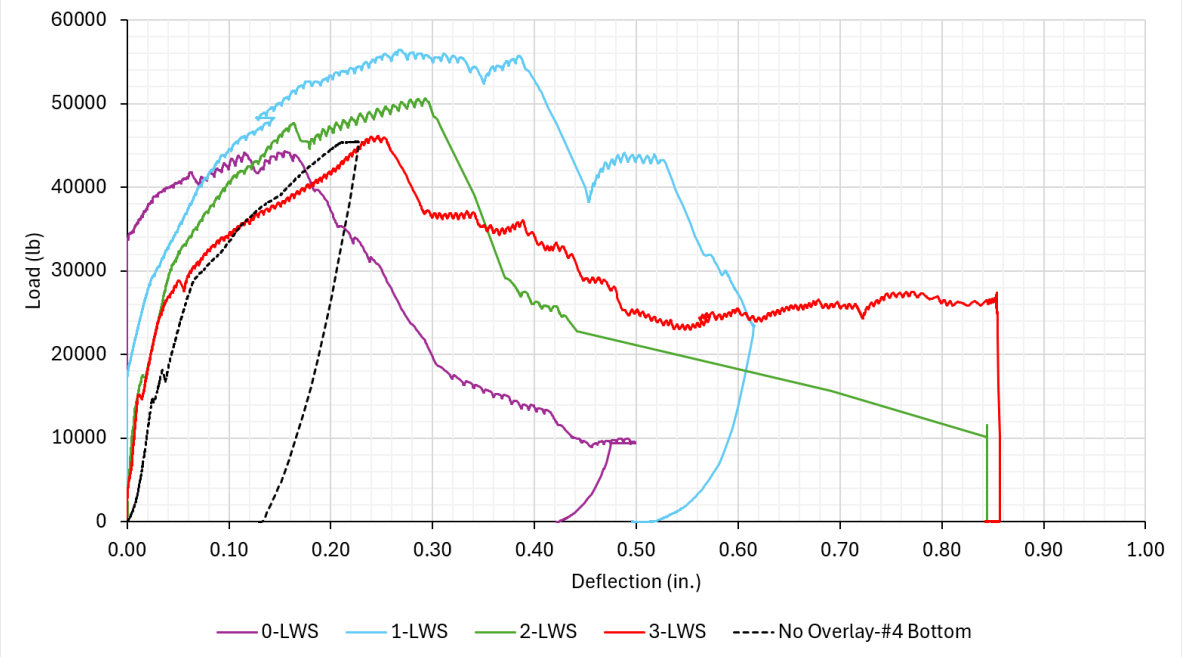


Figure 3.20: Load vs. deflection curves for specimens tested with the overlay in compression

3.3.2.3 Reinforced Beams with UHPC Overlay in Tension

For beams tested with the No. 3 bar (and overlay) at the bottom, which represents the negative moment zone of a bridge deck, cracking was mainly vertical and concentrated near midspan. This pattern led to crack localization or concentration into a single crack within the UHPC overlay. Reduction in flexural capacity from the specimens with the overlay on the compression side is primarily due to the reduced effective depth from the greater top cover and smaller area of the No 3 rebar. The No. 3 bar ruptured at ultimate load, at which point loading was stopped.

The load vs. deflection response of beams with the UHPC overlay in tension is presented in Figure 3.21. The dashed curve in Figure 3.21 shows the load response of the control beam with similar orientation and no overlay. All the specimens with overlay in tension exhibited linear behavior up to the formation of first crack after which there was a drop observed in the load-deflection curve. Onward, the response was similar to that of the control beam. All specimens including a UHPC overlay exhibited higher loads at initial cracking. This indicates that the overlay improved the cracking load of the beam specimen. The peak load for specimens UHPC-0 LWS and UHPC-1LWS are almost identical and the ultimate load decreases with increase in LWS content. Following crack localization in the UHPC overlay, all specimens exhibited behavior similar to that of the specimen with no overlay (e.g. a conventional tension controlled reinforced concrete beam) up to the final fracture of the tension bar.

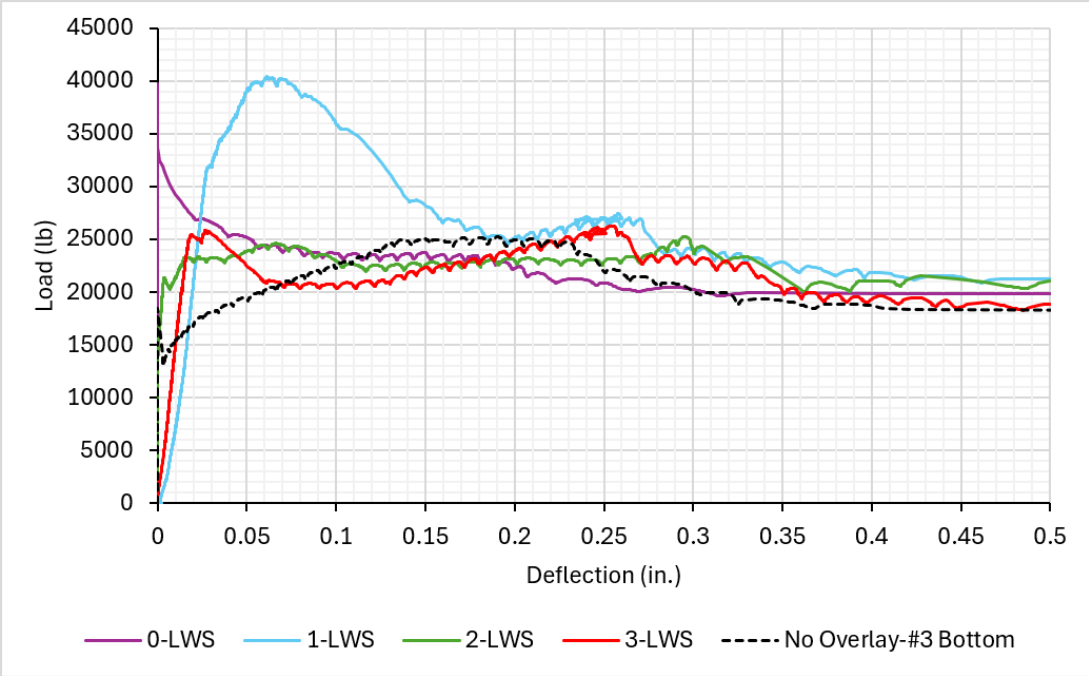


Figure 3.21: Load vs. deflection curves for Specimens tested with the overlay in tension

Pictures of the overlay specimens at failure are shown in Figures 3.22-3.25.



Figure 3.22: Failure of 8 in. x 8 in. x 30 in. No Overlay beam specimens with (a) No. 4 bar at the bottom and No. 3 bar at the top (positive moment) and (b) No. 3 bar at the bottom and No. 4 bar at the top (negative moment)



Figure 3.23: Failure of 8 in. x 8 in. x 30 in. UHPC-0LWS overlay beams with (a) overlay in compression and (b) overlay in tension



Figure 3.24: Fibers bridging the crack in the UHPC in an overlay tested in tension



Figure 3.25: Failure of 8 in. x 8 in. x 30 in. UHPC-1LWS overlay beams with (a) overlay in compression and (b) overlay in tension



Figure 3.26: Failure of 8 in. x 8 in. x 30 in. UHPC-2 LWS overlay beams with (a) overlay in compression and (b) overlay in tension



Figure 3.27: Failure of 8 in. x 8 in. x 30 in. UHPC-3 LWS overlay beams with (a) overlay in compression and (b) overlay in tension

3.3.3 Comparison of Experimental and Calculated Capacity

3.3.3.1 UHPC in Tension

The moment and shear capacities of all specimens were calculated. For specimens in which UHPC was placed on the tension side, the tensile contribution of UHPC was considered in analysis. According to (Garber, 2024; Haber 2022) the minimum effective cracking strength and localization strain in direct tension of UHPC were taken as 0.75 ksi and 0.0025, respectively, and these values were used in the flexural capacity calculations for UHPC in tension. Experimental cracking moment capacity reported in Table 3.7 is based on the initial cracking load obtained from the load deflection curve. For specimens with UHPC in tension, the compressive stress in the conventional concrete was considered to follow a triangular stress distribution and to remain within the elastic range.

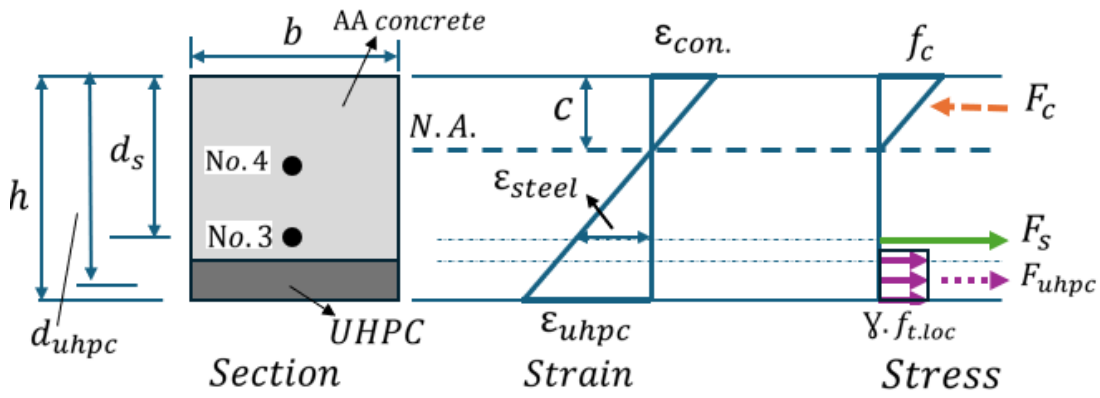


Figure 3.28: Mechanics used for UHPC overlay in Tension

The capacity calculations are based on force equilibrium among the three primary forces: compression in concrete, tension in steel reinforcement and tension in UHPC, as shown in Figure 3.28. During the analysis, the depth of the concrete compression block is iteratively adjusted until equilibrium between the resultant tension and compression forces is achieved. The compression block depth obtained from this force equilibrium is then used to calculate the flexural moment capacity. The contribution of reinforcement close to neutral axis is neglected due to its minimal influence on the overall response. In addition, the value of γ used for calculating UHPC tensile stress is assumed to be 1.0. The transverse shear capacity was calculated using ACI equation $Vc = 2\sqrt{fc'}b_w d$ (ACI 318-19); and to be conservative the compressive strength of the substrate was used in this equation.

Table 3.7. Experimental and theoretical values for beams with overlay in tension

Beam	Measured Values			Cracking Moment prediction		Shear Calculations	
	Measured P_{cr}* (kip)	M_{cr} (kip-in)	Shear capacity V_c (kip)	M_{cr} (kip-in)	Meas/Pred	Predicted V_c (kip)	Meas/Pred
No Overlay	19	79	9.5	71.38	1.06	8.02	1.18
UHPC-0 LWS	39.5	158	19.75	74.26	2.13	8.02	2.46
UHPC-1 LWS	40	160	20	75.5	2.12	8.02	2.49
UHPC-2 LWS	21	84	10.5	74.26	1.13	8.02	1.31
UHPC-3LWS	26	104	13	84.88	1.23	8.02	1.62

* Cracking load

After finding the ratio of measured-to-predicted cracking moment capacity it was observed that the ratio exceeds 2.0 for the UHPC-0 LWS and UHPC-1 LWS mixtures, indicating a substantial difference between experimental and predicted cracking moments. Initially, it was hypothesized that the difference might have resulted from error during specimen fabrication or testing. To verify the results and eliminate this possibility, an additional beam specimen was cast and tested for each of the two mixtures. Figure 3.29 presents the load vs. deflection curve obtained from the additional UHPC 0-LWS and UHPC 1 LWS beam tests.

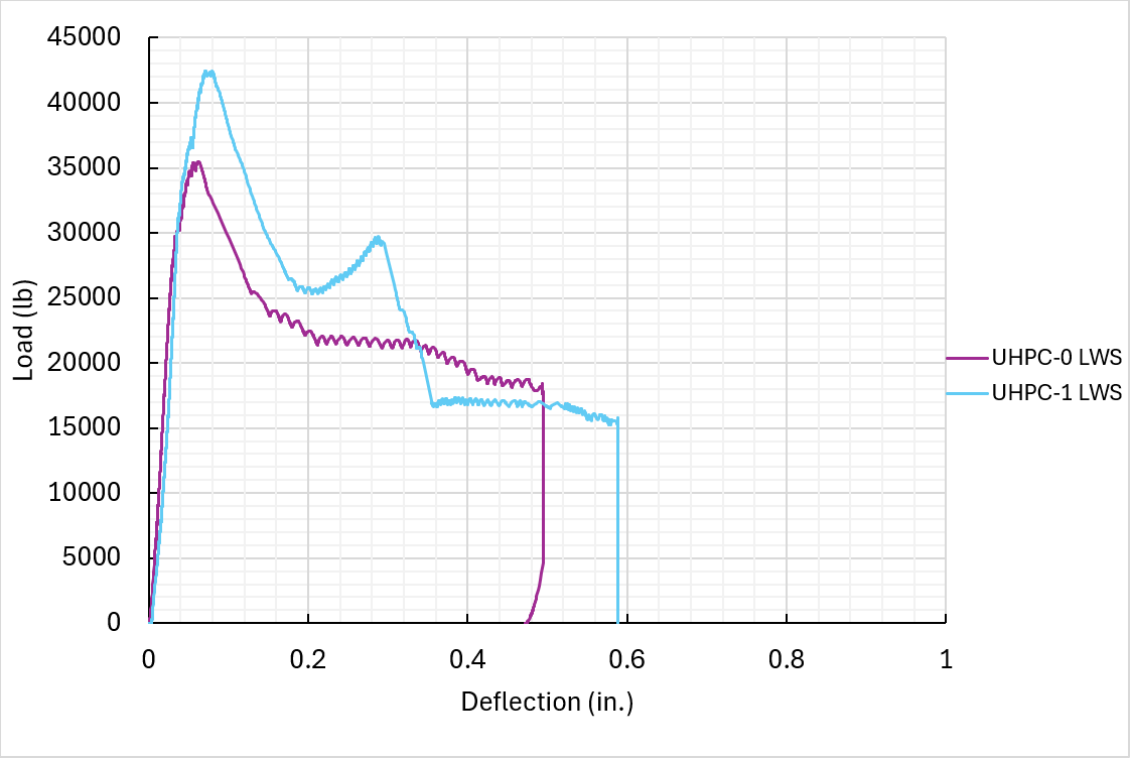


Figure 3.29: Additional load vs. deflection curves for UHPC-0 LWS and UHPC- 1 LWS specimens tested with the overlay in tension

Test results yield a cracking load of 35 kip and 42 kip for UHPC-0 LWS and UHPC-1 LWS specimens, respectively, which are in good agreement with the previously measured cracking loads of 39.5 kip and 40 kip. The consistency between the original and repeated tests confirms the reliability of the experimental results and further supports that UHPC overlays containing 0 LWS and 1 LWS enhances the flexural capacity of the overlay. The measured cracking load was approximately twice those of the corresponding specimens without overlay.

3.3.3.2 UHPC in Compression

For the specimens in which the overlay is in compression, the ultimate load obtained from the load-deflection curve was used to determine the experimental moment capacity. The analytical procedure is similar to determination of the ultimate flexural capacity for a singly reinforced

beam. The actual effective depth of the broken specimens was measured after the test and was used as the moment arm for finding the theoretical moment capacity. The depth of the neutral axis was determined by equating the tensile force in steel to the compressive force in the UHPC, and the corresponding UHPC compressive strength for each mix was used to evaluate the compression resultant.

Table 3.8. Experimental and Theoretical Values for Beams with Overlay in Compression

Beam	Measured Values			Theoretical Values			
	Measured P_{ult}* (kip)	Measured M_n (kip-in)	Measured V_c (kip)	Predicted M_n (kip-in)	Moment (Meas/Pred)	Predicted V_c (kip)	Shear (Meas/Pred)
No Overlay	46	184	23	79.80	2.31	10.18	2.26
UHPC-0 LWS	44	176	22	84.98	2.07	10.75	2.05
UHPC-1 LWS	56	224	28.	80.46	2.78	10.19	2.75
UHPC-2 LWS	51	204	25.5	80.46	2.54	10.19	2.50
UHPC-3LWS	46	184	23	80.43	2.29	10.19	2.26

* Ultimate load

3.4 Conclusions and Recommendations

This experimental study investigated the influence of a UHPC overlay with varying amounts of internal curing provided by LWS on the flexural capacity of simulated bridge deck specimens. The experimental program included design and construction of the specimens, characterization of fresh and hardened concrete properties of base concrete and UHPC mixes, and flexural testing of the overlay specimens. The test data were used to plot load vs. deflection behavior and the results for different UHPC mixes with varying amounts of LWS were compared. Based on the experimental results, the following conclusions were drawn:

- Surface preparation using Coca Cola® provided a ¼ in. amplitude exposed aggregate surface which facilitated sufficient bond between the UHPC and substrate concrete throughout the test.
- The application of all UHPC overlays enhanced the flexural capacity while maintaining composite action with the substrate.
- For beams with the UHPC overlay in compression, the failure initiated with vertical flexure cracking at midspan, followed by the development of diagonal shear cracks that resulted in sudden failure. The load-deflection curves for the specimens with the UHPC overlay in compression indicate that ultimate applied load for the overlay mixes with LWS were higher than the UHPC overlay without LWS.
- The reduction in the residual interfacial shear stress from reduced shrinkage likely contributed to increased load carrying capacity prior to failure for the UHPC-1 LWS and UHPC-2 LWS specimens with the overlay tested in compression.
- For beams with the UHPC overlay in tension, the failure started as a flexure crack at a higher load compared to the control specimen, and continued crack widening ultimately led to the rupture of the tension reinforcement. The load-deflection curves for this case show that UHPC-0 LWS and UHPC-1 LWS exhibited a similar crack localization load, however, the UHPC-2 LWS and UHPC-3 LWS had a reduced crack localization load.
- For the specimens tested with the overlay in tension, the 0-LWS and 1-LWS mixtures developed the highest cracking moment, achieving values approximately two times greater those of the control specimens without an overlay.
- For the specimens tested with overlay in compression, the UHPC-1 LWS and UHPC-2 LWS mixtures exhibited the highest cracking moment among all the mixtures evaluated.

- Performing a quantitative investigation of the interface shear behavior between substrate and UHPC overlay is recommended.
- Since the distance between girders of bridges are higher than the length of the overlay specimens, increasing the length of the composite overlay specimens can better represent the bridge deck behavior.

3.5 References

1. Aaleti, S., McDonald, N., Sritharan, S., and Abu-Hawash, A. (2013). *Enhancing durability of bridge decks using ultra-high performance concrete (UHPC)*. PCI/NBC Conference Proceedings, Precast/Prestressed Concrete Institute, Chicago, IL.
2. ASTM C143/C143M. (2020), *Standard Test Method for Slump of Hydraulic-Cement Concrete*, ASTM International, https://compass.astm.org
3. ASTM C1753/C1753M, (2022), *Standard Practice for Evaluating Early Hydration of Hydraulic Cementitious Mixtures Using Thermal Measurements*. ASTM International. https://compass.astm.org
4. ASTM C231/C231M-26*. (2026). Standard Test Method for Air Content of Freshly Mixed Concrete by the Pressure Method.* ASTM International https://compass.astm.org
5. Bridge Design Standards & Specifications. *State Bridge Design Standards - 2009 - English - LRFD. (n.d.).* https://www.odot.org/bridge/2009-sb/brd_std_2009-lrfd-sb-index.php
6. Garber, D., Helou, R., Graybeal, B., and Ocel, J. (2024). *Experiences from Early Implementations of UHPC Overlays.* Federal Highway Administration (FHWA), FHWA-RC-24-0008, Washington, DC.-U.S.
7. Graybeal, B. A., and B. Stone. 2012. "*Compression Response of a Rapid-Strengthening Ultra-High Performance Concrete Formulation*." FHWA-HRT-12-065. Washington, DC: Federal Highway Administration.
8. Graybeal, B. A., Haber, Z. B., Munoz, J. F., and De la Varga, I. (2018). *Ultra-High Performance Concrete for Bridge Deck Overlays.* TechNote, Report No. FHWA HRT-17-097, Federal Highway Administration, U.S.

9. Haber, Z. B., Foden, A., McDonagh, M., Ocel, J., Zmetra, K., and Graybeal, B. (2022). *Design and Construction of UHPC-Based Bridge Preservation and Repair Solutions.* Report No. FHWA-HRT-22-065, Federal Highway Administration, U.S.

10. Haber, Z. B., McDonagh, M., Foden, A., and Sadasivam, S. (2022). *Ultra-High Performance Concrete (UHPC) Overlays: An Example of Lifecycle Cost Analysis.* TechNote, Report No. FHWA-HRT-23-012, Federal Highway Administration, U.S.

11. Haber, Z.B, Munoz, J. F, Graybeal, B.J. (2017). *Field Testing of an Ultra-High Performance Concrete Overlay*. Report No. FHWA-HRT-17-096. Federal Highway Administration, U.S.

12. Khayat, K. H, Valipour, M. (2018). *Design and Performance of Cost-Effective Ultra High-Performance Concrete for Bridge Deck Overlay*. Report No. cmr 18-006, Missouri Department of Transportation. U.S.

13. Newtson, C. M., Weldon, B. D., Al-Basha, A. J., Manning, M. P., Toledo, W. K., & Davila, L. D. (2018). Bridge Deck Overlays Using Ultra-High Performance Concrete. Project No. 17CNMS01, Final Research Report, Transportation Consortium of South-Central States (Tran-SET), Louisiana State University, U.S.

14. Moffatt, E. G., M. D. A. Thomas, A. Fahim, and R. D. Moser. 2020. "*Performance of Ultra- High-Performance Concrete in Harsh Marine Environment for 21 Years*." American Concrete Institute Materials Journal 117, no. 5: 105-112.

15. Starke, J., Matteson, K., and Berry, M. (2024). *Exploration of UHPC Applications For Montana Bridges*. Report No. FHWA/MT-24-002/10000-844. Montana Department of Transportation, Canada.

16. Garber, D., El-Helou, R., & Graybeal, B. (2024). *Structural Design with UHPC Workshop Manual* (Report No. FHWA-RC-24-0006). Federal Highway Administration, U.S. Department of Transportation.

Chapter 4

4. Shrinkage and Creep Behavior of CSA Cement Concrete Incorporating Internal Curing

4.1 Literature Review

4.1.1 Calcium Sulfoaluminate (CSA) Cement

CSA cement was first introduced around 1960 (Thomas et al., 2018) following work by Alexander Klein at the University of California-Berkeley (Bescher, 2024) and has been in use in U.S. for more than 30 years (Besher, 2019). CSA cement comes in different types: as an additive to portland cement, as a single-component cement, or as a shrinkage compensating cement. CSA cement exhibits rapid setting, enhanced early age strength, and reduced shrinkage compared to conventional portland cement. Furthermore, CSA cement production involves lower calcination temperatures and reduced clinker content, leading to significant reduction in carbon emissions (Akerele et al., 2025).

The chemical composition of the CSA differs from that of portland cement. In portland cement, the oxide compositions are mainly calcium oxide (CaO) and silica (SiO_2) whereas for the CSA cements the main oxide is alumina (Al_2O_3), as illustrated in Figure 4.1

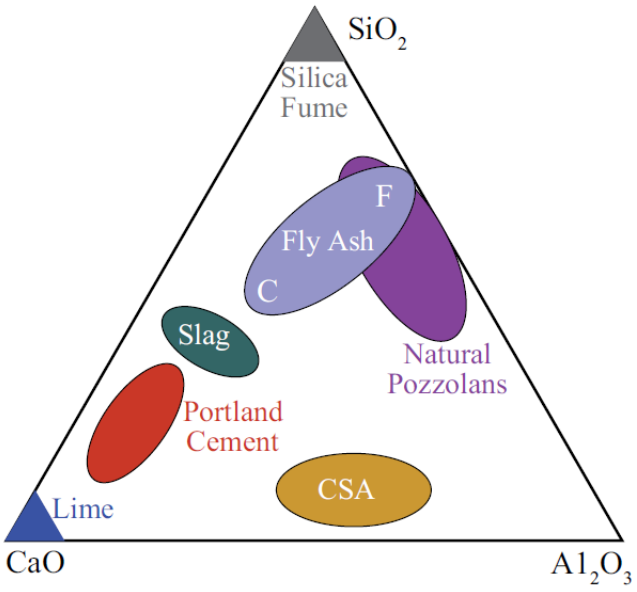


Figure 4.1: Oxide composition of CSA and other common cementitious materials (% by mass)

The main constituents of the CSA clinker are ye'elimite ($C_4A_3\overline{S}$), along with other phases such as belite (C_2S), ferrite (C_4AF), mayenite ($C_{12}A_7$) and anhydrite, depending on the raw material used (Glasser, 2001). To control setting time, strength, and volume stability, CSA clinkers are typically combined with about 20% calcium sulfate by mass, resulting in a system composed of two primary constituents. The amount of calcium sulfate also affects the water-cementitious material (w/c) ratio required for the hydration of the CSA cement. Portland cement requires a w/c near 0.42 to complete its hydration, however, this ratio is as high as 0.78 for the CSA cement which is also affected by the addition of belite and other phases in the cement (Thomas et al., 2018; Sirtoli et al., (2018)). Eqs 4.1 and 4.2 highlight the hydration of the CSA cement and the formation of ettringite crystals (Bescher et al., 2018):

$$C_4A_3S+8CS+6C+96H \rightarrow 3C_6AS_3H_{32} \qquad (4.1)$$

$$C_4A_3S+2CS+38H \rightarrow C_6AS_3H_{32}+2AH_3 \qquad (4.2)$$

The main hydration product of CSA cement is ettringite (AFt) ($C_6AS_3H_{32}$) needles, formed through the interaction of ye'elimite, lime, and sulfates (Sirtoli et al., 2018). The amount of the ettringite formed depends on the sulfate content of the cement controlled by the added amount of calcium sulfate during cement production (Thomas et al., 2018). An alternative to the pure CSA cement is using a blend of the system having both CSA and portland cement. In such a system, early-age hydration is governed by the CSA cement, while portland cement contributes primarily at later ages (Pelletier et al., 2010).

The initial setting time of CSA cement can be as fast as 10 minutes for lower w/c ratios. Similar to portland cement, setting time can be extended by increasing the w/c or decreasing the temperature. Retarding agents like citric acid can be used to increase the setting time, but setting time beyond 1 hour is hard to achieve. CSA cement mixtures can gain 50% of their strength within a few hours and 90% of their ultimate strength within 3 days (Thomas et al., 2018).

Concrete mixtures with CSA cement typically have desirable mechanical properties like high early strength, low shrinkage, and excellent durability. Besides high early compressive strength, CSA cement is also used as a shrinkage-compensating cement for two reasons. First, less excess water will remain in the concrete after hydration, therefore, the drying shrinkage is low. Second, the rate of gain of tensile strength in the CSA cement is faster than the rate of developing tensile stress that causes shrinkage cracks, which reduces formation of shrinkage cracks (Tanksley, 2018).

Similar to portland cement which is divided into five types, CSA cement is also divided into different categories by Bescher et al. (2018) based on the amount of each phase included in its composition. The main components in CSA cement are CSA, belite (C_2S), and calcium sulfate. Depending on the ratio of components, CSA cement can be rapid setting, shrinkage-

compensating, self-stressing, or a combination of the above (Bescher et al., 2018). Table 4.1 shows the classification of the CSA cement by Bescher et al. (2018).

Table 4.1. Types of CSA binders (Bescher et al., 2018)

	Calcium Sulfoaluminate	Dicalcium Silicate	Calcium Sulfate	Other
Type A - Accelerating Additive	35 - 45%	0 - 20%	10 - 30%	5 - 55%
Type B - Belitic Calcium Sulfoaluminate Cement	20 - 30%	40 - 60%	5 - 25%	0 - 35%
Type C - Expansive Additive	10 - 20%	10 - 30%	40 - 60%	0 - 40%
Type K - Shrinkage Compensating Cement	1 - 10%	30 - 50%	1 - 20%	20 - 70%

Different binders result different microstructures in the hardened paste. For instance, the portland cement (PC) system results in mainly calcium-silicate hydrate (C-S-H), whose creep and shrinkage behavior are mainly dependent on internal RH. On the other hand, the main hydration product of CSA cement is ettringite, whose porosity is radically different from the C-S-H. Ettringite is dimensionally stable and less sensitive to RH. Therefore, the creep and shrinkage behavior of CSA cement concrete is different than the PC concrete (Sirtoli et al., 2018).

Type K cement is a shrinkage-compensating CSA cement that replaces a portion of portland cement in the concrete mix design. Type K cement is a blend of portland cement, CSA, calcium sulfate, and lime (Thomas et al., 2018). Type K is typically used for its shrinkage compensating purposes which helps minimize drying shrinkage cracking by offsetting the anticipated shrinkage. The quick formation of ettringite crystals causes expansion which counteracts the tension produced by shrinkage of the portland cement concrete in a restrained condition (Tanksley, 2018). The hydration of CSA cement in Type K also prevents water bleeding by binding the water molecules with the ettringite crystals. The expansion of the shrinkage

compensating concrete should not exceed 0.1% at 7 days or 0.15% for 28 days. These limits are selected to avoid changing the reinforcement or joint details if existing concrete is replaced with Type K cement concrete (Rice, 2012).

Production of CSA cement results in 30% less carbon emissions than portland cement, potentially making it a more environmentally friendly choice (Bescher et al., 2018).

In 1970 a large research project was conducted in China on Belitic CSA (BCSA) cement to advance understanding of this class of binders which led to the standardization of cement and concrete mixes incorporating CSA cement (Sirtoli et al., 2018).

An important property of concrete is its creep and shrinkage behavior which is influenced by the cement type. These time-dependent deformations play important roles in long-term performance of structures by affecting member shortening, deflection, camber development in prestressed elements, stress redistribution, and the initiation and propagation of cracking.

The creep and shrinkage behavior of CSA cement concrete was investigated by Sirtoli et al., (2018). In this comparative study, the performance of pure CSA cement was evaluated against portland limestone cement (CPC) as well as a 50/50 ratio blend of CSA and portland cement labelled as CMIX. Specimens were tested in two conditions: sealed condition which represents the state of the structure before demolding and was used to measure autogenous shrinkage and exposed condition which was used to measure the drying shrinkage observed after demolding. Sealed conditions were maintained by completely covering the specimens with adhesive aluminum tape to avoid moisture loss. Volume change under both loaded and unloaded conditions (creep and shrinkage) was measured for autogenous and drying conditions until 364 days. The specimens were 120 mm x 120 mm x 360 mm prisms cast in stainless steel molds and

covered with plastic sheets after casting. The specimens were stored on the first day after casting in a climatic room of 20± 0.5 ˚C and RH>95%. The samples were demolded after 24 h and the test started. Duplicate creep specimens were placed in the creep loading setup, where the same load was applied to all vertically stacked specimens. For this research, three sequential loadings were applied at specimen ages of 1, 7, and 28 days. At each loading age, the sustained load was increased so that the total applied load on the specimen equaled one-third of the compressive strength corresponding to that age. The strain results were expressed by subtracting the strain due to instantaneous deformation and shrinkage strains from a companion specimen from the total measured strain of the creep specimens.

The results indicated that the autogenous shrinkage measured from the sealed specimens was similar across all three cement concretes at the end of 1 year. In contrast, drying shrinkage was highest and most rapid for CPC compared to the CSA and CMIX cements (Sirtoli et al., 2018). CMIX displayed a distinct shrinkage pattern compared to the pure CSA and CPC mixes. Following an initial shrinkage of 7 days, the sealed CMIX specimens exhibited expansion, which was followed by shrinkage. Notably, for the CMIX mixture only, the autogenous shrinkage (the shrinkage under sealed condition) exceeds the corresponding drying shrinkage (shrinkage of the exposed specimens). The expansion of the CMIX under sealed condition could be due to a two-phase hydration process. Early hydration is dominated by CSA, which reacts suddenly and shows minimal reactivity of CSA after the first week. In contrast, portland cement hydration is slower and typically begins to dominate 3 to 4 weeks after water addition. Because PC hydration starts after setting the CSA matrix has already hardened, which could be a possible reason for the expansion observed between 7 to 28 days. However, when specimens are exposed to early-age drying, a large amount of moisture is lost which limits further PC hydration, as its autogenous

behavior requires RH value above approximately 70-80%, resulting in minimal continued reaction (Sirtoli et al., 2018). Overall, the results indicate that the total shrinkage was lower for the CSA and CMIX mixes compared to the CPC mix, particularly under drying conditions.

The creep under sealed conditions was marginally lower for CPC than for CSA. The higher early-age strength of CSA cement concreted resulted in a higher applied stress, resulting in a higher specific creep value compared to the CPC mix. The data also indicated that CMIX showed a higher creep for the sealed conditions compared to drying conditions which was similar to its observed shrinkage behavior.

Microindentation studies have shown that C-S-H, the primary hydration product of portland cement, exhibits a greater creep rate than any other tested hydration products including ettringite. Nevertheless, ettringite has also demonstrates microindentation creep. Although low creep of CSA at early age can be advantageous, it may limit stress relaxation and increase the likelihood of cracking due to restrain-induced stresses.

This study by Sirtoli et al., (2018) also examined two predictive models. Model Code 2010 distinguished between early age and long-term behavior for both creep and shrinkage and breaks it down to autogenous and drying stages. However, ACI 209.R-92 does not differentiate between early age and long term shrinkage and creep. It rather uses a single formulation to represent the overall deformation. For the CSA mixes, the experimental results deviated significantly from both predictive models. The discrepancy is believed to be in inability of the models in capturing the early age shrinkage of the CSA cement. It is believed that incorporating parameters to address the early age rapid and intense self-desiccation could improve the predictability of the models.

The research concluded that creep and shrinkage of CSA cement concrete were lower than those of portland cement concrete. Both shrinkage and creep were higher under sealed condition than the drying condition which may be attributed to continuous hydration of the sealed specimen due to higher degree of saturation. Considering the fact that the difference between autogenous and drying shrinkage of CSA cement is minimal and because of their low drying shrinkage, it is advantageous to use CSA cement concrete for situations where shrinkage is a concern.

In a different study by Akerele et al. (2025), effectiveness of rapid setting CSA was studied in pavement applications and was compared with Type III portland cement. Type III portland cement, which is characterized by its rapid strength gain, has been used historically for pavement applications. However, the limitations with type III cement are extended curing time, high shrinkage, and high cement content- often exceeding 700 lb per cubic yard- which contributes to a higher environmental impact due to its high carbon footprint. These drawbacks highlight the need for alternative material with faster strength gain and improved sustainability.

Test results of the study by Akerele et al., (2025), indicate that CSA cement with optimized w/cm below 0.40 exhibits reduced shrinkage, minimizing the possibility of cracks. The conclusion comes following test results using the ASTM C157 procedure in which two different specimens of CSA mixtures were compared with Type III cement specimens. The two CSA mixtures exhibited minimal shrinkage values of (-0.0127%) and -0.0053%) at 4 days; both of which were significantly lower than that of traditional Type III mix (-0.018%). At 28 days, the shrinkage values of the CSA mixes were -0.024% and 0.0183% which remained lower than the corresponding value for the Type III mixture (-0.054%). The results also indicate that CSA cement concrete mixes with lower shrinkage demonstrated higher flexural resistance. Conversely, the flexural capacity was lower for Type III cement concrete mixture with a higher

shrinkage value. Therefore, the combination of low shrinkage and high flexural strength of the CSA cement concrete makes CSA cement an ideal material for pavement applications, particularly in minimizing the risk of cracking.

4.1.2 Internal Curing

4.1.2.1 Introduction

In addition to the mechanical loading, thermal deformation and shrinkage of the concrete can cause structural members to crack if restrained. Shrinkage produces tensile stress in the concrete causing shrinkage cracks which is a main reason for a reduction in the service life of the structure. While cracking may not cause a reduction in the load-bearing capacity of the member, it compromises the longevity of exposed structures through increasing susceptibility to freeze and thaw cycles. Penetration of chloride ions through cracks also results in corrosion of the reinforcement and subsequent spalling of the concrete. Concrete cracking is affected by more than just tensile stress due to shrinkage. Other factors like restraint degree, shrinkage rate, fineness of cement, type of cement, aggregate, incorporation of fibers, water-cement ratio, admixtures, curing, stress relaxation, and elastic modulus can also contribute to early-age shrinkage and cracking in concrete (Wu et al., 2017).

There are different types of shrinkage that occur in concrete including autogenous shrinkage (internal desiccation), chemical shrinkage, drying shrinkage (loss of moisture to the environment), and thermally induced shrinkage. The primary types of shrinkage are early-age (autogenous and chemical) and long-term (drying) shrinkage which contribute to most of the shrinkage-related cracks. Autogenous shrinkage, which is an early age shrinkage also known as self-desiccation, happens when the internal relative humidity (IRH) of the paste decreases due to cement hydration. While autogenous shrinkage is not well understood, it is generally believed

that this type of shrinkage is related to the change in relative humidity of the capillary pores in cement paste. The Japanese Concrete Institute defines autogenous shrinkage as the macroscopic volume reduction of cementitious materials when cement hydrates after the initial setting (Ghanem et al., 2024; Wu et al., 2017). For typical formulations of portland cement concrete, early-age shrinkage is much lower than drying shrinkage. However, for high-performance concrete (HPC) and UHPC formulations having high cementitious materials contents and silica fume as supplementary cementitious material, early-age shrinkage can cause micro or macro cracks in the concrete. Water demand for hydration of silica fume is more than the portland cement which results in a higher amount of chemical shrinkage.

The volume of the water and cementitious materials before mixing is more than their volume after the hydration reaction, which results in chemical shrinkage. This indicates that some water is lost due to hydration resulting in chemical shrinkage. In addition, chemical shrinkage shows how much water per unit of cementitious material is required to complete 100% hydration. For instance, the chemical shrinkage of portland cement is 0.07 which means 7% mass of water per mass of the portland cement is needed to complete the hydration; however, this number is 0.22, 0.18, and 0.10 for silica fume, slag, and fly ash, respectively (Ideker et al., 2013). This indicates that compared to portland cement more water is required to complete the hydration for the mentioned supplementary cementitious materials. For internally cured concrete, a portion of the water is added by the coarse lightweight aggregate (LWA), fine lightweight aggregate (FLWA), or super absorbent polymer (SAP).

Drying shrinkage happens when the internal relative humidity (IRH) of the environment is lower than the hardened paste and water loss continues until the IRH of the paste is equivalent to that of the environment (Wu et al., 2017). Although drying shrinkage in CSA is generally not

significant, rapid autogenous shrinkage can take place at early ages which can be mitigated by internal curing. By slowing the onset of self-desiccation by internal curing, additional time is provided for stress relaxation, resulting in reduced microscopic cracks. Different types of shrinkage act simultaneously on the concrete which means it is necessary to perform an early-age shrinkage test along with the drying shrinkage test to determine the magnitude of each type independently and fully understand the shrinkage behavior of the material.

To reduce cracks due to shrinkage, the water in the cement paste consumed due to cement hydration or lost to the environment due to evaporation must be replenished. There are two ways to supply water to concrete: external curing and internal curing. External curing is the process of supplying water to the surface of the concrete from an external source and is the typical way concrete is cured. Examples of external curing include water curing, steam curing, and membrane curing. For high-strength concrete with a low water-to-binder (w/b) ratio like UHPC, the permeability of the concrete surface decreases and external curing water cannot penetrate the surface. For such a scenario there is a need to provide water through some internal source. According to ACI, internal curing is defined as "supplying water throughout a freshly placed cementitious mixture using reservoirs, via pre-wetted lightweight aggregates, that readily release water as needed for the hydration or to replace moisture lost through evaporation or self-desiccation" (Ideker et al., 2013). The water intended for internal curing disperses inside the concrete after it hardens and contributes to the hydration process. The materials used for internal curing can be divided into two main types: materials containing physically absorbed water (e.g., SAP) and porous materials (e.g., LWA). The water from LWA is sucked from the reservoirs by the cement paste during curing due to capillary pressure and is transported to the surrounding concrete. Hence there is more hydration in the cement surrounding the LWA in the interfacial

transition zone (ITZ) which creates a stronger bond between the cement and LWA. The advantages of internal curing are increased hydration, improved strength development, reduced early-age shrinkage and cracking risk, low permeability, high durability, and reduced water requirements for external curing. Figure 4.2 shows a schematic comparative model of internal and external curing. Internal curing is especially beneficial to mixtures containing a high volume of supplementary cementitious materials like silica fume, fly ash, and slag due to a higher water demand compared to the portland cement.

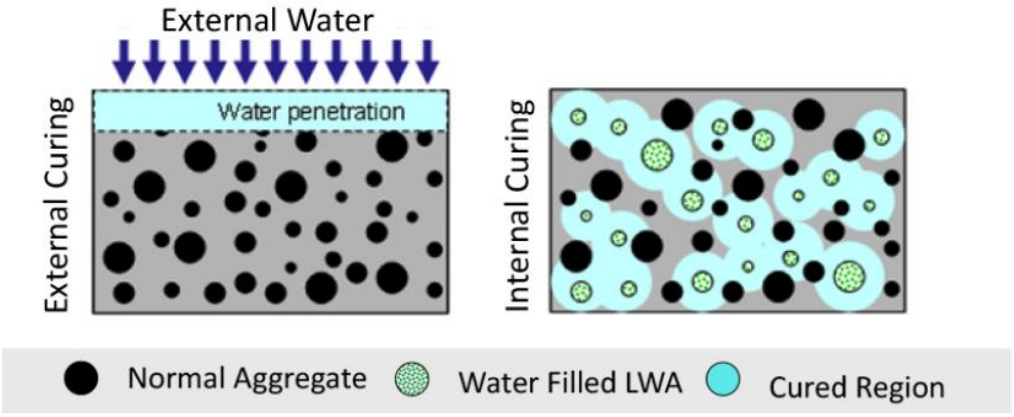


Figure 4.2: Schematic Model of External vs. Internal Curing (Weiss, 2016)

4.1.2.2 Internal Curing Water Requirement

North America typically uses LWA for internal curing of concrete (Weiss, 2016). It is mainly because of its availability and approval by most of the highway agencies and cost efficiency. Using LWA for internal curing of concrete has increased since 2000 (Ideker et al., 2013). The water in the lightweight aggregate leaves the pores of the lightweight aggregate as the negative pressure in the pore fluid develops with the setting of paste and increases thereafter. Eq 4.3 can be used to find the quantity of LWA in a mix required for providing internal curing (ASTM C1761, 2023; Bentz et al., 2005; Ideker et al., 2013).

$$M_{LWA} = \frac{C_f \, x \, CS \, x \, \alpha_{max}}{S \, x \, \phi_{LWA}} \qquad (4.3)$$

Where:

M_{LWA} = mass of (oven-dry) LWA needed per unit volume of concrete (kg/m^3 or lb/yd^3);

C_f = cementitious materials content for the concrete mixture (kg/m^3 or lb/yd^3);

CS = chemical shrinkage of cementitious materials at complete 100% hydration (kg of water/kg of cement or lb/lb);

α_{max} = maximum expected degree of hydration of cementitious materials (0 to 1.0);

S = degree of saturation of pre-wetted aggregate relative to the wetted surface dry condition (0 to 1). Note: Eq 4.3 is only valid for non-zero values of S, otherwise the amount of LWA diverges to infinity.); and

ϕ_{LWA} = Mass of water released by lightweight aggregate in going from the wetted surface dry condition to the equilibrium mass at the relative humidity of 94%, expressed as a fraction of the oven-dry mass (kg water/kg dry LWA or lb/lb).

In Eq 4.3, for a w/c ratio less than 0.36, the maximum expected degree of hydration can be taken as 0.36. If the w/c ratio of a mix exceeds 0.36 then the maximum expected degree of hydration can be conservatively taken as 1.0 (Bentz et al., 2005).

Eq 4.3 can be used to find the amount of LWA required for supplying a fixed amount of water into the concrete. The numerator of Eq 4.3 shows the water demand to fill the empty capillary pores in the paste resulting from the chemical shrinkage. The denominator shows the released amount of water per unit mass of the LWA in the oven-dry condition. Eq 4.3 is intended for a w/c less than 0.45. It can be applied to a higher w/c ratio, but it does not address the potential

bleeding problem (Bentz et al., 2005). For a blend of more than one cementitious material, the water demand (the numerator of the equation) is the sum of individual water demand for each binder (for example, i=1,2,3,4 for cement, fly ash, slag, silica fume) and can be computed using Eq 4.4 (Bentz et al, 2011).

$$\text{Water_demand} = {C_f}^i \; x \; CS^i \; x \; {\alpha_{max}}^i \qquad (4.4)$$

The w/c ratio of CSA cement concrete can be as high as 0.78 (Thomas et al., (2018)) due to different hydration requirements which means this equation may need modification to be applied for internal curing of the CSA cement concrete.

The LWA used for internal curing must be uniformly distributed throughout the concrete to be effective. Even distribution of LWA is necessary for the later curing since with time the permeability of the cement paste decreases and water travel inside the concrete can be limited to hundreds of micrometers. For this reason, a more dispersed fine LWA is more beneficial compared to coarse LWA. Using fine LWA is preferred over the coarse LWA since fine LWA provides sufficient distribution of water across the section and is generally less expensive compared to coarse LWA.

4.1.2.3 Fine LWA Absorption and Desorption Testing

The best internal curing agents should have a high absorption capacity and should desorb the water when needed. According to ASTM C1761/C1761M-23, “Standard specification for lightweight aggregate for internal curing of concrete,” the 72-h absorption of LWA used for internal curing should not be less than 5%. There are different ways to determine the absorption capacity of the fine LWA. ASTM C1761 outlines the absorption test to determine the mass of the lightweight aggregate needed to provide the required quantity of water for internal curing. Oven-

dry fine LWA is soaked in water for different time intervals (72-h) to determine the rate of absorption (ASTM C1761).

To determine the potential of fine LWA to release the imbibed water at high relative humidity (90% or higher), desorption isotherms should be performed. According to ASTM C1761, LWA should be able to release at least 85% of its water at 94% RH. After achieving the saturated surface dry condition, LWA is placed in a series of desiccators each with a known RH. The LWA is placed in a desiccator with high RH and allowed to desorb the imbibed water until hygroscopic equilibrium is achieved. Then the LWA is transferred to a desiccator with a relatively lower RH. For better analysis, the result of the test can be plotted in a graph, as shown in Figure 4.3. For developing a mix design, other aggregate properties like specific gravity after 48 h of soaking, and fineness modulus need to be determined.

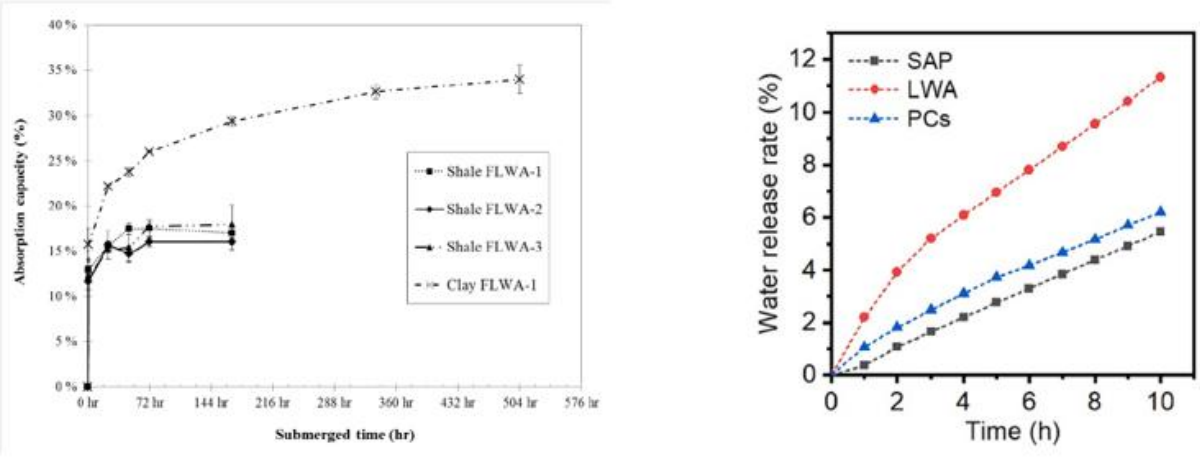


Figure 4.3: Example water (a) absorption capacity and (b) release characteristics of different internal curing agents (Ideker et al., 2013)

4.1.3 Shrinkage Measurement

There are different ways to measure shrinkage of concrete out of which two will be discussed here. The working principles for both the tests are similar. Concrete is poured into a rigid form with low friction and its change in length is measured over time using either a Linear Variable Differential Transformer (LVDT) or a comparator. One test procedure is described in the modified ASTM C157 test method. This test is performed to measure the unrestrained length change of the specimen for drying shrinkage. However, if the specimen is completely sealed this procedure can be used for measuring autogenous shrinkage as well. The ASTM C157 procedure is usually performed starting at 24 h age which results in missing shrinkage measurements for the first 24 hours as shown in Figure 4.4. To capture the full profile of shrinkage a better procedure is using VWSGs (explained later) or the corrugated tube method as described in ASTM C1698. In the corrugated tube method, concrete is poured into a corrugated plastic mold which offers little resistance to the length change of the specimen. The specimen is sealed and stored at a constant temperature. The time corresponding to the final setting of the cement is the starting time for measuring autogenous shrinkage. Change in length is measured at a regular interval and is used to calculate the autogenous shrinkage strain. The mentioned tests are well suited for concrete with a high w/c, however, problems can arise for the concrete with w/c less than 0.42. For concrete with a lower w/c ratio (e.g., high and ultra-high performance concrete) the value of autogenous shrinkage is high and should be recorded and added to the shrinkage result of the ASTM C157 test (Ideker et al., 2013).

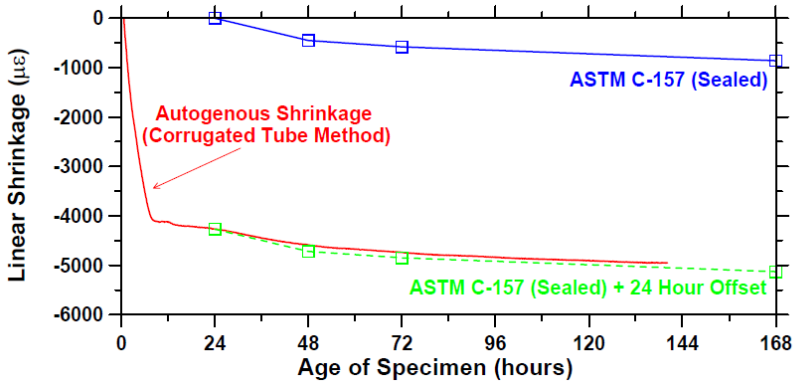


Figure 4.4: Comparison of Autogenous Shrinkage Measured in Sealed Specimens Using ASTM C157 (Beginning at 24 H) And Corrugated Mold Procedure (Beginning Immediately After Mixing) For A w/c = 0.30 mixture (Sant et al., 2006)

4.2 Experimental Procedure

4.2.1 Mix Design

4.2.1.1 Belitic Calcium Sulfoaluminate (BCSA) Cement

The BCSA concrete mix design started by conducting some trial mixes based on a spreadsheet already developed by a previous student at the University of Oklahoma (Tanksley, 2018). The goal of the trial mixes was to achieve baseline compressive strength by adjusting the citric acid dosage while using conventional rock and sand without the addition of LWS. After specifying the material quantity per unit volume of the baseline mix, a specific volume of the conventional sand was replaced with LWS, providing the internal curing for the concrete. The compressive strength of baseline mix was used as a benchmark to determine the amount of LWS to be replaced with conventional sand for internal curing such that it did not severely affect the compressive strength of the concrete. The saturated surface dry (SSD) mix proportion of baseline mix is given in Table 4.2.

Table 4.2. Baseline mix proportion of BCSA cement concrete

Material	Quantity
Rapid Set Cement (lb/yd^3)	658
5/8 in. Limestone (lb/yd^3)	1800
Sand (lb/yd^3)	1334
LWS (lb/yd^3)	0
w/c	0.4
Water (lb/yd^3)	263
Air Entraining Admixture (fl.oz/cwt)	2.0
Citric Acid (% of cement wt)	0.3*

*This percentage was decided after multiple trial tests discussed in the procedure section.

A number of baseline concrete trial mixes were used to determine the amount of citric acid needed to provide the required workability and working time. Citric acid is a set retarder which is particularly used with BCSA cement in order to avoid quick loss of workability. The addition of citric acid also affects the early age strength of the BCSA mix which is a key property for this type of cement, therefore, the optimal citric amount was picked to avoid quick sitting of the mix while yielding at least 3000 psi for the 6 h compressive strength.

The first trial test (BCSA-1) started with mixing 2 ft^3 of BCSA concrete without the addition of citric acid. The mix quickly lost its workability with close to zero slump value 10 minutes after cement addition. This quick slump loss made it difficult to work with the mixture so citric acid dosages of 0.25%, 0.3%, and 0.4% of cement weight were added in consecutive mixes (BCSA-2, BCSA-3, and BCSA-4) to observe the impact of citric acid on workability over time. Since it is important to know the quantity of water needed to reach a target compressive strength, High Range Water Reducer (HRWR) was not added to the mix at this stage.

After determining the optimal citric acid dosage, the next step involved incorporating LWS into the mixture. Eight trial mixes with varying LWS content were prepared to identify the two mixes with highest feasible replacement level without adversely impacting the strength. The amount of LWS was selected to supply internal curing water as a percentage of the cement weight. In the first trial mix, the LWS content was determined to provide 5 lb of internal curing water per 100 lb of cementitious material. In the subsequent mixes, the replacement content was increased to 7 lb, 10 lb, 12 lb, all normal sand replaced with LWS, a mix with both sand and coarse aggregate replaced with LWS and Livingstone LW rock (the same manufacturing source as LWS used in this study), and a baseline mix without any LWS. The amount of citric acid was kept constant for all the mixes containing LWS.

Concrete mix designs are typically proportioned assuming aggregate is in a saturated surface dry condition which requires converting the unsoaked weight of LWS to its saturated surface dry weight. This was done by multiplying the dry weight by (1+Absorption capacity) of LWS. The LWS was soaked in water for 48 h before its use for the mix. The LWS was then drained through a geosynthetic filter placed at the base of a perforated bucket for 15 minutes. After 15 minutes the sand was agitated to help in releasing the surfaced water trapped between the sand particles and was rested to drain for another 5 minutes. Once again, the sand was agitated and rested for another 5 minutes to drain the excess water. Once drained, a sample of LWS was taken for determining the moisture content which was later used to specify the actual water content of LWS in that mix. To address this issue, a representative sample of LWS was oven dried and the moisture content value was used for the weight adjustment of the LWS and water for the subsequent mixes.

Once moisture contents were adjusted and all the materials were weighed, the next step was to add them into the mixer in the following sequence:

- Pour the air entraining agent into the sand (if applicable);
- Dump the sand, LWS and rock into the mixer;
- Dry mix for 2-3 minutes;
- Add all the Citric acid and HRWR (Glenium) into the water container(s) and mix it with a rod thoroughly until the content is dissolved and distributed uniformly;
- Add half of the water (containing HRWR and citric acid) with the aggregate into the mixer;
- Mix for 1 minute;
- Add the rapid setting BCSA cement into the mixer followed by adding the remaining water;
- Mix for 1 minute and visually observe the workability;
- If needed add extra dose of HRWR directly into the mix while keeping the mixer drum rotating;
- After achieving a desired flow dump the mixer contents into a cart and utilize for testing.

For every added volumetric unit of LWS the same volume of the regular sand was removed to maintain a constant total mixture volume. Due to the lower density of LWS compared to the regular sand, the mass of the sand removed is greater than the LWS added, leading to a reduction in unit weight of the resulting mixture.

Slump was measured for each mix at different time intervals to ensure proper workability as shown in Figure 4.5.



(a) (b)

Figure 4.5: Slump test for (a) BCSA cement concrete and (b) Type K cement concrete

For each mix, 15 cylinders of 4 in. x 8 in. dimensions were cast and placed in a controlled room of 68˚F after casting. Three cylinders were tested for each 6 h, 1-day, 3-day, 7-day and 28-day compressive strength test. The data were then related to the citric acid dosage, workability and outside temperature which were used to determine the final mix design.

4.2.1.2 Type K Plus Portland Cement

The Type K plus portland cement mix design was based on previous research by a former student at the university of Oklahoma (Tanksley, 2018). The amount of replaced LWS was selected to introduce 8 lb and 10 lb of internal curing water, similar to the values selected for BCSA cement. The mix proportion of the Type K at the SSD condition is given in Table 4.3.

Table 4.3. Baseline mix proportion for Type K plus portland cement concrete

Material	Quantity
Portland Cement (lb/yd^3)	423
Type K Cement(lb/yd^3)	141
5/8 in. Limestone (lb/yd^3)	1430
Sand (lb/yd^3)	1715
LWS (lb/yd^3)	0
w/c	0.5
Water (lb/yd^3)	282

The mixing sequence used for these mixes is as follows:

- Dump the aggregate into the mixer and dry mix for 2-3 minutes;
- Mix all the citric acid and half of HRWR into half the water and add it over the aggregate into the mixer;
- Mix the ingredients for a few minutes to allow uniform distribution of water into the mix;
- Add the cementitious materials into the mixer;
- Add the remaining half of water mixed with the remaining half of HRWR into the mixer and mix for 2-3 minutes. Since the Type K cement is rapid setting, it is best to adjust the HRWR dosage earlier so that the material does not start setting while in the mixer.

The mix ingredients of the Type K plus portland cement mix are shown in Figure 4.6.



Figure 4.6: The mix ingredients of Type K cement concrete

During mix proportioning, the amount of LWS in the Type K mixes was initially determined based on the SSD condition. Although the mixing water was adjusted for the actual moisture content of the LWS, which was higher than the SSD moisture, the aggregate weight itself was not corrected to account for additional moisture which resulted in providing lesser LWS than intended. Since the total water was adjusted, the water to cement ratio was generally not affected, and the overall influence of this discrepancy is expected to be limited.

4.2.2 Specific Gravity and Absorption Tests for the LWS

Based on ACI 211.2-98, a pycnometer test was conducted to determine the specific gravity of the LWS. For this purpose, LWS was immersed in water and was kept in a control room with temperature of 68˚F for 48 h. The 48-h soaking time was selected based on research by Tanksley (2018) on a similar source LWS. After soaking, the water and LWS was filtered through a geosynthetic placed at the base of a perforated filter bucket. The water drained through the geosynthetic in 25 minutes and the settled LWS was stirred after 15 and 20 minutes to help with the drainage from the fine particles. Next, the LWS was emptied into a flat container and was surface dried using paper towels. The drying continued until no water was absorbed by the paper towels and all the surface water of the fine LWS was absorbed. The specific gravity was determined using a pycnometer and the procedures of ACI 211.2-98, and was determined to be

1.35. Meanwhile, an absorption test was performed on the same LWS by putting a certain amount of the presoaked and surfaced dried LWS into the oven. The LWS was weighed before and after 24 h drying and the absorption of the LWS was determined to 36.5%.

4.3 Results

4.3.1 Slump

Due to rapid loss of workability of the CSA cement concretes, it was necessary to use a set retarder to provide ample time for placing the concrete. For this purpose, varying amounts of citric acid were used and the impact of this variation on slump of the BCSA concrete was observed over 20 minutes using procedure described in ASTM C143, as shown in Figures 3.7 and 3.8.

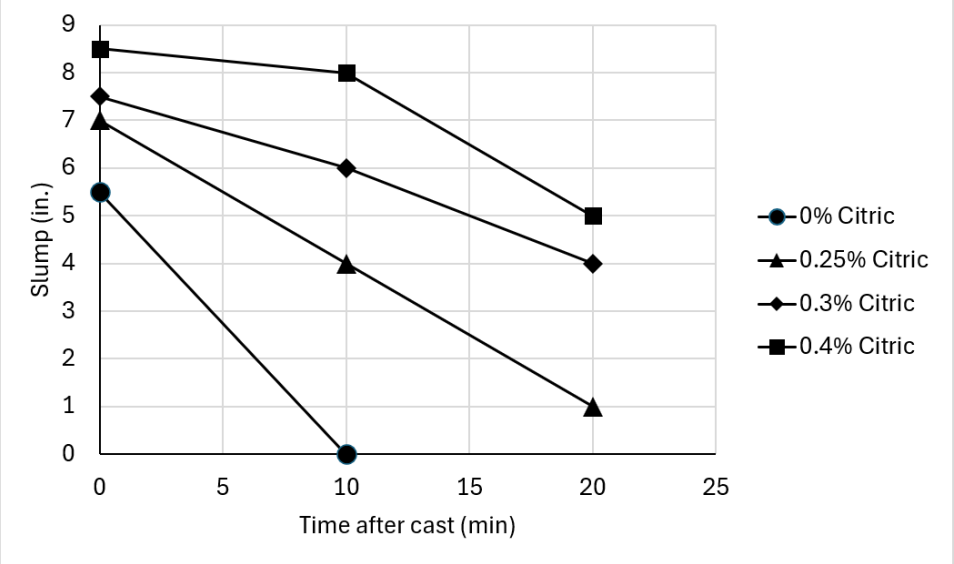


Figure 4.7: Slump variation graph over time for the baseline BCSA concrete mix with different citric acid contents

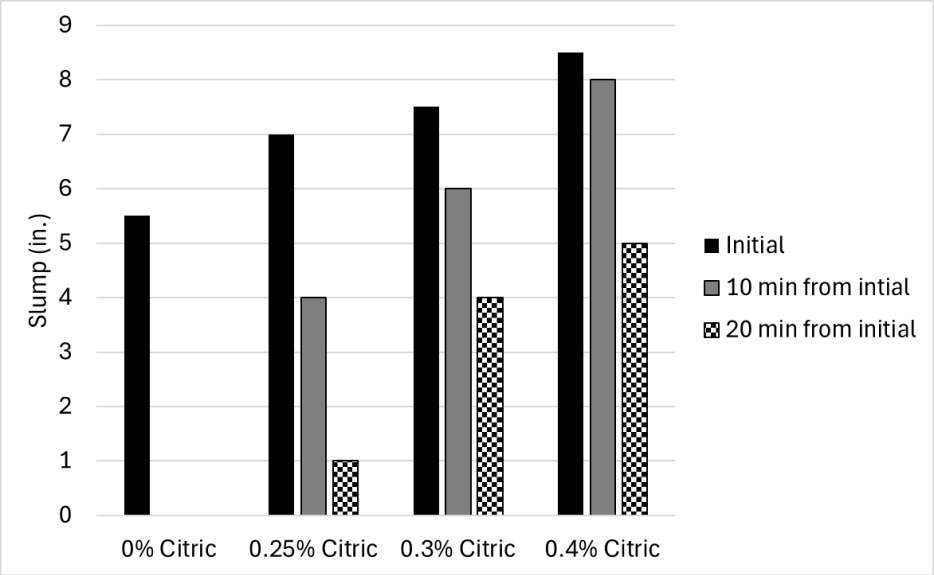


Figure 4.8: Slump variation chart over time for the baseline BCSA concrete mix with different

The results indicate that using the 0.3% and 0.4% weight of cementitious material citric acid dosages provide workability during the first 20 minutes after mixing, which is the desired timeframe for placing the concrete. To further narrow down the final citric acid dosage for the BCSA mixes, early age compressive strength testing was conducted. The goal was to achieve 3000 psi within 6 h of casting. A comparative of citric acid dosage with slump, outside temperature and 6 h compressive strength is provided in Table 4.4.

Table 4.4. Workability and strength for different dosages of citric acid-baseline BCSA mix

Designation	Citric Acid (%)	Outside Temp (˚F)	Slump (in.)			Compressive Strength (psi)- 6 h
			Initial	10 min from Initial	20 min from Initial	
BCSA-1	0.00	78.6	5.5	0	0	3370
BCSA-2	0.25	77.0	7.0	4	1	3320
BCSA-3	0.30	78.4	7.5	6	4	3030
BCSA-4	0.40	78.6	8.5	8	5	1255

The results indicate that the 0.3% citric acid dosage (as highlighted in green) can provide both workability during first 20 minutes and more than 3000 psi compressive strength at 6 h. Therefore, the 0.3% citric amount was chosen onward for the creep and shrinkage mixes.

4.3.2 Volumetric Air Content and Unit Weight Tests

For the mixes with LWS, a volumetric air content test procedure based on ASTM C173 was used to determine the air content of the mix. A few trial batches were performed to optimize the amount of air entrainer admixture into the mix.

The conventional pressure method (ASTM C231) for determining air content assumes that the rocks are impermeable, and air voids are only present in the paste. However, LWS has pores which are filled with air and the air inside the pores is compressible. Therefore, using the pressure method for determining the air content of the mixes with LWS would overestimate the air content. The volumetric procedure used for air content determination of the mixes with LWS measures the air content of the mortar fraction of the concrete by displacing it with water and is not affected by the air which is inside the pore of aggregate particles (ASTM C173, 2024).

In ASTM C173, the apparatus's bowl is filled with concrete in two layers, each layer rodded 25 times and tapped on the side 10-15 times with a rubber mallet for proper compaction. Then the top section of the apparatus is placed and tightened. Water is added to the mix with a small amount of alcohol after which the top cap is sealed and the apparatus is agitated and rolled to release the air from the concrete into the water column as shown in Figure 4.9. The air content is read from the calibrated neck and is adjusted to the amount of alcohol added.



Figure 4.9: Volumetric air content test

The results indicate that air content for all mixes was within the range of 5-6% specified by ACI 318-19. For the first four mixes (except 7 LWS) the measured air content increased with increase in LWS, and then decreased for the 12 LWS, LWS+Rock, and LWS+LW Rock, as indicated in Figure 4.10.

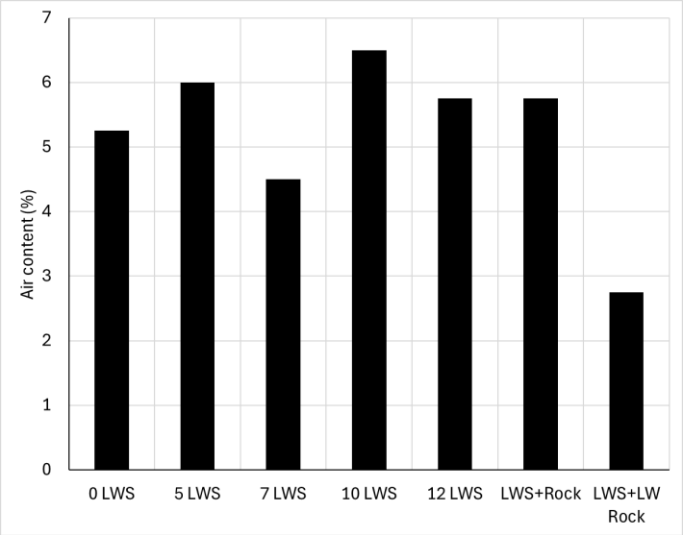


Figure 4.10: Measured volumetric air content with different amounts of LWS for BCSA cement concrete

The unit weight of the BCSA mix with varying amount of LWS was determined using the procedure described in ASTM C138 and the volumetric air content setup container was used to measure the weight of fresh concrete. The results follow a gradual decrease in unit weight with increasing amount of LWS, as shown in Figure 4.11.

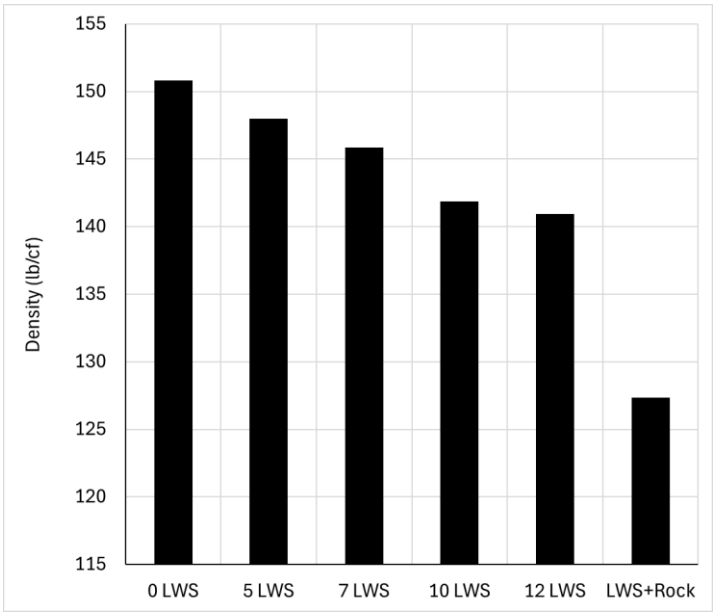


Figure 4.11: Unit weight of BCSA concrete with different amounts of LWS

4.3.3 Compressive Strength Test

Compressive strength testing was performed to observe the impact of citric acid on the early age and long-term strength of the BCSA mix. The initial set of tests were performed for the baseline mixes without any LWS which is for citric acid amount determination. The results in Figure 4.12 indicate that the impact of citric acid is more pronounced for the first six hours (0.25 days) and diminishes as concrete age increases. The compressive strength at 1, 3, 7, and 28 days indicated a slight increase with the addition of citric acid which could be attributed to the proper placement and compaction for the mixes with better workability.

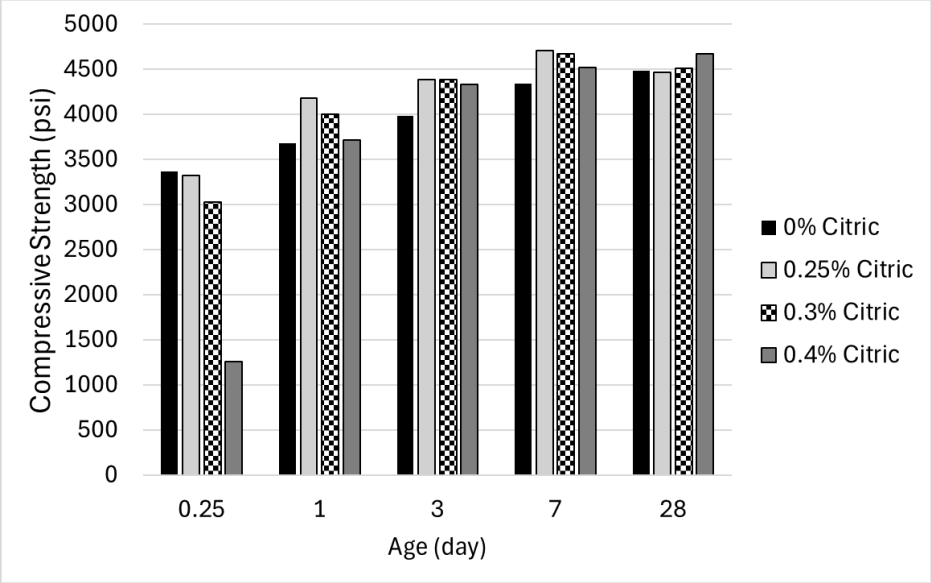


Figure 4.12: Compressive strength of BCSA-cement concrete with 0 LWS

Addition of LWS caused a reduction in the compressive strength of the mix, as indicated by Figure 4.13. However, the reduction in strength was least for the 7 LWS and 10 LWS mixes. On the other hand, the change in compressive strength between the 7 LWS and 10 LWS mixes was minimal. In order to better utilize the impact of internal curing, the final mixes used for preparing the creep, shrinakge, and MOR mixes were designed to provide 8 LWS and 10 LWS.

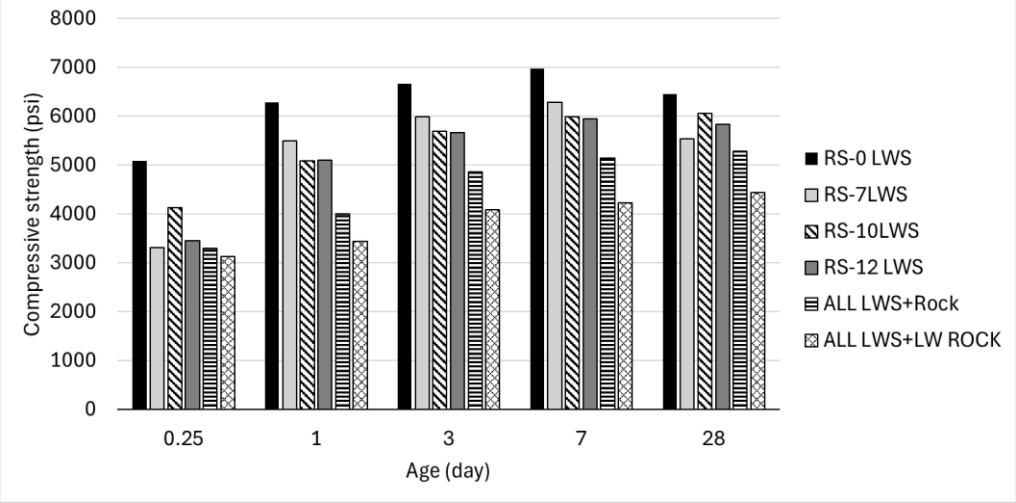


Figure 4.13: Compressive strength of BCSA concrete with varying amount of LWS (0.30% citric acid)

4.3.4 Modulus of Rupture (MOR) Test

Modulus of rupture (MOR) testing was conducted based on ASTM C78/C78M to determine the flexural strength of the rapid setting BCSA and Type K mixtures with and without LWS. Three mixes were mixed and tested for this purpose. For the first mix, no LWS was used, and second and third mixes included LWS to provide 8 lb and 10 lb of internal curing water, respectively. The 6 in. x 6 in. x 21 in. prism and 4 in. x 8 in. cylinder molds were oiled and filled with concrete in two layers. According to ASTM C192/C192M, each of the two layers of prims concrete was compacted 63 times with a 5/8 in. rod and were struck 3-4 times by a rubber mallet to ensure proper compaction. The cylinders were rodded 25 times per layer using a 3/8 in. steel rod. The specimens were kept in a 68 ˚F temperature-controlled room and were covered with a plastic sheet to avoid excess evaporation. Test were conducted for the BCSA mix at 6 h, 1 day, and 28 days whereas for the Type K cement concrete tests were conducted at 3 days, 7 days, and 28 days. Three prisms were tested to failure in flexure using third point loading for each time interval using a hydraulic compression machine, as shown in Figure 4.14. The broken prisms were measured from three points along height and width, and the average values were used to measure the MOR of the specimens, as shown in Figures 3.15 and 3.16. Meanwhile, three 4 in. x 8 in. cylinders were tested to find the corresponding value for the compressive strength at each testing age.



Figure 4.14: MOR test setup

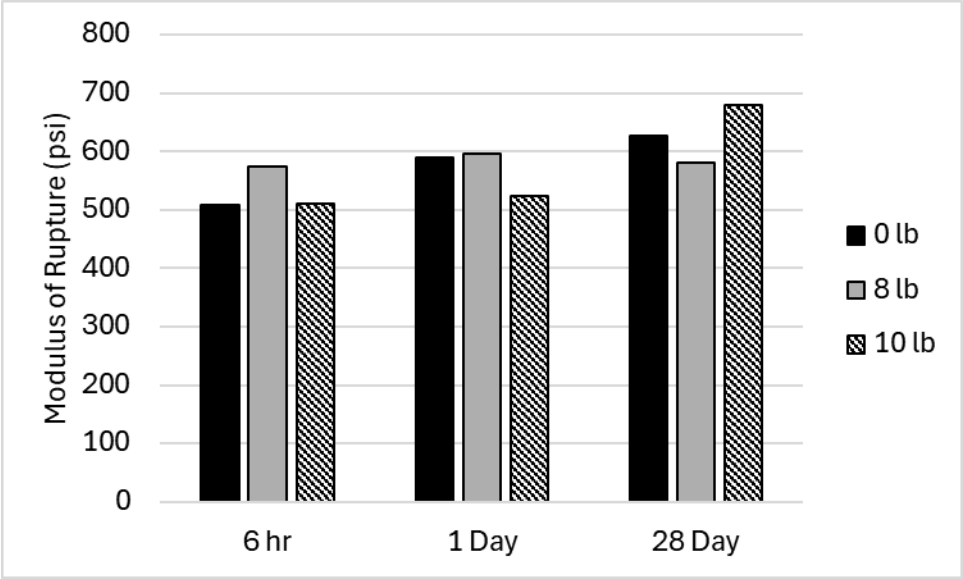


Figure 4.15: MOR test results for BCSA cement concrete

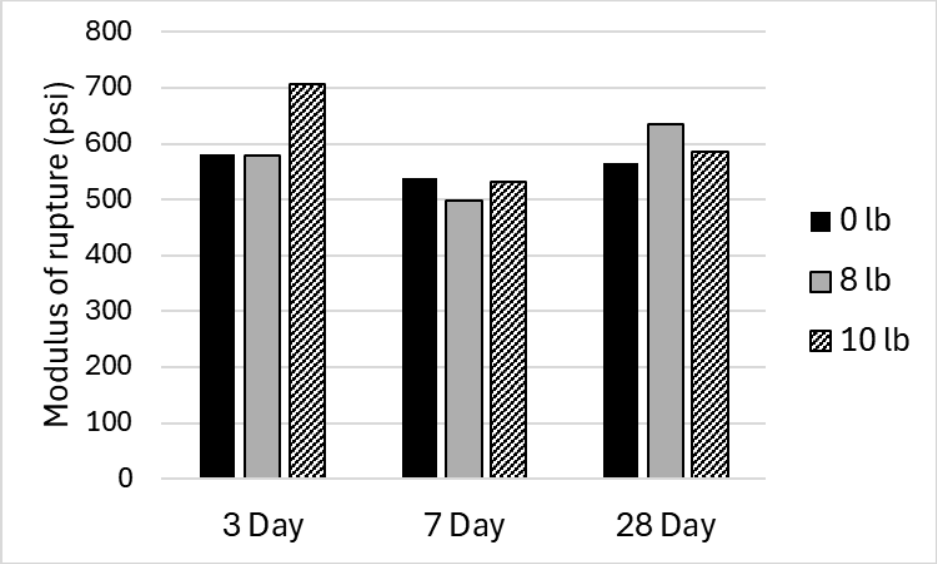


Figure 4.16: MOR test results for Type K cement concrete

4.3.5 Calorimetry Test Results

Calorimetry test for the BCSA and Type K mixes was conducted to observe the hydration of cement over time. The test procedure was discussed in Chapter 2. The results for BCSA mix indicate that LWS did not contribute to a noticeable change in setting time of the matrix, as indicated in Figure 4.17. The measured setting time for BCSA concrete mixes for all LWS contents is 80 minutes. For all the mixes, the ingredients were stored in a temperature controlled room before casting to maintain a constant starting temperature and to avoid sudden temperature rise. Material cooling resulted in a 25 mintues delay in setting compared to the mix in which material was not pre-cooled.

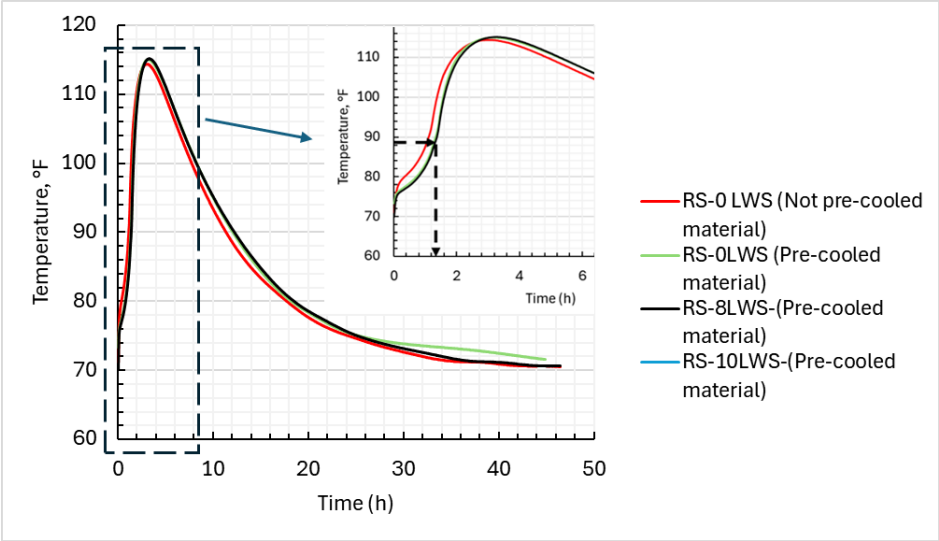


Figure 4.17: Calorimetry test results for BCSA concrete with different LWS content

Setting time for the Type K cement concrete mixes is presented in Figure 4.18, which increased with the addition of LWS. The setting time values for Type K cement concrete mixes with 0 LWS, 8 LWS, and 10 LWS mixes were 5.7 h, 7.5 h, and 7 h, respectively.

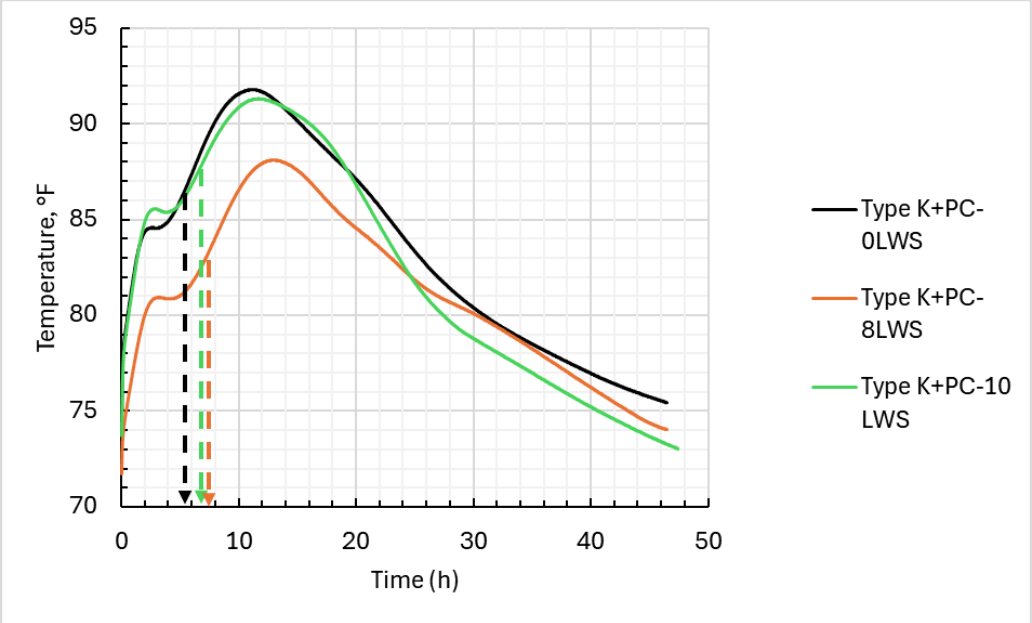


Figure 4.18: Calorimetry test results for Type K cement concrete mixes with different LWS content

4.3.6 Shrinkage and Creep Measurement

Creep and shrinkage tests were performed to capture the long-term impact of internal curing on BCSA and Type K cement concrete mixes. Two measurement procedures were adopted. The first approach was based on placing VWSG inside 6 in. x 12 in. concrete cylinders which captured the creep and shrinkage deformation of the specimens from the casting time up to 365 days. The second approach was measuring shrinkage deformation using the procedure discussed in ASTM C157. The advantages of using VWSG are recording the deformation from the moment of casting and collecting data points in short intervals (5-15 minutes) which results in a smoother curve with limited possibility for measurement error. The ASTM C157 shrinkage measurements started at 1 day and 3 days for each of the BCSA and Type K mixes, respectively, which misses the pre-setting and early age data points and is a drawback of this test procedure. In addition, ASTM C157 lacks the precision of the VWSG procedure and measurements are recorded in longer intervals, with results being susceptible to both instrumental and measurement errors.

The actual moisture content of the LWS was adjusted after moisture content measurement for each mix for both BCSA and Type K mixes used for creep and shrinkage testing. The provided internal curing water amounts based on these moisture contents are presented in Table 4.5. However, for consistency, the mix designations used in presented results were kept based on the intended amount of internal curing water provided by LWS.

Table 4.5. Actual internal curing water provided by LWS for both BCSA and Type K cement concrete mixes

Designation	Assumed LWS (lb/cwt)	Actual LWS (lb/cwt)
BCSA_8 LWS	**8.0**	**8.5**
BCSA_10 LWS	**10.0**	**8.6**
Type K_8 LWS	**8.0**	**6.97**
Type K_10 LWS	**10.0**	**7.75**

Note that, after adjustment using the measured moisture contents, the internal curing water content of both BCSA mixtures were relatively close to one another. While this may be true, the measured moisture content may have been affected by a potential oven malfunction which could have produced incorrect measurements. This assumption is further backed up by the fact that LWS used for both mixtures was soaked for the same duration and under the same environment prior to batching which may require interpreting the measured moisture content results with caution. Figures 3.19 and 3.20 show the compressive strength development of the BCSA and Type K creep specimens, respectively. Applied creep load was set at 60% of the compressive strength measured immediately prior to loading. The 6-h compressive strength of BCSA-10 LWS was lower than the 6 h compressive strength of BCSA-8 LWS. Since the BCSA-10 LWS mixture reached the loading strength of 6440 psi at 1 day after casting, creep loading was applied at that age. However, the compressive strength of both the mixtures converged by the 28-day. The difference in early age strength of BCSA-8 LWS and BCSA-10 LWS is attributed to the citric acid dosage and becomes less significant with time.

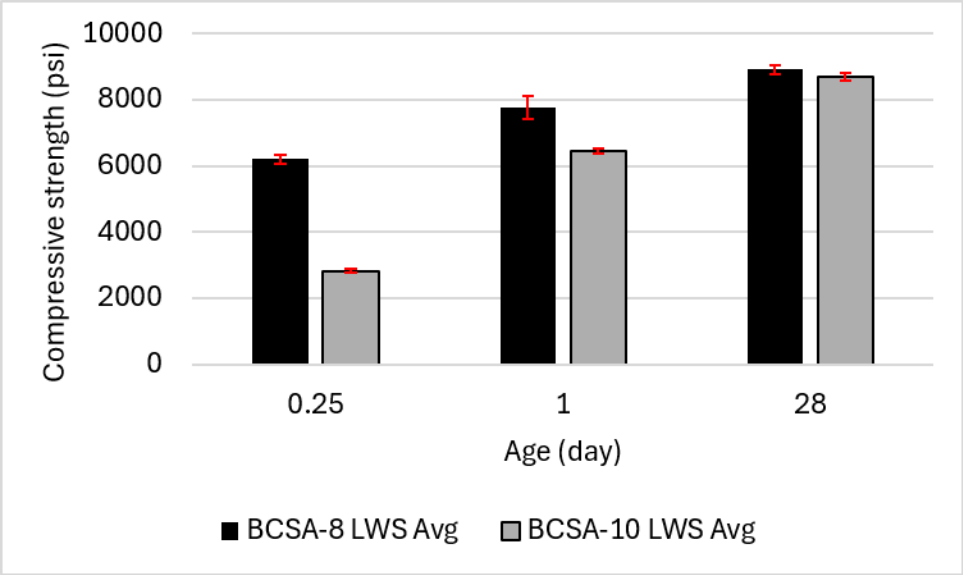


Figure 4.19: Compressive strength of the BCSA creep specimens

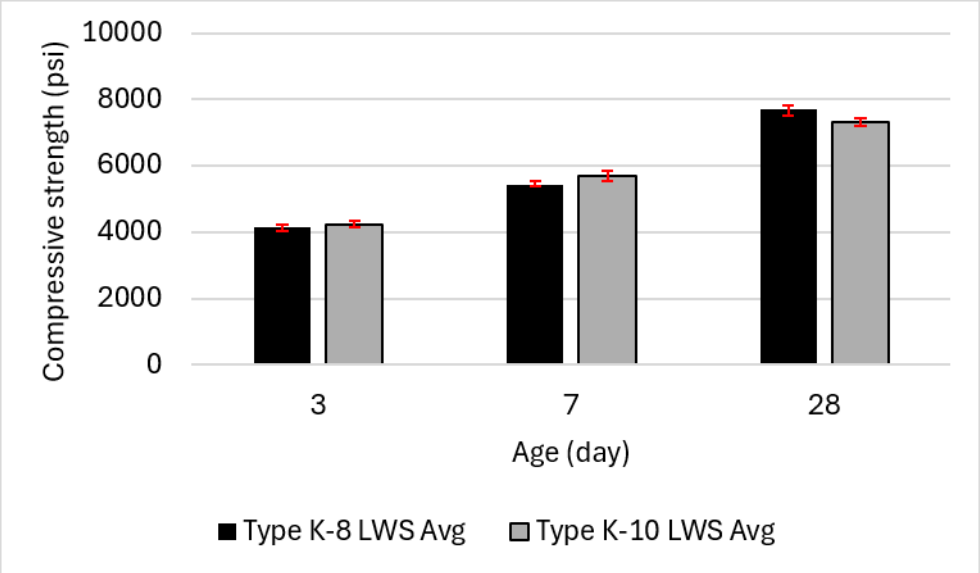


Figure 4.20: Compressive strength of the Type K creep specimens

4.3.7 Shrinkage Measurement Using ASTM C157 Procedure

The ASTM C157 Shrinkage test is used to measure the change in length of an unrestrained concrete specimen from causes other than externally applied loads and temperature. After conducting trial batches to find the optimum amount of LWS was selected to maintain compressive strength close to the mix without LWS while providing adequate internal curing. Shrinkage tests were performed according to ASTM C157/C157M. Three different mixes were used for each of the BCSA and Type K cement concrete mixes. For the first batch, no LWS was used to set a baseline value for shrinkage comparison. The second and third batches, included LWS intended to provide 8 lb and 10 lb of internal curing water per 100 lb of cement for the mixes, respectively. Construction of the specimens started by assembling and applying form-release oil to the molds used for the shrinkage prisms (Figure 4.21(a)) and companion compressive strength cylinders. After the prism molds were oiled, gauge studs were installed at the end of the molds. Care was taken to prevent any contact between the oil and the studs to ensure accurate length-change measurement. After mixing all the components in the mixer, a slump was measured per ASTM C143/143M. The prisms and cylindrical molds were filled in two layers, and each layer was rodded using a 3/8 in. rod with 34 strokes per layer for prisms and 25 strokes per layer for cylinders as specified in ASTM C192/192M. While placing the second layer of concrete in the shrinkage specimen molds, the concrete was consolidated thoroughly around the gage studs with a finger. After filling the molds and finishing the tops of the specimens, the end plate screws were loosened to avoid disturbance of gauge studs while demolding the specimens.

The BCSA concrete specimens were demolded after 6 h and Type K cement concrete were demolded 3 days after casting, and initial shrinkage values were measured using a comparator,

shown in Figure 4.21(b). Care was taken to position each specimen in the same orientation for every measurement. During testing, the specimen was rotated in a consistent direction until comparator reading stabilized, and the final reading was then recorded. The specimens of each batch were divided into two groups of three, with one group being soaked in water continuously and the other under unsoaked conditions, as shown in Figure 4.22(a). Both were stored in a temperature-controlled chamber after casting. To allow free circulation of air around the specimen, they were stored in a rack with a sufficient gap on all four sides, as shown in Figure 4.22(b). Three 4 in. x 8 in. concrete cylinders were tested for compressive strength of each batch at 6 h, 1 day, and 28 days. During the first week after casting, shrinkage measurements were recorded daily. Thereafter, measurements were taken weekly for the following three months and monthly for the remainder of the one-year monitoring period.



(a) (b)

Figure 4.21: (a) Prism molds and (b) Shrinkage measurement using comparator



(a) (b)

Figure 4.22: (a) Wet curing and (b) dry specimens stored in a rack

4.3.8 Shrinkage Measurement Using VWSG

The second procedure used for shrinkage measurement was conducted using VWSG. For this method, model 4200 GEOKON VWSGs were used as shown in Figure 4.23(a). These VWSGs have a 153 mm gauge length and 1 με sensitivity and are commonly used for concrete strain measurements in foundations, piles, bridges, dams, tunnel linings, etc. For shrinkage measurement, the VWSGs were placed vertically in the center of 6 in. x 12 in. cylindrical molds that were then filled with concrete. For this procedure the 0 LWS mix was excluded from the tests since previous research had examined this mix design (Roswurm (2023); Starks (2023)). Only the amount of LWS corresponding to 8 lb and 10 lb of internal curing water was considered for both shrinkage and creep measurements using VWSGs.



(a) (b)

Figure 4.23: (a) Model 4200 GEOKON VWSG, and (b) Manual Readout for VWSG Adjustment and Checking

To ensure that strain gauges were initially set to record the correct range of measurements, a handheld readout (Figure 4.23(b)) was used to adjust the initial strain value to 2600 με. This was done to provide enough stroke for measuring the potential elongation or shortening of the specimens. To adjust the initial strain, the reader was turned on, and the strain gauge wires were attached with the same color wires of the handheld readout. The strain value was adjusted by rotating the flat ends of the strain gauge until the value approached 2600 με. Each gauge was placed vertically at the center of the diameter in a 6 in. x 12 in. cylinder and was held in place by zip ties. The gauges were placed approximately 3.75 in. from the bottom of the cylinders. Care was given to avoid contact between the flat ends of the gauge and zip ties to avoid restraining the movement of the VWSG.

The ends of the cylinders were covered, as shown in Figure 4.24, to create the same volume to surface area ratio of the creep specimens. The cylinders were not wet cured but stored in a temperature controlled room.

The VWSGs were connected to a data logger which was recording the strain readings, outside temperature, and concrete temperature in specified time intervals. The advantage of this procedure is that it starts measuring the shrinkage as soon as the sensors come in contact with the concrete, whereas the intitial shrinkage behavior (between casting and demolding of prisms) is not recorded in the ASTM C157 procedure. Another advantage of using VWSGs is that it minimizes the measurement/instrumentational errors since it does not require human operation of the comparator. In addition, VWSGs provide the readings at short time intervals which captures the instantanous shrinkage behavior of the mixture. To better capture the initial deformation of the specimens, the data collecting interval was set to 5 minutes immediately after casting through the first few days and then switched to 15 minutes onward.



Figure 4.24: Shrinkage Measurement Using VWSGs

4.3.9 Creep Measurement

Three 6 in. x 12 in. creep specimens and two companion shrinkage specimens were cast for both the BCSA and Type K cement concrete mixes. The VWSGs were placed into cylindrical molds for the creep specimens, similarly to the previously discussed shrinkage specimens. Meanwhile nine

4 in. x 8 in. concrete cylinders were prepared for each mix to measure compressive strength at different intervals. The 6 in. x 12 in. creep and shrinkage cylindrical specimens were filled in three layers, and each layer was rodded 25 times. The VWSG made it impossible to rod the middle of the cylinders, therefore, they were gently tapped with a hand and rubber mallet to compact the concrete. The 4 in. x 8 in. cylinders were filled in two layers with each layer being rodded 25 times. The specimens' surface was levelled and sealed with a plastic sheet to avoid loss of moisture.

Three days after casting, all the specimens were demolded and ground to make the surfaces level as shown in Figure 4.25(a). Three 4 in. x 8 in. cylinders were tested to measure the 3-day compressive strength. The creep load was set at 60% of the average crushing load, determined from the mean compressive strength of three companion cylinders. The age of concrete at the time of loading for creep was 6 h for the BCSA-8 LWS, 1-day for BCSA-10 LWS concrete and 3 days for the Type K cement mixtures. Table 4.6 shows the creep load and at the given age of all CSA specimens.

Table 4.6. Creep load and age of all the CSA specimens

Specimen	Age at creep load (day)	Creep load (kip)
Type K-8 LWS	3.0	31.1
Type K-10 LWS	3.0	31.8
BCSA-8 LWS	0.25	46.8
BCSA-10 LWS	1.0	48.5

The ground creep specimens were put into the frame as specified in ASTM C512/C512M and were centered by measuring the distance of the specimens from all four sides of the reaction plate. A top steel plate was placed over the specimens on which a hydraulic cylinder was mounted. A 200-kip load cell placed over the hydraulic jack was used to measure the applied load and was connected to a data acquisition system, as shown in Figure 4.25(b). A GEOKON data logger recorded the

VWSG readings, indicating deformation of the specimens under sustained load, which were later downloaded to a computer. The companion shrinkage specimens were covered at the top and bottom to maintain a similar volume to surface area condition as the creep specimens. In addition to examining shrinkage behavior the readings of the shrinkage specimens were used to determine pure creep behavior by subtracting the shrinkage deformation out of total measured deformation of the creep specimens.



(a) (b)

Figure 4.25: (a) Grinding creep and shrinkage cylinders, and (b) creep test setup

4.3.10 Creep and Shrinkage Results Based on VWSG Measurements

The data recoding began immediately after casting when the concrete came into contact with the strain gauges. Since the strain readings before setting do not induce stresses within the concrete, the readings before setting were excluded from analysis.

The experimental results are presented in two stages: early age behavior, which covers the first few days after setting, and long-term behavior, which includes the measurements collected for at least one year. Each dataset consists of three graphs: a shrinkage curve, a total measured creep curve, and a net creep curve obtained by subtracting the shrinkage strain from the total measured deformation. In these curves positive strain values indicate expansion, whereas negative values represent contraction of the concrete specimens.

The total creep curves consist of two distinct segments. The initial segment which is between setting time and the application of sustained loading, while the second segment begins immidiately after loading and is distinguished by a vertical shift associated with the instantaneous elastic strain. For the net creep curves, the portion of the measured strain before setting is ignored and only the deformation response due to loaded (excludig shrinkage) is presented in the graphs.

4.3.10.1 Type K-8 LWS

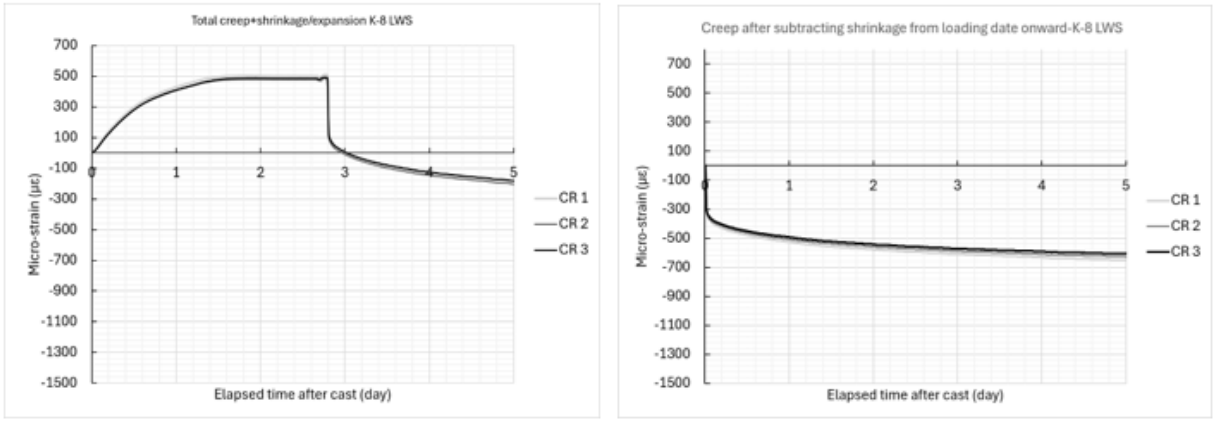
Early age behavior: Early age shrinkage behavior of the 8 LWS Type K cement concrete mixture exhibited an initial expansion of +480 με between setting and two days after casting, as shown in Figure 4.26. The deformation halted between 2 to 3 days after casting followed by shrinkage at the start of the third day. This initial expansion compensated for a significant portion of the subsequent shrinkage deformation of the specimen. The small fluctuation observed in the shrinkage curve at three days corresponds to the vibration recorded due to grinding of specimens,

which was performed to ensure that both shrinkage and creep specimens were subjected to similar surface preparation and testing conditions.



Figure 4.26: Early-age shrinkage of Type K-8 LWS mix

The portion of the curve prior to three days is identical for all Type K-8 LWS specimens. For both the total and net creep, the vertical jump in the curve corresponds to the elastic deformation of the specimens loaded with 60% of the corresponding crushing load of concrete. The lower magnitude of total measured strain indicates that a portion of the shrinkage deformation was countered by the early-age expansion of the specimens. In Figure 4.27(a) and 4.27(b), the x-axis represents the time after the cement setting and the time after creep load application, respectively.



(a) (b)

Figure 4.27: Short-term behavior for (a) Total measured creep plus shrinkage and (b) Net creep of Type K-8 LWS using VWSG procedure

Long-term behavior: The long-term shrinkage curve of the Type K cement concrete mixture containing 8 LWS exhibited an initial expansion followed by gradual shrinkage, as shown in Figure 4.28. The curve reached an equilibrium point of zero net deformation at 120 days after casting. Beyond this point, shrinkage deformation continued to develop until 310 days, after which the curve started to plateau. The final shrinkage at the end of 365 days was -90 με and remained relatively s thereafter, indicating minimal long-term deformation.

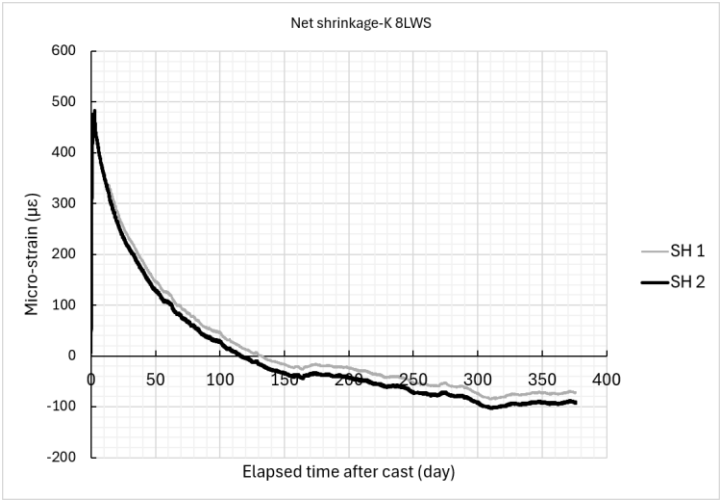
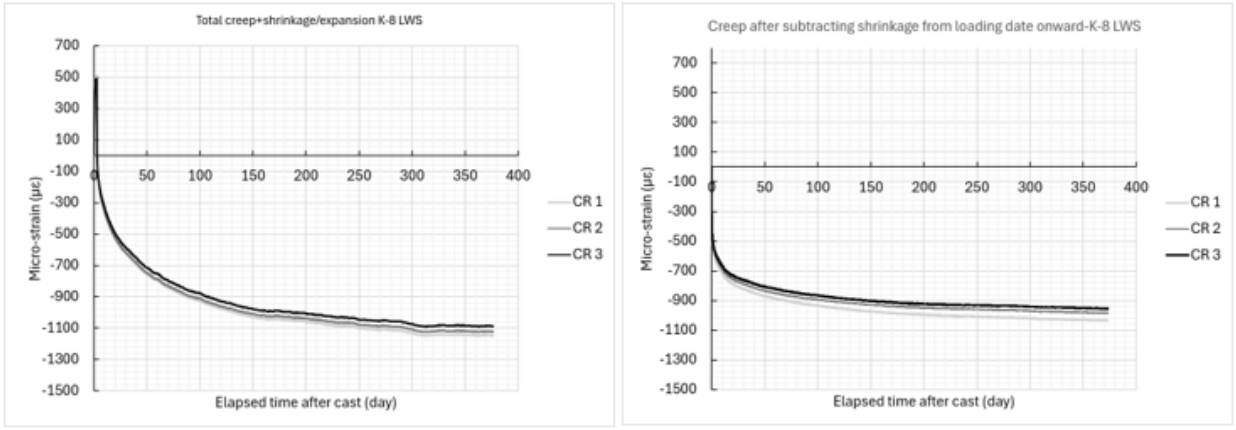


Figure 4.28: Long-term shrinkage strain of Type K 8-LWS mixture

The initial expansion of the Type K cement concrete resulted in a reduced creep rate during the first 120 days of the measured total creep deformation, corresponding to the period before reaching zero net deformation as shown in Figure 4.29(a). During this stage, the early-age expansion partially offset the compressive deformation induced by sustained loading, thereby reducing the overall rate of deformation. This behavior can be beneficial at early ages, when concrete is more vulnerable to cracking and restrained shrinkage damage. After the expansion phase ended and deformation crossed the zero strain point, the creep response become progressively dominanted by long term shrinkage and sustained load effect. At 365 days, the measured strain of total creep specimens was -1100 με while the corresponding net creep strain was slightly less than-1000 με, as presented in Figure 4.29(b).



(a) (b)

Figure 4.29: Long-term (a) total measured creep plus shrinkage and (b) net creep of Type k cement concrete with 8 LWS using VWSG procedure

4.3.10.2 Type K-10 LWS

Early age behavior: Similar to the Type K cement mixture containing 8 LWS, the Type K 10 LWS mixture exhibited an average early-age expansion of +490 με during the first three days after casting, as shown in Figure 4.30. The expansion then remained s for 0.5 day before the

specimen began to undergo shrinkage. The measured expansion was +30 με greater than that observed for the Type K 8-LWS specimens.

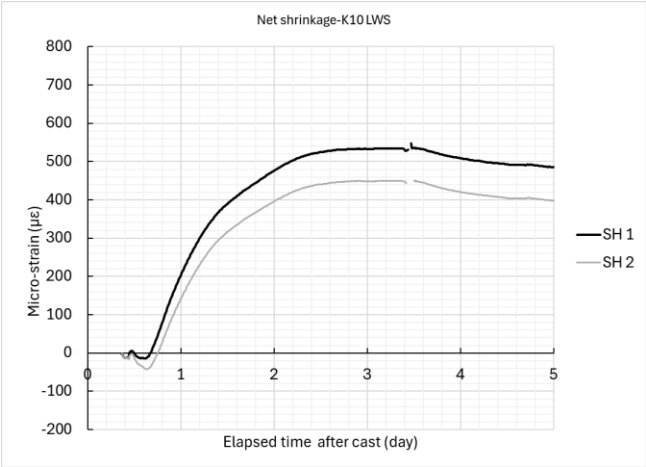
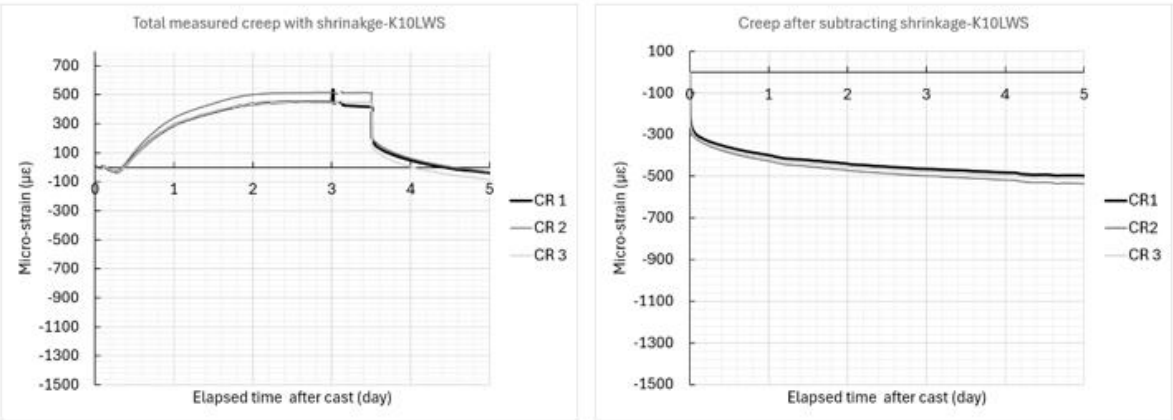


Figure 4.30: Early-age shrinkage of Type K-10 LWS mixture

The specimens were loaded in creep at 3.5 days after casting and underwent -290 με elastic deformation which is the vertical drop in the curves of Figures 4.31(a) and 4.31(b) with load application.



(a) (b)

Figure 4.31: Short-term (a) total measured creep plus shrinkage and (b) net creep of Type K cement concrete with 10 LWS using VWSG procedure

Long-term behavior: Long-term shrinkage behavior of the Type K-10 LWS was generally similar to the Type K-8 LWS mixture. However, the curve reached the point of zero net deformation at 140 days after casting which is a 10 day increase compare to the 8 LWS mixture, as shown in Figure 4.32. The impact of the increase in internal curing water on shrinkage is minimal between 8 LWS and 10 LWS mixes. At the end of the 365 days monitoring period, the measured shrinkage strain was approximately -90 με which remains relatively constant with increase in age.

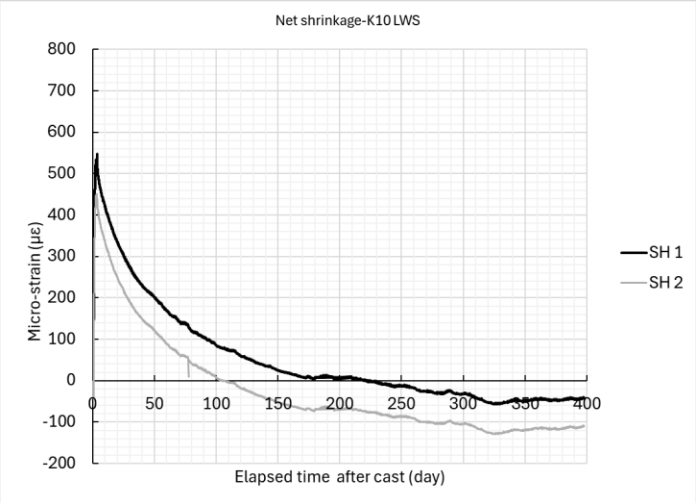


Figure 4.32: Long-term shrinkage strain of Type K-10 LWS mixture

The creep behavior of the Type K-10 LWS mixture was similar to that of the Type K-8 LWS mixture. At the end of the 365 days monitoring period, the total measured creep strain value was -900 με while the corresponding net creep strain was -750 με, as shown in Figures 4.33(a) and 4.32(b). A -200 με (18%) reduction in total strain at 356 days was observed with the increase in internal curing from 8 LWS to 10 LWS. This behavior suggests that increasing the level of internal curing contributed to a reduction in the long-term creep deformation of the Type K cement concrete.

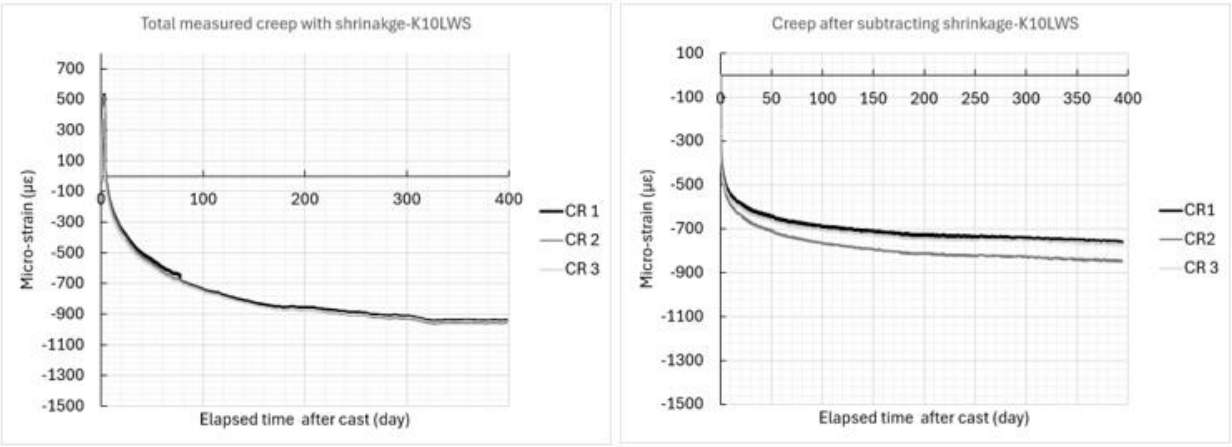


Figure 4.33: Long-term (a) Total measured creep plus shrinkage and (b) net creep of Type K cement concrete with 10 LWS using VWSG procedure

4.3.10.3 BCSA-8 LWS

Early-age behavior: The early-age shrinkage of the BCSA-8 LWS mixture exhibited a peak expansion of +100 με at 0.4 day after casting, followed by a gradual transition into shrinkage, as shown in Figure 4.34.

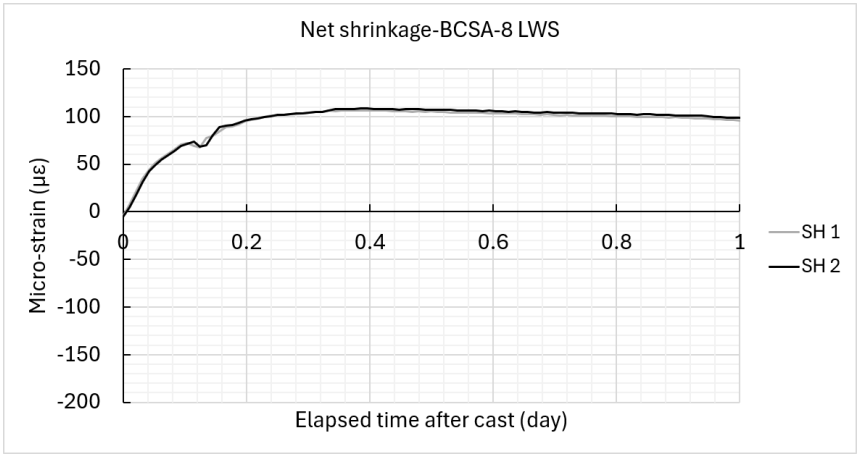
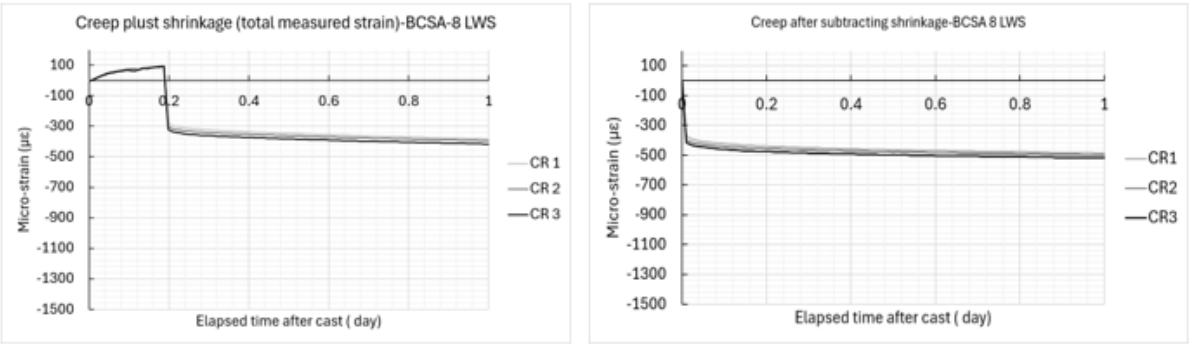


Figure 4.34: Early-age shrinkage of BCSA-10 LWS mixture

Following the application of sustained load at 6 h after casting, creep specimens experienced an instantaneous elastic strain of -400 με and the creep deformation started after stabilization of the sustained load. The total measured creep and net creep strains for the first day after casting is shown in Figures 4.35(a) and 4.34(b).



(a) (b)

Figure 4.35: Short-term (a) total measured creep plus shrinkage and (b) net creep of BCSA-8 LWS mixture using VWSG procedure

Long-term behavior: The shrinkage of the BCSA-8 LWS mixture began 0.4 days after casting with a higher early-age shrinkage rate compared to the Type K cement concrete, as shown in Figure 4.36. The curve intersected the x-axis and achieved zero deformation at 70 days after casting. The curve began to plateau after 300 days and at the end of the 365 days monitoring period, the shrinkage strain reached -150 με. Although the initial expansion of BCSA is lower than the Type K cement concrete, its shrinkage strain at the end of one year is comparable to the Type K 8 LWS shrinkage strain at the same age.

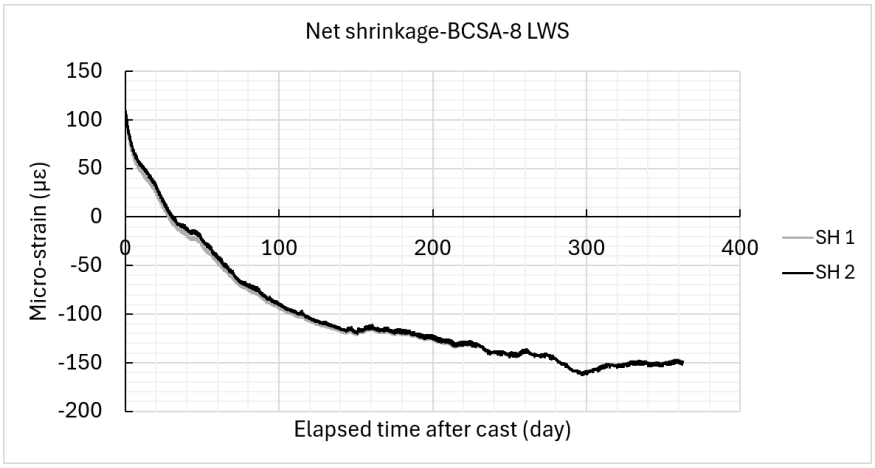
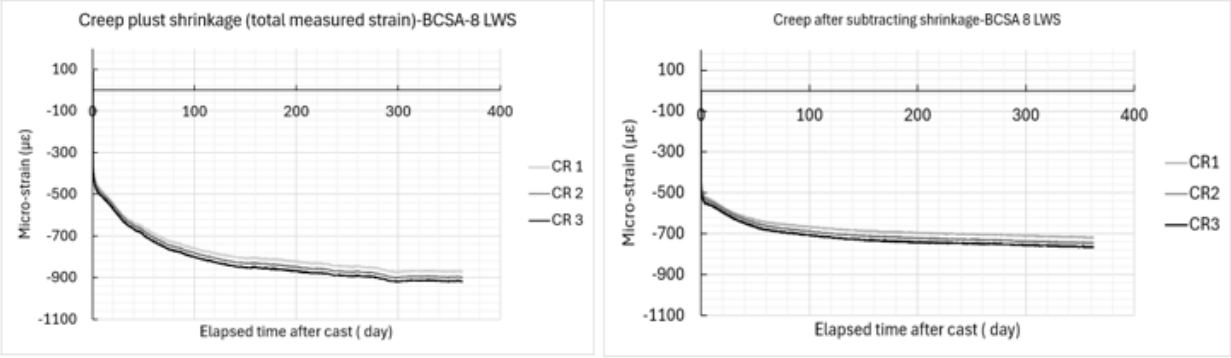


Figure 4.36: Long-term shrinkage of BCSA-8 LWS mixture after setting time

Since the initial expansion of the BCSA mixture was less than that of the Type K cement concrete, its contribution to mitigate the total creep deformation before 70 days is also limited. At the end of 365 days, the total measured creep strain in Figure 4.37 (a) and the corresponding net creep strain at Figure 4.37 (b) reached -900 με and -760 με, respectively.



(a) (b)

Figure 4.37: Long-term (a) Total measured creep plus shrinkage and (b) net creep of BCSA-8 LWS mixture using VWSG procedure

4.3.10.4 BCSA-10 LWS

Early-age behavior: With the increase in internal curing water included in the BCSA-10 LWS mixture, the initial expansion of the BCSA cement mix also increased to +220 με, as shown in Figure 4.38, which is nearly twice the the intital expansion observed in the BCSA-8 LWS mix.

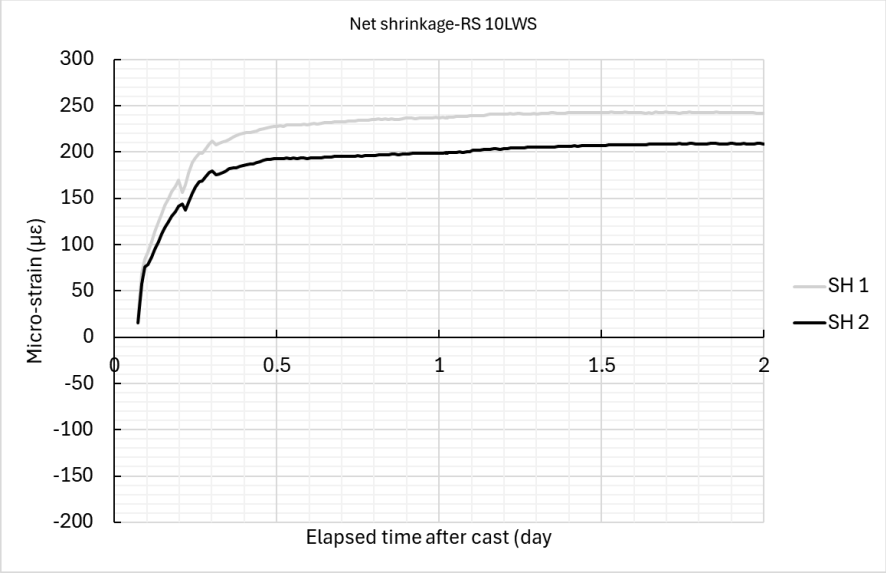
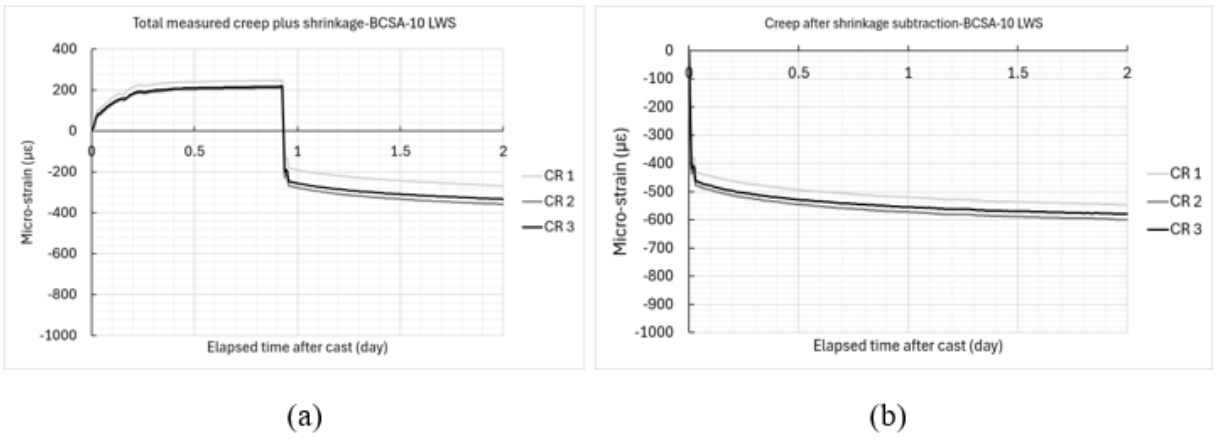


Figure 4.38: Early-age shrinkage of BCSA-10 LWS mixture after setting time

Unlike the BCSA-8 LWS mixture, this set of specimens did not gain sufficient strength up to one day after casting; therefore, the creep load was applied at one day after casting. Figures 4.39(a) and 4.39(b) show the total and net creep measurement of the BCSA-10 LWS mixes measured over 2 days.



(a) (b)

Figure 4.39: Short-term (a) Total measured creep plus shrinkage and (b) net creep of BCSA 10 LWS mixture using VWSG procedure

Long-term behavior: The advantage of increasing the internal curing level to 10 LWS was the extension of the zero-strain point to approximately 240 days after casting as given in Figure 4.40. This behavior indicates that the net deformation of concrete remained in expansion for nearly 240 days before transitioning to shrinkage. In comparison, the BCSA-8 LWS reached the zero strain point at 30 days from casting. This additional expansion period could help prevent developing premature shrinkage cracks at early ages.

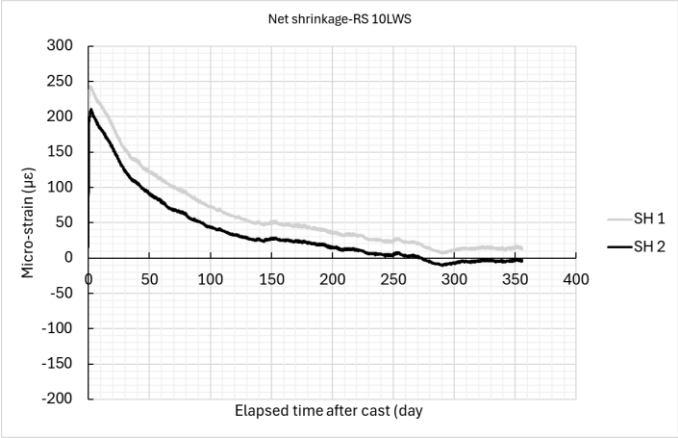
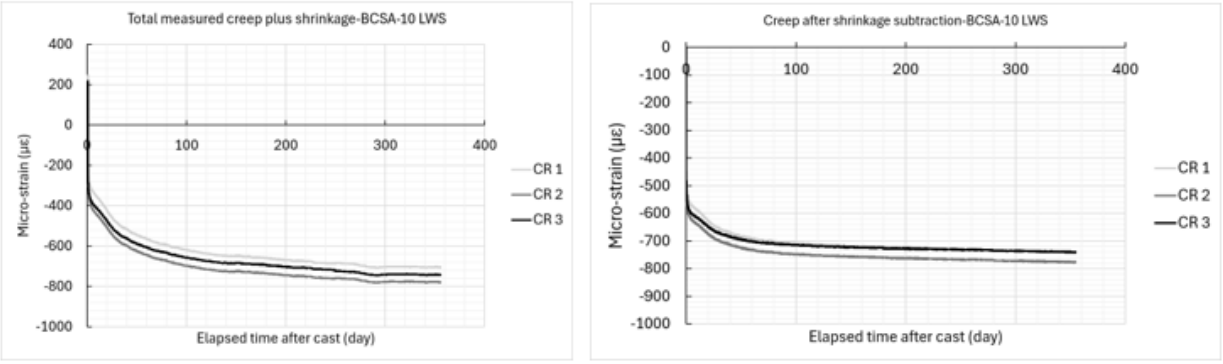


Figure 4.40: Long-term shrinkage of BCSA-10 LWS mixture after setting time

Creep of BCSA-10 LWS is similar to the BCSA-8 LWS mixture which indicates that increasing LWS did not have a noticeable change in the creep behavior, as shown in Figure 4.41. However, LWS resulted in a higher creep coefficient compared to the mix without LWS which is discussed in the next section.



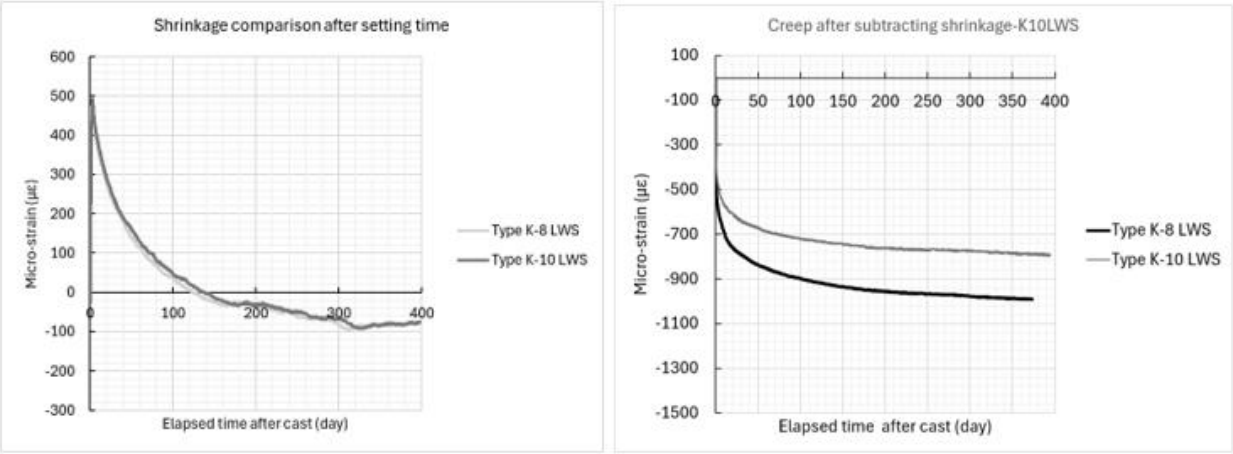
(a) (b)

Figure 4.41: Long-term (a) total measured creep plus shrinkage and (b) net creep of BCSA 10 LWS mixture using VWSG procedure

4.3.11 Comparison of Shrinkage and Creep Behavior of Each Type of Cement with Different LWS Content

4.3.11.1 Type K Cement Concrete

The shrinkage results in Figure 4.42(a) indicate that increasing the LWS content from 8 LWS to 10 LWS had only a minimal effect on the ultimate shrinkage strain of the Type K cement concrete. However, a study by Starks (2023) reported an ultimate shrinkage strain of -400 με shrinakge at the end of 200 days for Type K concrete without LWS. Compared with this control mixture, the use of internal cuing with either 8 LWS or 10 LWS resulted in a 90% reduction in 200 days shrinkage compared to the mix with no LWS. The incorporation of 10 LWS for internal curing reduced the net creep deformation by approximately 120 με compared to the 8 LWS mixture, as shown in Figure 4.42(b).

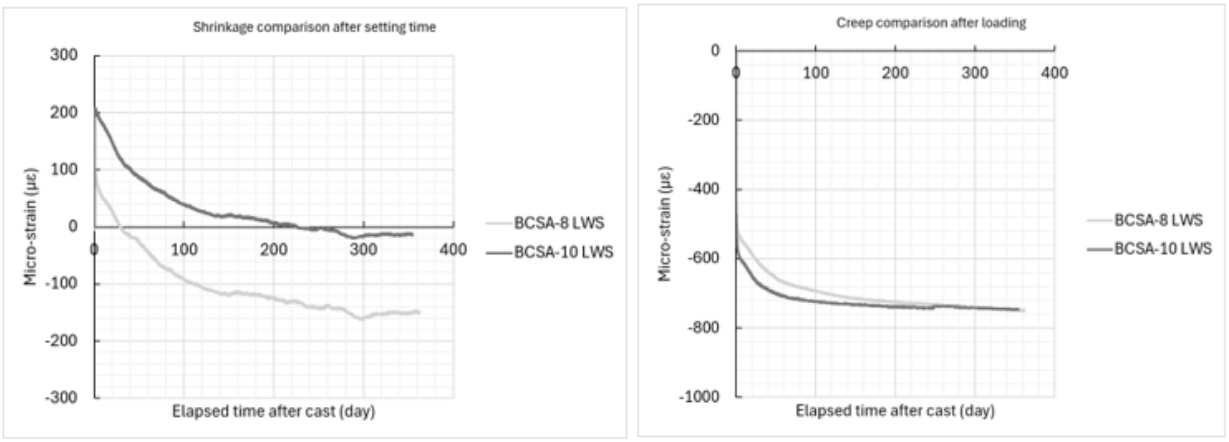


(a) (b)

Figure 4.42: Comparison of (a) Shrinkage and (b) Net creep for Type K cement concrete for 8 and 10 LWS

4.3.11.2 BCSA Cement Concrete

For the BCSA mixture, increase in internal curing level from 8 LWS to 10 LWS reduced the ultimate shrinkage strain by 125 με (87%). Since most of the expansion of the BCSA-10 LWS occurs before creep loading, therefore, its contribution in creep deformation is minimal and both the BCSA-8 LWS and BCSA-10 LWS have similar net creep deformation. The comparative shrinakge and creep curves of BCSA mix are provided in Figures 4.43(a) and 4.43(b) respectively.



(a) (b)

Figure 4.43: Comparison of (a) shrinkage and (b) creep for BCSA cement concrete for 8 and 10 LWS

Table 4.7 summarizes the elastic/instantaneous strain, creep strain and 1 year creep coefficient measured using VWSGs for each of the three specimens within a given mixture. Creep coefficient, defined as the ratio of the creep strain to the elastic strain, represents the additional deformation resulting from sustained loading relative to the initial elastic deformation. The strain values used in the creep coefficient calculation were obtained from the net creep curves.

The elastic strain, creep strain, and creep coefficient values for the Type K and BCSA mixtures without LWS, presented in Table 4.7, were obtained from the studies conducted by Starks (2023) and Roswurm (2023), respectively. Although the BCSA mix design reported by Roswurm was a self-consolidating concrete (SCC), which is different than the mix used in present study, nonetheless the results provide a useful baseline for comparing the creep behavior of the BCSA mixture with and without LWS.

Table 4.7. A summary of elastic strain, creep strain, and creep coefficients

Mix Type	Specimen	Elastic Strain	Creep Strain	Creep Coefficient
Type K-0 LWS	#1	430	580	**1.35**
Type K-8 LWS	#1	312	721	2.31
	#2	319	664	2.08
	#3	305	649	2.12
	Avg.	312	678	**2.17**
Type K-10 LWS	#1	231	533	2.31
	#2	256	594	2.32
	#3	248	526	2.12
	Avg.	245	551	**2.25**
BCSA-0 LWS	#1	823	549	0.66
	#2	850	512	0.60
	#3	813	475	0.58
	Avg.	828	512	**0.61**
BCSA-8 LWS	#1	372	347	0.93
	#2	397	348	0.87
	#3	415	350	0.84
	Avg.	395	348	**0.88**
BCSA-10 LWS	#1	391	349	0.89
	#2	437	339	0.77
	#3	419	321	0.77
	Avg.	415	336	**0.81**

The values presented in Table 4.7 indicate that incorporation of LWS increased the creep coefficient of all the mixtures. For the Type K mixture, the addition of 8 LWS and 10 LWS resulted in a one-year creep coefficient of 60% and 67%, respectively, relative to the mixture without LWS. For the BCSA mixture, the corresponding increase was 44% and 33% for the 8 LWS and 10 LWS mixtures, respectively.

4.3.12 Shrinkage Results-ASTM C157

The drying shrinkage behavior of the Type K and BCSA cement concrete was also evaluated in accordance with ASTM C157. The measured shrinkage strains are presented for all specimens

under different curing conditions. Overall, the replicate specimens for each mix exhibited consistent behavior with relatively small variation throughout the monitoring period.

The lack of a relatively smooth trend in the shrinkage curve of ASTM C157 procedure may be attributed to fluctuation in temperature of the measurement room or comparator measurement procedure inconsistencies on the measured strain value; however, temperature correction has been applied for all the readings to minimize the influence of temperature variation on the measured strain value.

For the BCSA mixture, the strain measurement began six hours after casting. However, to ensure that the concrete had developed sufficient strength beyond the influence of citric acid retarder, the strain reading at one day was used as the baseline measurement. Since the initial reference reading for the BCSA mixture was taken one day after casting, and for the Type K mixtures at three days after casting, the early-age expansion of the concrete was not captured, which is a limitation of this test procedure.

The shrinkage rate was relatively high at early ages for both cement types but decreased gradually with time and eventually plateaued at later ages. This behavior is consistent with the VWSG measurement results. To better illustrate the shrinkage behavior, the average of the three specimens for each mix were also plotted for both dry and wet curing conditions.

4.3.12.1 Type K cement concrete

The ultimate shrinkage of the Type K cement concrete specimens measured between 3 and 365 days using the ASTM C157 procedure, as shown in Figure 4.44, remained within -500 με which is comparable to average strain reading of -560 με recorded by VWSGs. Increasing the LWS

content did not change the ASTM C157 shrinkage behavior of Type K cement concrete which is consistent with the results obtained from the VWSG measurements.

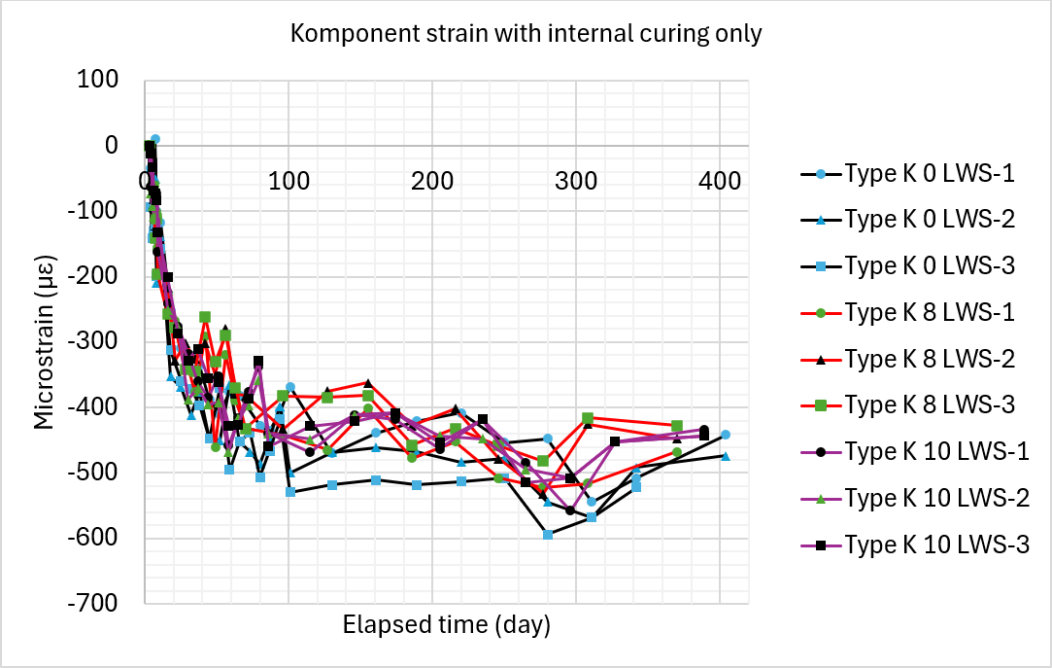


Figure 4.44: Shrinkage strain for Type K cement concrete with different LWS content - (dry external curing)

To better identify the influence of internal curing, the average shrinkage strain of the three specimens for each mixture are presented in Figure 4.45. During the first 100 days, the rate of shrinkage of the specimens was relatively higher, followed by a gradual reduction in deformation that eventually plateaued after 300 days. This behavior is consistent to the trend observed from VWSGs measurement.

The results indicate that, on average, internal curing reduced the shrinkage strain compared to the control mix without LWS. Although the lack of a smooth shrinkage curve makes it difficult to precisely quantify the reduction due to internal curing, an average reduction of approximately 50 με can be noticed compared to the baseline mix containing 0 LWS. However, there was not a noticeable difference in shrinkage between Type K-8 LWS and Type K-10 LWS mixtures.

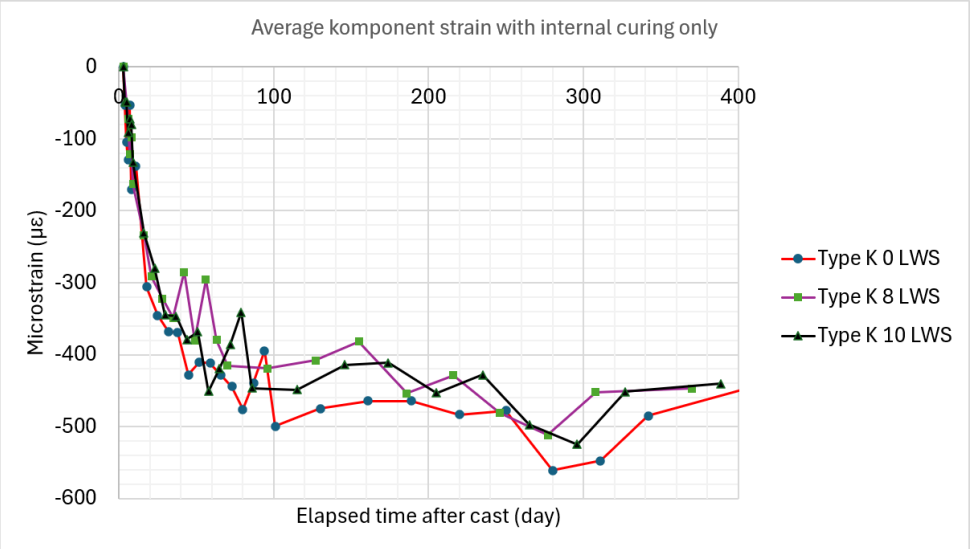


Figure 4.45: Average shrinkage measurement of Type K cement concrete using ASTM C157 procedure (dry external curing)

Figure 4.46 presents the deformation of the specimens subjected to both internal and external curing conditions. Since the specimens were continuously submerged in water, drying shrinkage did not occur, and the specimens exhibited expansion throughout monitoring.

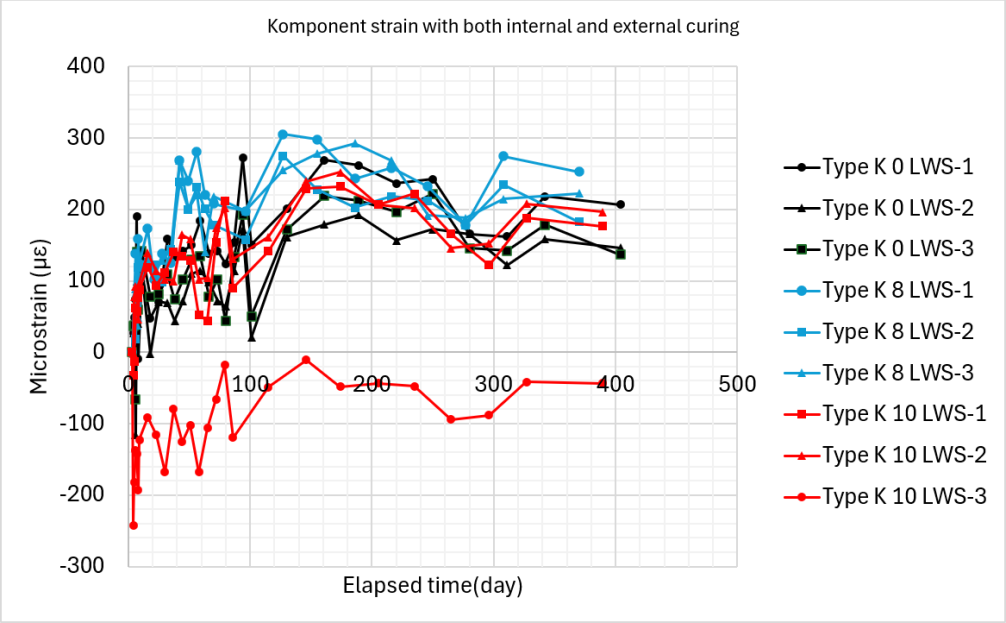


Figure 4.46: Strain of Type K specimens (wet external curing)

The average strain values shown in Figure 4.47, indicate that all the specimens under wet-curing condition with different LWS content expanded; however, no clear relationship was observed between the level of internal curing and the magnitude of the measured expansion.

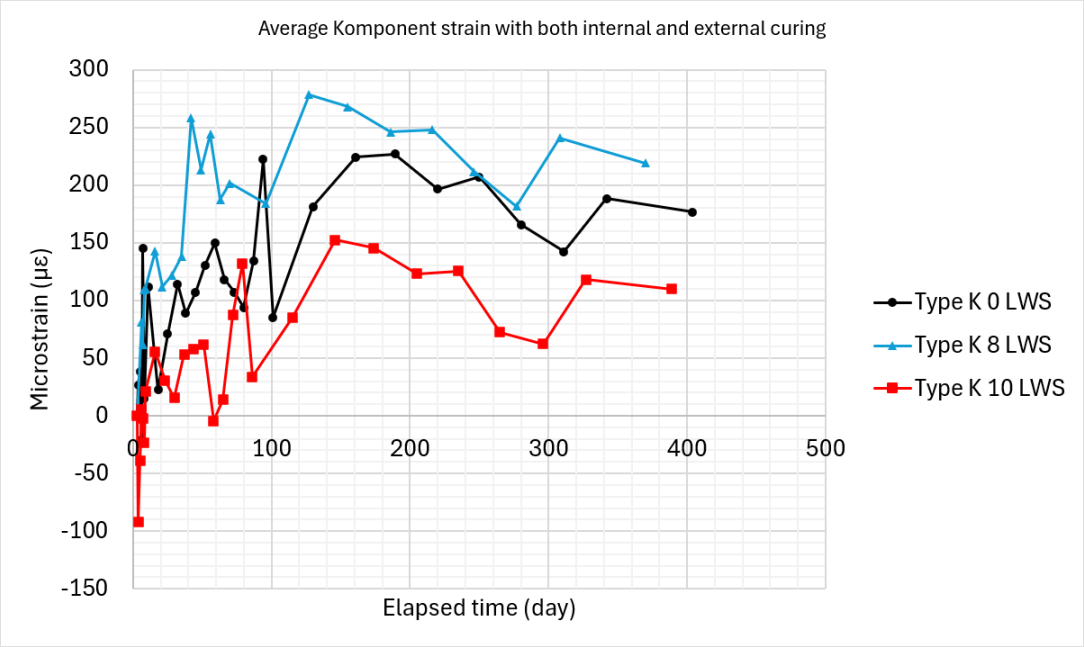


Figure 4.47: Average strain of Type K specimens with both internal curing and wet external curing

4.3.12.2 BCSA Cement Concrete

The shrinkage measurements for the internally cured BCSA specimens obtained based on ASTM C157 are presented in Figure 4.48. The ultimate shrinkage strain for the 0 LWS mix at the end of 365 days was approximately -200 με and this value was around -300 με for both 8 LWS and 10 LWS mixes. The average shrinkage strain presented in Figure 4.49 remained within a similar range, whereas VWSGs measurements indicate lower shrinkage strain for the BCSA-10 LWS mixture compared to the BCSA-8 LWS mixture.

For all BCSA mixtures, the shrinkage rate was relatively hight during the first 100 days after casting, followed by a gradual reduction in deformation rate and eventually plateauing at later

ages. However, unlike ASTM C157, the VWSGs results exhibited continuous shrinkage for 300 days before approaching a relatively constant value.

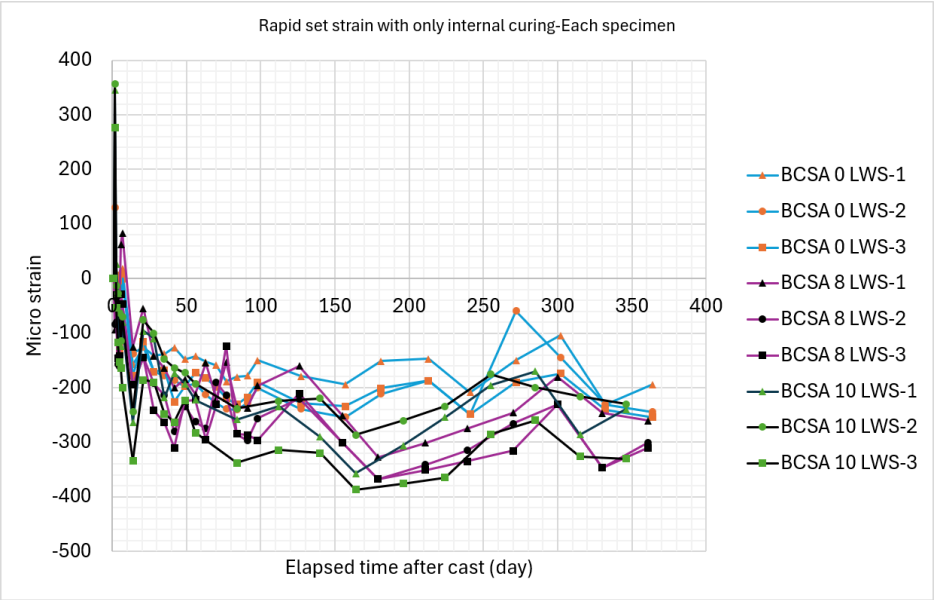


Figure 4.48: Shrinkage strain for BCSA cement concrete with different LWS content (dry external curing)

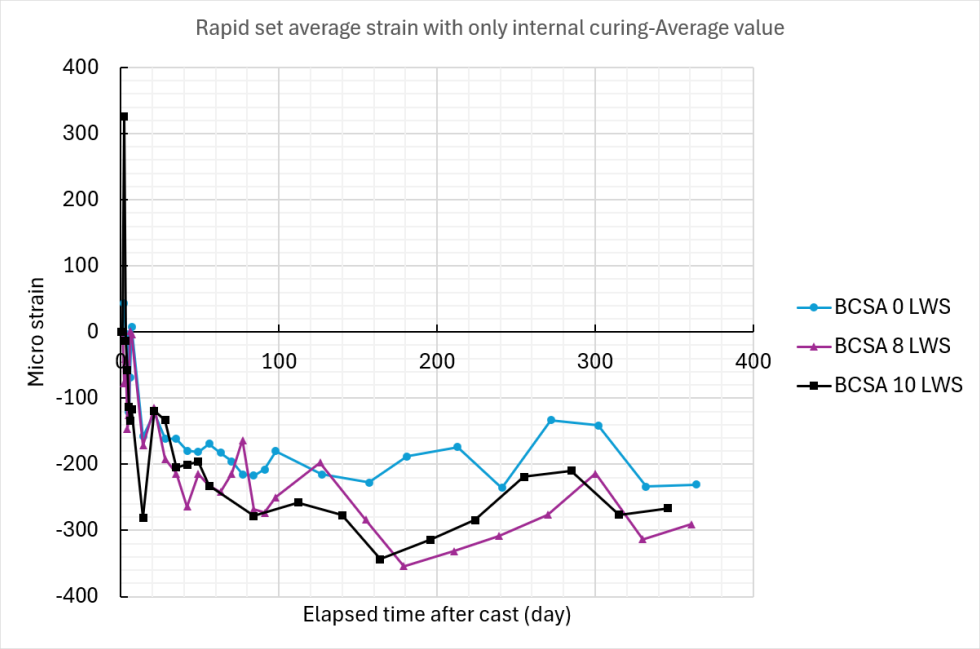


Figure 4.49: Average shrinkage strain for BCSA cement concrete with different LWS content (dry external curing)

Unlike the Type K mixtures, which exhibited noticeable expansion under combined internal and wet curing, the BCSA mixes did not show significant expansion for the first 200 days after casting. A mild expansion beginning at 200 days after casting, following by plateauing of the deformation after 350 days, as shown in Figure 4.50 and the average values in Figure 4.51. This result indicates that the presence of continuous moisture effectively prevented shrinkage in the BCSA mixtures.

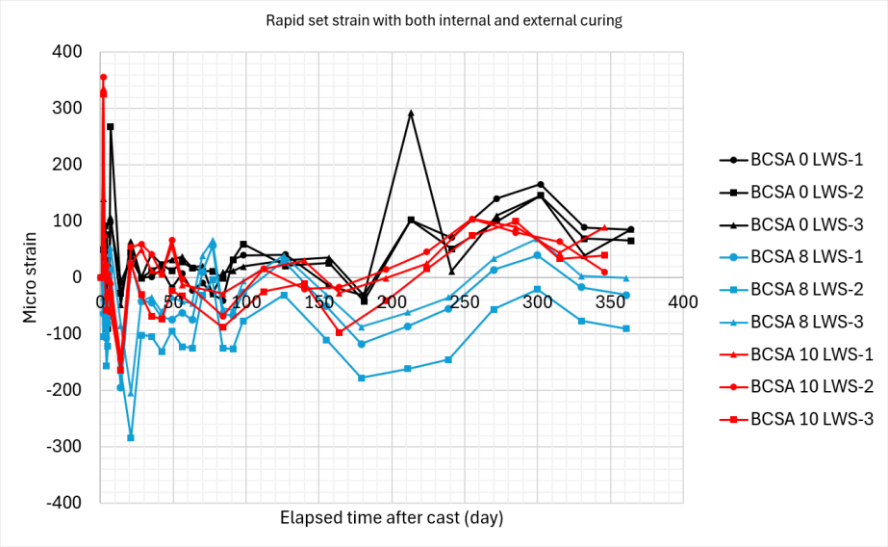


Figure 4.50: Shrinkage strain for BCSA cement concrete with different LWS content (both internal curing and external wet curing)

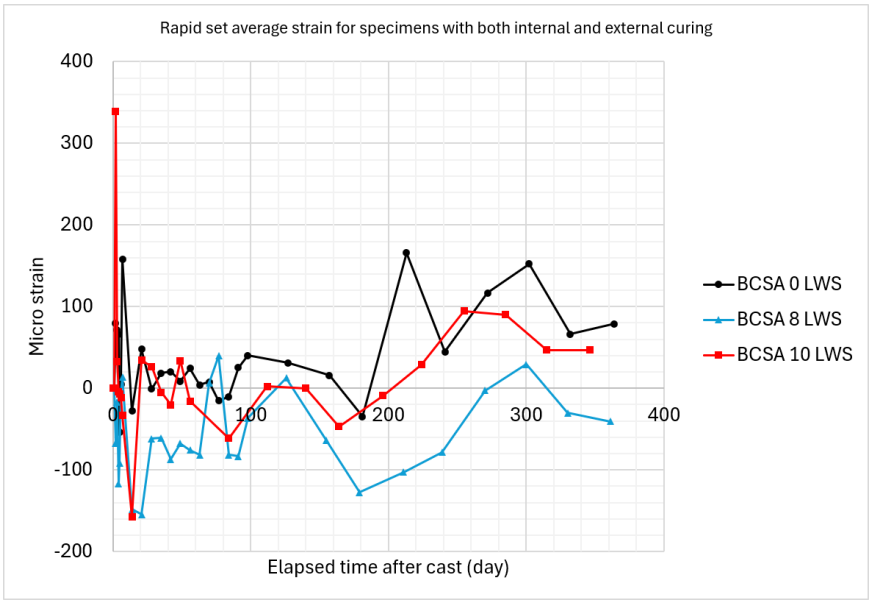


Figure 4.51: Average shrinkage strain For BCSA cement concrete with different LWS content (both internal and external curing)

4.4 Summary

In summary, two different procedures were used to measure the strain in concrete: using VWSGs and the ASTM C157 method. The data obtained by VWSGs were smoother and allowed continuous measurements at shorter time intervals beginning immediately after casting. In contrast, the data collected by the ASTM C157 procedure started at 1 day and 3 days after casting for BCSA and Type K cement mixes, respectively, and had larger data collection interval. Consequently, the ASTM C157 procedure is more susceptible to measurement inconsistencies and does not capture pre-setting deformation.

The results obtained using VWSGs indicate that both mixes of Type K exhibit expansion during the first three days followed by shrinkage for the next 300 days after casting. Although the ASTM C157 procedure did not capture the early-age expansion, the total shrinkage of Type K mixtures between 3-300 days was approximately 500 με which is around 100 με less than the total shrinkage measured using the VWSGs. Internal curing reduced the 200 days shrinakge by approximately 90% compared to the Type K mixure without LWS, however, the difference in shrinakge ofType K-8 LWS and Type K-10 LWS mixtures wasminimal.. Meanwhile, internal curing reduced the creep strain of Type K cement mixes, as illustrated by VWSG measurements. For the specimens with both internal and wet external curing, expansion was noted from the ASTM C157 measurements for all the Type K specimens.

For the BCSA mixes, the VWSG measurements indicated shrinakge strain of approximately -150 με for 8 LWS and -25 με for 10 LWS at 365 days which indicates an 83% reduction in shrinkage of BCSA-10 LWS with repect to BCSA-8 LWS. However, the measured strain for all the LWS amounts using ASTM C157 procedure ranged between -200 με for 0 LWS and -300 με for both 8 LWS and 10 LWS which is higher than the shrinkage measured by VWSG. Specimens with both

internal and wet external curing did not expand for the first 200 days after casting and exhibited a mild expansion after that. Overall, the dual cured BCSA specimens exhibited an approximately net zero deformation. The creep results indicate an increase in creep strain of Type K mixtures with increasing LWS content, suggesting that higher level of internal curing may have an adverse influence on the creep behavior of Type K cement mixtures.

4.5 Conclusions and Recommendations

- The incorporation of 0.3% citric acid dosage for the BCSA mixture provided the desired workability without compromising the targeted early-age compressive strength.
- Change in LWS dosage had a negligible effect on the measured air content of the BCSA mixtures.
- An increase in the LWS content resulted in a reduction in the unit weight of the concrete mixture.
- The influence of citric acid on the compressive strength of BCSA cement concrete was primarily observed at early ages, while its effect become less significant with concrete age.
- Increasing the LWS content reduced the compressive strength of both the CSA concrete mixes. Full replacement of the conventional sand with LWS led to a substantial reduction in the compressive strength and is not recommended where higher strength and stiffness of concrete is desired.
- Calorimetry test results indicate that incorporation of LWS had a negligible impact on the setting time of the BCSA mixture.

- In contrast, setting time of Type K mixture was affected by LWS addition. Compared to the control mix with 0 LWS, the setting time increased by 1.8 h and 1.3 h with the addition of 8 LWS and 10 LWS, respectively.
- VWSG measurements indicate that the Type K 8 LWS and 10 LWS mixes exhibited initial expansion of +455 με and +490 με, respectively, during the first 3 days after casting, followed by a gradual shrinkage. The net shrinkage for both mixtures was -90 με at the end of 365 days indicating that increasing the LWS content from 8 LWS to 10 LWS did not change the shrinkage behavior, however, both Type K-8 LWS and Type K-10 LWS resulted in a 90% reduction in shrinkage compared to the Type K mixture with no LWS. Shrinkage measurement obtained from ASTM C157 procedure indicate approximately -500 με shrinkage between 3 and 365 days, which is in reasonable agreement with the average strain of -560 με measured by VWSGs.
- The results obtained by ASTM C157 indicate that Type K specimens subjected to both internal and wet external curing expanded throughout the monitoring period.
- Increasing the internal curing from 8 LWS to 10 LWS reduced the ultimate net creep deformation of the Type K mixtures by 120 με. This reduction could be attributed to the additonal degree of hydration provided by internal curing water resulting in a denser microstructures with reduced microcracking after hardening, therefore, improving the creep resistance of the concrete.
- Based on VWSG measurements, the BCSA-8 LWS and BCSA-10 LWS mixtures exhibited initial expansion of +100 με and +230 με, respectively, during the first 0.4 day after casting. Increasing the LWS content reduced the ultimate shrinkage measured at the end of 365 days with the shrinkage of approximately -150 με for 8 LWS and -25 με for 10

LWS, indicating 83% reduction in shrinkage of BCSA-10 LWS specimens compared to the BCSA-8 LWS. Excluding the initial expansion, the shrinkage measured between 1 and 365 days was -200 με and -210 με for the BCSA-8 LWS and BCSA-10 LWS mixtures, respectively, based on the VWSG measurements; however, this value is approximately -300 με for both mixes using ASTM C157 procedure. The results obtained by ASTM C157 procedure did not show difference in shrinakge of BCSA mixes associated with the increase in LWS content. In addition, some differences in shrinkage are expected due to different volume to surface area ratios of the specimens used for the VWSG and ASTM C157 shrinakge measurements.

- BCSA specimens subjected to both internal and wet external curing exhibited no shrinkage throughout the 365-day monitoring period.
- The creep results for BCSA mixtures indicate ultimate net creep strain of -750 με and -750 με for the 8 LWS and 10 LWS mixes, respectively. These values indicate that creep of BCSA mixtures are not affected with changing the LWS content.
- Creep coeffient values indicate an increase in creep coefficient with incorporation of LWS indicating a reduction in stiffness with addition of LWS.
- Conducting additional shrinkage and creep studies by varying one parameter at a time (either the internal curing condition or the cement type) can help to modify the existing models to develop creep and shrinkage prediction models for the inernally cured CSA cement concrete.

4.6 References

1. Thomas, R. J., Maguire, M., Sorensen, A. D., & Quezada, I. (2018) "*Calcium Sulfoaluminate Cement Benefits and Applications*. Concrete international.
2. Bescher, E., & Kim, J. (2019). *Belitic calcium sulfoaluminate cement: History, chemistry, performance, and use in the United States.* In Proceedings of the 1st International Conference on Innovation in Low-Carbon Cement & Concrete Technology, Los Angeles, CA, USA.
3. Akerele, D. D., and Aguayo, F. (2025). "*Effectiveness of Rapid-Set CSA Concrete Mixes for Sustainable Pavement Repair."* CIB Conferences, Vol. 1, Article 164.
4. Glasser, F. P., and Zhang, L. (2001). "High-Performance Cement Matrices Based on Calcium Sulfoaluminate-Belite Compositions." *Cement and Concrete Research*, 31(12), 1881–1886. https://doi.org/10.1016/S0008-8846(01)00649-4
5. Sirtoli, D., Wyrzykowski, M., Riva, P., Tortelli, S., Marchi, M., and Lura, P. (2019). "Shrinkage and creep of high-performance concrete based on calcium sulfoaluminate cement." *Cement and Concrete Composites*, 98, 61–73. https://doi.org/10.1016/j.cemconcomp.2019.02.006
6. Bescher, E. P., Kim, J., Ramseyer, C., and Vallens, J. K. (2018). "Low Carbon Footprint Pavement: History of Use, Performance and New Opportunities for Belitic Calcium Sulfoaluminate." *Proc., 13th International Symposium on Concrete Roads*, Berlin, Germany, June 2018.
7. Pelletier, L., Winnefeld, F., and Lothenbach, B. (2010). "The Ternary System Portland Cement-Calcium Sulphoaluminate Clinker-Anhydrite: Hydration Mechanism and Mortar

Properties." *Cement and Concrete Composites*, 32(7), 497–507. https://doi.org/10.1016/j.cemconcomp.2010.03.010

8. Tanksley, S. D. (2018). *Internal Curing of Calcium Sulfoaluminate Cement Concrete Using Lightweight Aggregate*. Master's thesis, University of Oklahoma, Norman, OK.
9. Rice, E. (2012). "*History of Type K Shrinkage Compensating Cement."* ACI Fall 2012 Convention*,* Toronto, ON, Canada.
10. ASTM International. (2017). *ASTM C157/C157M-17, Standard Test Method for Length Change of Hardened Hydraulic-Cement Mortar and Concrete*. ASTM International, West Conshohocken, PA.
11. Wu, L., Farzadnia, N., Shi, C., Zhang, Z., and Wang, H. (2017). "Autogenous Shrinkage of High Performance Concrete: A Review." *Construction and Building Materials*, 149, 62–75. https://doi.org/10.1016/j.conbuildmat.2017.05.064
12. Ghanem, H., Ramadan, R., Khatib, J., and Elkordi, A. (2024). "A Review on Chemical and Autogenous Shrinkage of Cementitious Systems." *Materials*, 17(2), 283.
13. Ideker, J. H. (2013). *Internal Curing of High-Performance Concrete for Bridge Decks*. Oregon Department of Transportation, Salem, OR.
14. Weiss, J. (2016). *Internal Curing for Concrete Pavements*. FHWA-HIF-16-006, Federal Highway Administration, Washington, DC.
15. ASTM International. (2023). *ASTM C1761/C1761M-23, Standard Specification for Lightweight Aggregate for Internal Curing of Concrete*. ASTM International, West Conshohocken, PA. https://doi.org/10.1520/C1761_C1761M-23
16. Bentz, D. P., Lura, P., and Roberts, J. W. (2005). "Mixture Proportioning for Internal Curing." *Concrete International*, 27(2), 35–40.

17. Sant, G., Lura, P., and Weiss, J. (2006). "Measurement of Volume Change in Cementitious Materials at Early Ages." *Transportation Research Record: Journal of the Transportation Research Board*, 1979(1), 21–29. https://doi.org/10.1177/0361198106197900104

18. ASTM International. (2022). *ASTM C78/C78M-22, Standard Test Method for Flexural Strength of Concrete (Using Simple Beam with Third-Point Loading)*. ASTM International, West Conshohocken, PA

19. American Concrete Institute (ACI). (1998). *ACI 211.2-98: Standard Practice for Selecting Proportions for Structural Lightweight Concrete*. American Concrete Institute, Farmington Hills, MI.

20. ASTM International. (2019). *ASTM C192/C192M-19, Standard Practice for Making and Curing Concrete Test Specimens in the Laboratory*. ASTM International, West Conshohocken, PA.

21. ASTM International. (2017). *ASTM C231/C231M-17a, Standard Test Method for Air Content of Freshly Mixed Concrete by the Pressure Method*. ASTM International, West Conshohocken, PA.

22. ASTM International. (2024). *ASTM C173/C173M-16, Standard Test Method for Air Content of Freshly Mixed Concrete by the Volumetric Method*. ASTM International, West Conshohocken, PA. https://doi.org/10.1520/C0173_C0173M-16

23. Calmetrix, Inc. (n.d.). *Application Videos for F-Cal*. Calmetrix, Bedford, MA. Accessed May 31, 2026. Calmetrix Application Videos for F-Cal

24. Starks, J. G. (2023). *Mechanical Performance of Post-Tensioned Residential Foundation Slabs Using Expansive BCSA Cements* (Master's thesis). University of Oklahoma, Norman, OK.

25. Roswurm, S. (2023). *Application of Rapid-Setting Belitic Calcium Sulfoaluminate Cement in Pretensioned Prestressed Concrete* (Doctoral dissertation). University of Oklahoma, Norman, OK.

Chapter 5

5. The Flexural Fatigue Life of Internally and Externally Cured Expansive BCSA and Type K Cement Concrete for Pavements

5.1 Literature review

Members designed to resist a specific amount of static loading will not be able to take the same load if applied repetitively. The repeated application of a load causes fatigue which reduces the stiffness of the member and results in fracture due to the progressive growth of micro-cracks. The micro-cracks in concrete are due to imperfections such as micro-sized capillary pores and millimeter-sized air voids that result from hydration, shrinkage, and other causes.

A fatigue test on the concrete samples is conducted by applying sinusoidal stress having a maximum amplitude (σ_{max}) and minimum amplitude (σ_{min}) as a percentage of the stress corresponding to the modulus of rupture MOR of concrete (fr). The applied stress level ($S= \sigma_{max}$ /fr) is then related to the number of load cycles (N) causing failure. The reason for using S is to account for the effects of the compressive strength of concrete on fatigue life (N). After finding the number of load cycles at failure corresponding to different stress levels, the data is plotted in a graph with stress level (S) on the y-axis and fatigue life (N) on the x-axis. Fatigue tests can be conducted with a range of loading frequencies from 1 to 20 Hz, which based on the previous literature should not affect the fatigue life of plain concrete (Sohel et al., 2022).

Most of the available data related to fatigue are regarding conventional/normalweight concrete with portland cement as a binder. The objective of this research is to develop an S-N curve for the flexural fatigue life of concrete with expansive BCSA cement and a mixture of Type K cement with portland cement as binders. Type K and expansive BCSA cement are types of

Calcium Sulfualuminate (CSA) cement that gain strength much faster than traditional portland cement and exhibit expansion. More explanation is provided later in this document.

The S-N curve, also known as the Wohler fatigue curve, is used to predict the design life of concrete members under repetitive loading. The value of the stress level S corresponding to two million cycles of the load is known as fatigue strength. In other words, fatigue strength is defined as the maximum flexural stress at which the beam can withstand 2 million cycles of non-reversed fatigue loading (Rama et al., 1989). Endurance limit is another term that describes the maximum cyclic stress that a material can endure indefinitely without failing. Below the stress level corresponding to the endurance limit, the material theoretically does not fail regardless of the number of loading cycles. For plain concrete the fatigue endurance limit is 50-55 percent of its static flexural strength (Rama et al, 1989).

Fatigue has been studied since 1900, but many of the studies were dependent on the subjective experience of the individuals (Lloyd et al., 1968). Three general forms of the S-N equation have been used to evaluate fatigue. The first one is a relationship between stress level S and the number of load cycles N corresponding to fatigue failure. (X.P. Shi et al., 1993):

$$S = \frac{\sigma_{max}}{fr} = a - b\ Log(N) \qquad (5.1)$$

Where the coefficients a and b represents the intercept and slope of the S-N line developed from experimental data, respectively, which depend on the loading rate (Vicente, 2024) as well as other loading conditions such as tension, compression, or flexure and the other terms were defined previously Most classical studies assume that if the maximum cyclic stress is equal to the static strength, the element fails in first cycle which makes a=1 in Eqs. (5.1) and (5.2) however, this assumption ignores the contribution of dynamic component of the cycling and load rate

application on concrete strength (Vicente, 2024). According to (Vicente, 2024) if the stress level (S) is equal to 1.0, the fatigue strength is expected to be greater than one cycle, and the value of intercept is always greater than 1 and increases with increase in frequency.

The second form of the equation is the modified Wholer equation proposed by Aas Jackobsen in which an addition parameter, stress ratio (R), is added to Eq. (5.1) and this was the first equation to consider the influence of minimum stress level (X.P. Shi et al., 1993; Vicente, 2024). R is the ratio of $\frac{\sigma_{min}}{\sigma_{max}}$ which simulates the actual condition of stress on a structure where the minimum value of the repeated stress is not equal to zero.

$$S = \frac{\sigma_{max}}{fr} = a - b(1 - R)\, Log(N) \qquad (5.2)$$

$$(R = \frac{\sigma_{min}}{\sigma_{max}}, 0 \leq R \leq 1) \qquad (5.3)$$

The value of b ranges from 0.064-0.08 (Wei et al., 2022) and Aas-Jackobsen used a value of 0.064 for compression fatigue (Vicente, 2024).

A fatigue equation was proposed by Petkovic which is applicable for fatigue life of less than 10^6 cycles (Vicente, 2024) and is applicable for the range of $0 \leq S_{min} \leq 0.8$ (International Federation for Structural Concrete, 2012). This equation is presented in Eq. (5.4).

$$S_{max} = 1 - \frac{\log(N)}{12+16 \cdot S_{min}+8 \cdot S_{min}^2} \qquad (5.4)$$

The International Federation for Structural Concrete (fib) 2010 Model Code also provides a widely used formulation for fatigue strength for 10^8 cycles or less which is shown in Eq 5.5 (Vicente, 2024).

$$S_{max} = 1 + \log N \cdot \frac{(Y-1)}{8} \qquad (5.5)$$

$$Y = \frac{0.45+1.8 \cdot S_{min}}{1+1.8 \cdot S_{min}-0.3 \cdot S_{min}^2} \qquad (5.6)$$

Fatigue stress prediction can also be obtained using the equation adopted in Eurocode 2, as cited by Vincent, 2024, and illustrated in Eq. (5.7).

$$S_{max} = 1 - \frac{(1-R)^{0.5}}{14} \log N \qquad (5.7)$$

A fatigue relationship derived from the AASHTO road test is widely used by pavement researchers which relates S with the number of load cycles N.

$$S = \frac{\sigma_{max}}{fr} = AN^{-B} \qquad (5.8)$$

Where A and B are regression coefficients and the other terms were defined previously.

As the number of load cycles (N) in Eq. (5.8) increases, the stress level (S) decreases which indicates that a higher number of load cycles decreases the capacity of the structure; however, the drawback of this representation of fatigues strength is that it does not include the stress ratio (R) (X.P. Shi et al, 1993).

Fatigue tests are conducted using different stress levels (S) and different stress ratios (R). Keeping S constant, there is a higher value of test fatigue life (N) for higher R which makes it difficult to come up with a unique N for different R values. To address this issue, the concept of equivalent fatigue life (EN) was introduced which converted the test data for different stress ratios to an equivalent fatigue life using Eq. (5.9) (Sohel et al., 2022):

$$EN = N^{1-R} \qquad (5.9)$$

Where EN is the equivalent fatigue life, and the remaining terms have been defined earlier. Eq. (5.9) can also be used to convert the equivalent fatigue life EN to test fatigue life N for different stress ratios (R).

Some researchers worked on improving concrete fatigue strength by adding different types of fibers in reinforced concrete. Table 5.1 shows the variation in fatigue strength (f_{fmax}) of the concrete based on added percentage of fibers and their type. Each of the fiber types A, B, C, and D in Table 5.1 indicate 2 in. long hooked-end steel fibers, low-carbon steel straight fibers, 2 in. long steel corrugated fibers, and ¾ in. long Polypropylene fibers respectively. The results indicate that fibers have greatly increased fatigue strength from 8 to 33 percent depending on the type of fiber, as shown in Table 5.1.

Table 5.1. Effect of different types of fibers on the flexural strength and endurance limit of concrete (Rama et al., 1989)

Fiber Type	A		B		C		D		Plain
Fiber Content(%)	0.5	1.0	0.5	1.0	0.5	1.0	0.5	1.0	Conc.
f_{fmax} (in psi)	749	1242	559	594	549	676	478	508	508
EL_1 (%)	95	158	71	76	71	86	61	65	65
EL_2 (%)	76	85	67	59	70	55	70	65	65

f_{fmax} - flexural strength.
EL_1 - Endurance limit expressed as a percentage of modulus of rupture of plain concrete.
EL_2 - Endurance limit expressed as a percentage of its modulus of rupture.

5.1.1 CSA Cement Application

The detailed discussion of the composition and properties of CSA cement is provided in Chapter 4. This section briefly highlights its practical application.

CSA cement concrete has been used for the construction of concrete pavements and runways in different places. For example, the California Department of Transportation (Caltrans) has used CSA cement concrete to replace 350 lane miles of freeway pavement. Between 1995 and 2012, approximately 30,000 cubic meters of CSA cement concrete was used to replace a large section of SeaTac airport in Washington state, which after approximately 20 years is still in perfect condition (Bescher, 2018). For the SeaTac airport, concrete placement started at midnight and ended at 6:00 a.m. Six hours after concrete placement the strength was enough to allow equipment to pass over it without causing any damage (Tunnel Business Magazine, 2013). In California, there is a $1,000 charge per minute of delay for reopening the pavement which highlights the need for a high early-strength material. According to the ASTM C845/C845M-18, expansive cement should conform to the physical requirements of Table 5.2. The 7-day expansion of the shrinkage compensating concrete should not exceed 0.1% and this value is 0.15% at 28 days. If the expansion exceeds 0.2% then it comes under the category of chemically prestressed concrete (Rice, 2012). These limits are selected to avoid changing the reinforcement or joint details if existing concrete is replaced with Type K cement concrete (ACI convention, 2012).

Table 5.2. Physical requirements of expansive cement (ASTM C845)

Time of setting, min, minutes	75
Air content, max, vol %	12.0
Restrained expansion of mortar:	
7-day expansion:	
min, %	0.04
max, %	0.10
28-day, percentage of 7-day expansion, max	115
Compressive strength, min:	
7-day, psi [MPa]	2100 [15]
28-day, psi [MPa]	3500 [24]

In 1963, Caltrans placed two one-mile sections of concrete pavement by blending 15% expansive cement (Type K) with the portland cement. This was done to address the high shrinkage issue encountered with some of the aggregates. Although it was not a rapid setting cement, the shrinkage compensating cement concrete resulted in fewer cracks in the pavement, which is still in service today (Bescher et al., 2018).

5.2 Procedure

5.2.1 Experimental Study

5.2.1.1 Beam Construction

For this research, a total of 88 beams with dimensions of 6 in. x 6 in. x 21 in. and 14 beams with dimensions of 8 in. x 8 in. x 30 in. were cast. To initiate a baseline for comparison, 16 out of the total 88- 6 in. x 6 in. x 21 in. specimens were conventional concrete beams and the remaining were divided between expansive BCSA cement and Type K cement concrete. A total of six trial batches were conducted to find the optimal amount of citric acid and High Range Water Reducer (HRWR) to get early strength while maintaining proper workability.

Mixing of the concrete started with adding sand and coarse aggregate to the mixer. Then half of the total water pre-mixed with citric acid was added over the aggregate and was mixed for 2-3 minutes. Next, the cementitious materials were loaded into the mixer followed by adding the remaining water that contained citric acid and HRWR. The mixing continued for 3-5 minutes or until the concrete was mixed thoroughly.

Multiple slump tests were conducted to observe the loss of workability over time. As shown in Figure 5.1, the concrete was poured into the oiled steel beam forms in three layers and each layer was rodded at the rate of 1 rod per 2 $in.^2$ of the surface area to ensure proper consolidation of concrete as specified by ASTM C192/C192M-19. Accordingly, the number of rods for the 6 in. x 6 in. x 21 in. and 8 in. x 8 in. x 30 in. specimens were 63 and 120 rods, respectively. Nine cylindrical specimens with 4 in. x 8 in. dimensions were cast for compressive strength test as shown in Figure 5.1 After leveling the fresh concrete, the specimens were covered with plastic sheets to avoid loss of moisture. Compressive strength tests were performed on each batch of concrete at different intervals to measure their strength gain.



Figure 5.1: 6 in. x 6 in. x 21 in. specimens along with 4 in. x 8 in. cylinders

Table 5.3 shows the mix design used for preparing conventional, CSA, and conventional cement concrete.

Table 5.3. Mix designs

Material	**Conventional Concrete**	**Expansive BCSA Cement Concrete**	**Type K Cement Concrete**
Portland Cement (lb/yd^3)	682	-	423
Expansive BCSA Cement (lb/yd^3)	-	564	-
Type K Cement (lb/yd^3)	-	-	141
Water (lb/yd^3)	300	282	282
Fine Aggregate (lb/yd^3)	1291	1697	1715
5/8 in. Limestone Coarse Aggregate (lb/yd^3)	1725	1415	1430
High Range Water Reducer (ADVA 575) (oz/-cwt)	1	3.0	5.0
Citric Acid Retarder (lb/yd^3)	-	2.82	0.39
Air Entrainer (% of cement)	2	-	-

Note: *1 lb= 4.44 N and 1 yd^3 = 0.764 m^3*

cwt: 100 lb. weight of total cementitious material

5.2.2 Fatigue and MOR Test Procedures

A third point loading was used to evaluate the failure of the specimen under pure flexure. The concrete specimen was placed on a steel beam supported by a cylindrical MTS actuator in a self-contained frame used to apply a cyclic up-and-down displacement to the test setup as shown in Figure 5.2. Since the movement of the loading setup was restricted at the top, a reaction was generated by the load cell and the readings from which were recorded as the load applied by the actuator.

The load was applied to the specimens through steel rollers positioned at the top and bottom of the specimen. These rollers were rested on the neoprene pads and were bolted to the top loading plate and bottom steel beam. These neoprene pads were placed to allow minor leveling adjustments and to ensure uniform load distribution along the width of the specimens while minimizing stress concentration. Therefore, the deformation of neoprene pads contributed to the total deformation measured by the MTS machine.

Before conducting the fatigue tests for each specimen set, two beams and three cylinders were tested to find the modulus of rupture (MOR) and compressive strength of the concrete, respectively. The modulus of rupture tests were conducted with a loading rate between 25 psi/sec and 35 psi/sec as specified by the ASTM C78/C78M-22. To prevent potential damage to the apparatus caused by the continued loading after the specimen failure, the test was performed in a displacement control mode at a rate of 0.01 in./minute, which produces a similar loading rate to that specified in ASTM C78/C78M-22. At least two beams were tested for the MOR of the concrete to account for concrete variability. The highest static failure load measured in the MOR test was used to determine the upper and lower limits of the load for the fatigue tests.

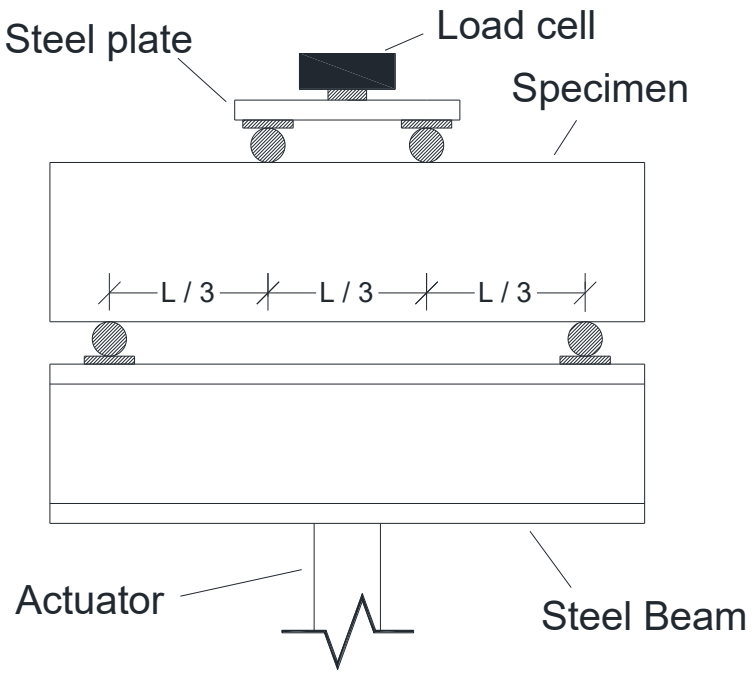


Figure 5.2: Loading setup for MOR and fatigue tests

The edges of the beams were smoothed using an abrasive grinding stone so that they would sit evenly on the loading frame and to promote even load distribution. Third point loading locations were marked for each of the specimens to ensure proper positioning into the loading frame. Special attention was given to ensure that the beams rested evenly on the rollers; uneven seating could cause twisting and premature failure. To achieve proper contact, bolts from both the steel plate and steel beam rollers were adjusted until the rollers contacted the beam uniformly. Fatigue loading was applied to the beams using a percentage of MOR load at the maximum magnitude while maintaining 10% of the MOR load as a minimum for cyclic loading. Unlike the MOR tests, fatigue tests were conducted in a load-controlled condition. Load cycles were applied until collapse of the specimen To protect the testing machine from damage due to specimen failure, a

displacement limit was programmed to shut off the hydraulic pump from the loading once the specimens failed. Dimensions of the failed specimens were measured from three locations along the height and the width, and the average was used for further analysis. The resulting data were then used to plot S-N curves using linear regression on log scale for different concrete types and specimen sizes.

5.3 Results

This section describes the fatigue test results for expansive BCSA cement and Type K cement concrete. To establish a baseline for comparison, 16 conventional concrete beams with dimensions of 6 in. x 6 in. x 21 in. were cast and tested in fatigue similar to the CSA cement concrete samples. The total number of CSA specimens is 72 beams with dimensions of 6 in. x 6 in. x 21 in. and 14 beams with dimensions of 8 in. x 8 in. x 30 in. The reason for using two different sizes of the specimen (6 in. x 6 in. x 21 in. and 8 in. x 8 in. x 30 in.) was to examine the size effect on fatigue strength. The tests also included using lightweight sand (LWS) for internal curing of the CSA cement concrete mixes and to observe the impact of internal curing on fatigue strength. A total of 198 cylinders (18 for each batch without LWS and 9 for the batches with LWS) were tested to obtain the compressive strength at different time intervals and for each fatigue test.

5.3.1 Fresh concrete tests

Based on Table 701:1 of the Oklahoma DOT Standard Specifications for Highway Construction, ODOT (2019), the maximum allowable slump for pavement concrete having a high-range water-reducer is 9.0 in. provided it causes no segregation; however, this limit is for portland cement concrete. Due to a lack of a specific slump recommendation for the CSA cement concrete, a 9.0-in. target slump was used for all the castings. Both the CSA and Type K cement concrete lose

workability at a higher rate than conventional concrete. For example, for the Type K cement concrete the slump dropped from 9 in. to 3 in. in 10 minutes. To increase the setting time for both the CSA cements citric acid was used as a percentage of total weight of cementitious materials as shown in Table 5.4. In Tables 5.4, 5.5, and 5.6 the letters K, C, and PC implies for Type K, expansive BCSA, and portland cement concrete mixtures, respectively.

Table 5.4. Slump, temperature, and citric acid dosage

Member	K1	K2	K3	K4	C1	C2	C3	PC1	PC2
Slump (in.)	9.0	9.0	8.25	9.25	9.0	7.0	9.5	9.0	9.0
Temperature (°C)	24.3	25.2	26.8	14.9	23.8	17.2	30.1	-	-
Citric Acid (% of cement weight)	0.07	0.07	0.07	0.07	0.40	0.40	0.40	-	-

1 in.=2.54 cm

5.3.2 Hardened Concrete Properties

The results of 28-day and test-day compressive strengths for CSA specimens with and without LWS are shown in Table 5.5.

Table 5.5. Compressive strength of fatigue test specimens

Specimen	28-day (psi)	Test-day (psi)
PC1	5470	5740
PC2	4860	5100
K1	5890	8500
K2	-	7550
K3	5210	7510
K4	3500	5422
C1	8010	9810
C2	10280	12250
C3	8000	9880
Type K_8 LWS	6520	6520
Type K_10 LWS	6650	6650

Specimen	28-day (psi)	Test-day (psi)
Expansive BCSA _8 LWS	11960	11960
Expansive BCSA _10 LWS	10550	10550

1 psi=0.00689 MPa

The compressive strength test for the K2 mix at 28 days was not performed and for the portland cement concrete, the test day strength was very close to the 28 days strength. There is a noticeable difference between the compressive strength of the Type K specimens at 28 days and the test day which affects its MOR strength. Since the result of the MOR test is used as an input load for the fatigue test, the time difference between the MOR test and the fatigue test should be kept minimal. In this research a new MOR test was conducted for each fatigue test if significant time had passed since the last MOR was completed.

5.3.3 Flexural Fatigue and MOR Test Results

Both the fatigue and MOR tests were conducted using a third-point loading as illustrated previously. Previous research described in the literature review indicated that the loading frequency does not affect the fatigue behavior of the specimen. For the loading setup used for this study, it was found that higher load frequencies caused vibration of the test setup which affected the upper and lower applied loads during the fatigue test. At the start of the research, fifteen specimens were tested with a 10 Hz loading frequency, but the results were not consistent and were discarded. A loading frequency of 1.0 Hz, and for some lower stress levels 3.0 Hz, was used for subsequent testing. After failure, the depth and width of the broken specimens cross-sections were measured from three different locations and their average used for calculating the stresses are shown in Tables 5.7 and 5.8.



Figure 5.3: Specimen C1-080 after testing

Table 5.6. Materials and dimensions of the specimens

Material and Size	Specimen Designation	Loading frequency (Hz)	Actual width, b (in.)	Actual depth, d (in.)	Effective span, L (in.)
6 in. x 6 in. x 21 in. Conventional Portland Cement Concrete (PC1)	PC1-MOR1	-	6.20	6.00	18.00
	PC1-MOR2	-	6.30	6.02	18.00
	PC1-095	1.0	6.13	6.03	18.00
	PC1-090	1.0	6.32	6.01	18.00
	PC1-090	1.0	6.20	6.00	18.00
	PC1085	1.0	6.14	6.03	18.00
	PC1-080	1.0	6.20	6.00	18.00
	PC1-075	1.0	6.25	6.01	18.00
6 in. x 6 in. x 21 in. Conventional Portland Cement Concrete (PC2)	PC2-MOR1	-	6.18	6.00	18.00
	PC2-MOR2	-	6.21	6.00	18.00
	PC2-095(1)	1.0	6.22	6.00	18.00
	PC2-095(2)	1.0	6.07	6.04	18.00
	PC2-090(1)	1.0	6.20	6.01	18.00
	PC2-090(2)	1.0	6.16	6.02	18.00
	PC2-085(1)	1.0	6.30	6.02	18.00

Material and Size	Specimen Designation	Loading frequency (Hz)	Actual width, b (in.)	Actual depth, d (in.)	Effective span, L (in.)
	PC2-085(2)	1.0	6.3	6.06	18.00
6 in. x 6 in. x 21 in. Expansive BCSA Cement Concrete (C2)	C2-MOR1	-	6.22	6.01	18.00
	C2-MOR2	-	6.30	6.01	18.00
	C2-095	1.0	6.25	6.05	18.00
	C2-090	1.0	6.27	6.01	18.00
	C2-085	1.0	6.18	6.00	18.00
	C2-085	1.0	6.20	6.00	18.00
	C2-080	1.0	6.20	6.04	18.00
	C2-075	1.0	6.22	6.01	18.00
6 in. x 6 in. x 21 in. Type K Cement Concrete (K2)	K2-MOR1	-	6.227	6.035	18.00
	K2-MOR2	-	6.216	6.00	18.00
	K2-095(1)	1.0	6.156	6.00	18.00
	K2-095(2)	1.0	6.30	6.06	18.00
	K2-090(1)	1.0	6.21	6.02	18.00
	K2-090(2)	1.0	6.13	6.00	18.00
	K2-090(3)	3.0	6.23	6.02	18.00
	K2-090(4)	3.0	6.28	6.02	18.00
8 in. x 8 in. x 30 in. Type K Cement Concrete (K1)	K1-MOR1	-	8.10	8.08	24.00
	K1-MOR2	-	8.10	8.08	24.00
	K1-095	1.0	8.10	8.08	24.00
	K1-090	1.0	8.10	8.08	24.00
	K1-090	1.0	8.10	8.08	24.00
	K1-080	1.0 and 3.0	8.27	8.06	24.00
8 in. x 8 in. x 30 in. Expansive BCSA Cement Concrete (C1)	C1-MOR1	-	8.27	8.07	24.00
	C1-MOR2	-	8.21	8.10	24.00
	C1-095	1.0	8.15	8.06	24.00
	C1-090	1.0	8.13	8.10	24.00
	C1-085	1.0	8.14	8.06	24.00
	C1-080	1.0	8.17	8.05	24.00
	C1-075	1.0	8.2	8.08	24.00
6 in. x 6 in. x 21 in. Expansive BCSA (C3)	C3-MOR1	-	6.18	6.00	18.00
	C3-MOR2	-	6.26	6.01	18.00
	C3-095	1.0	6.20	6.03	18.00
	C3-095	1.0	6.17	6.03	18.00
	C3-090(1)	1.0	6.13	5.99	18.00
	C3-090(2)	1.0	6.30	6.03	18.00
	C3-090(3)	1.0	6.24	6.05	18.00
	C3-090(4)	1.0	6.13	6.02	18.00
6.0 in. x 6.0 in.	K3-MOR1	-	6.22	6.01	18.00
	K3-MOR2	-	6.13	6.00	18.00

Material and Size	Specimen Designation	Loading frequency (Hz)	Actual width, b (in.)	Actual depth, d (in.)	Effective span, L (in.)
	K3-095	1.0	6.32	6.01	18.00
	K3-095	1.0	6.17	6.01	18.00
	K3-090(1)	1.0	6.13	6.00	18.00
	K3-090(2)	1.0	6.30	6.05	18.00
	K3-085(1)	1.0	6.28	6.01	18.00
	K3-085(2)	1.0	6.34	6.02	18.00
6.0 in. x 6.0 in. x 21 in. Type K Cement Concrete (K4)	K4-MOR1	-	6.21	6.09	18.00
	K4-MOR2	-	6.26	6.02	18.00
	K4-095(1)	1.0	6.33	6.04	18.00
	K4-095(2)	1.0	6.33	6.03	18.00
	K4-090(1)	1.0	6.26	6.02	18.00
	K4-090(2)	1.0	6.30	6.02	18.00
	K4-085(1)	1.0	6.25	6.02	18.00
	K4-085(2)	1.0	6.35	6.04	18.00

Since the applied stress limits were slightly different from the initial computed value based on the MOR test due to testing equipment limitations, the recorded data for each fatigue test was plotted to find the exact applied upper and lower load limits on the specimens as shown in Figure 5.4.

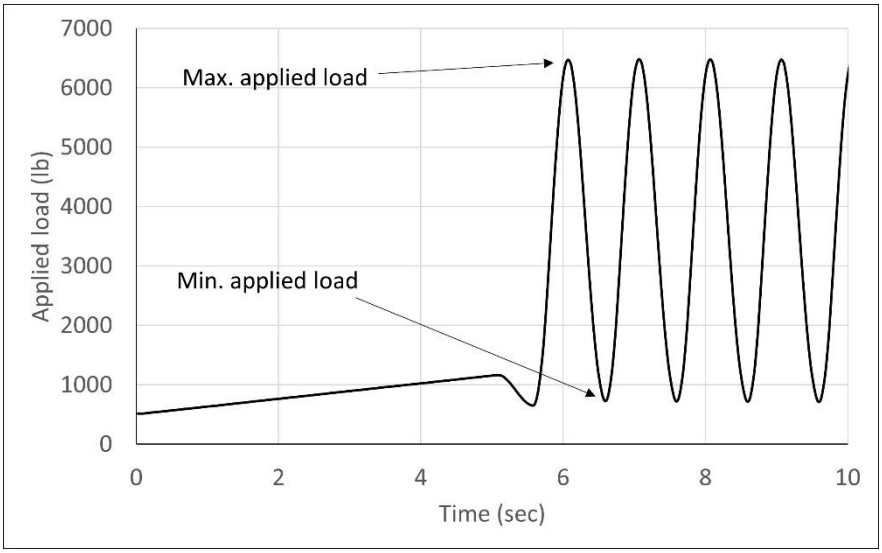


Figure 5.4: Curtailed applied load vs. time graph for specimen PC-080

The recorded values from the loading graph corresponding to the extremums of the sine waves were used to determine the stresses in Table 5.7. The difference between the actual and computed stress limits could be due to the deformation of neoprene bearing pads located below the rollers, the dynamic effects associated with the sinusoidal load and chosen loading frequency, or a combination of these. For most of the tests, the applied stress levels were selected based on the maximum MOR load (out of two MOR tests) to get a conservative fatigue behavior and to accelerate the test. Table 5.7 shows the detailed results for each fatigue and MOR test.

Table 5.7. Fatigue and MOR test results

Specimen	MOR failure load, P (lb)	Experimental MOR (psi)	Max. applied stress, σ_{max} (psi)	Min. applied stress, σ_{min} (psi)	Actual S_{max} (σ_{max}/ MOR)	Actual R (σ_{min}/ σ_{max})	No. of load cycles to failure
6 in. x 6 in. x 21 in. Conventional Concrete (PC1)							
PC1-MOR1	8045	648.8	-	-	-	-	-
PC1-MOR2	7826	617.0	-	-	-	-	-
PC1-095	8045	648.8	617.0	61.7	0.95	0.10	3
PC1-090	8045	648.8	570.9	57.1	0.88	0.10	9
PC1-090	8045	648.8	583.9	58.4	0.90	0.10	41
PC1-085	8045	648.8	551.5	55.1	0.85	0.10	132
PC1-080	8045	648.8	519.3	51.9	0.80	0.10	2994
PC1-075	8045	648.8	480.8	48.1	0.741	0.10	1109
6 in. x 6 in. x 21 in. Conventional Concrete (PC2)							
PC2-MOR1	7468	604.2	-	-	-	-	-
PC2-MOR2	6878	556.5	-	-	-	-	-
PC2-095(1)	7468	604.2	574	57.4	0.95	0.10	428
PC2-095(2)	7468	604.2	574	57.4	0.95	0.10	6
PC2-090(1)	7468	604.2	544	54.4	0.9	0.10	12250
PC2-090(2)	7468	604.2	544	54.4	0.9	0.10	122
PC2-085(1)	7468	604.2	514	51.4	0.85	0.10	175
PC2-085(2)	7468	604.2	514	51.4	0.85	0.10	12129
6 in. x 6 in. x 21 in. Expansive BCSA Concrete (C2)							
C2-MOR1	11055	885.7	-	-	-	-	-
C2-MOR2	9649	763.2	-	-	-	-	-
C2-095	11055	881.4	829.2	87.2	0.94	0.10	2
C2-090	11055	881.4	793.8	81.6	0.90	0.10	6

Specimen	MOR failure load, P (lb)	Experimental MOR (psi)	Max. applied stress, σ_{max} (psi)	Min. applied stress, σ_{min} (psi)	Actual S_{max} (σ_{max}/ MOR)	Actual R (σ_{min}/ σ_{max})	No. of load cycles to failure
C2-085	11055	881.4	752.4	78.0	0.85	0.10	1
C2-085	11055	881.4	750.6	86.7	0.85	0.11	2
C2-080	11055	881.4	703.0	75.4	0.80	0.10	59
C2-075	11055	881.4	667.3	71.0	0.75	0.10	117
6 in. x 6 in. x 21 in. Expansive BCSA concrete (C3)							
C3-MOR1	8168	661	-	-	-	-	-
C3-MOR2	6745	537	-	-	-	-	-
C3-095(1)	8168	661	628	62.8	0.95	0.10	30
C3-095(2)	8168	661	628	62.8	0.95	0.10	13
C3-090(1)	8168	661	595	59.5	0.90	0.10	135
C3-090(2)	8168	661	595	59.5	0.90	0.10	28
C3-090(3)	8168	661	595	59.5	0.90	0.10	9
C3-090(4)	8168	661	595	59.5	0.90	0.10	237
8 in. x 8 in. x 30 in. Type K Cement Concrete (K1)							
MOR1	10512	477.1	-	-	-	-	-
MOR2	11718	531.8	-	-	-	-	-
K1-095	11718	531.8	506.5	54.4	0.95	0.10	55
K1-090	11718	531.8	478.6	52.2	0.90	0.10	6404
K1-090	10512	477.1	429.6	45.7	0.90	0.10	2360
K1-080	11718	531.8	419.2	58.4	0.79	0.14	1281493
6 in. x 6 in. 21 in. Type K Cement (K2)							
K2-MOR1	6910	555	-	-	-	-	-
K2-MOR2	7625	619	-	-	-	-	-
K2-095(1)	7625	619	588	58.8	0.95	0.10	10967
K2-095(2)	7625	619	588	58.8	0.95	0.10	7531
K2-090(1)	7625	619	557	55.7	0.90	0.10	376
K2-090(2)	7625	619	557	55.7	0.90	0.10	456
K2-090(3)	7625	619	557	55.7	0.90	0.10	3893
K2-090(4)	7625	619	557	55.7	0.90	0.10	3773
6 in. x 6 in. 21 in. Type K Cement (K3)							
K3-MOR1	6782	553	-	-	-	-	-
K2-MOR2	6650	533	-	-	-	-	-
K3-095(1)	6782	553	525	52.5	0.95	0.10	26
K3-095(2)	6782	553	525	52.5	0.95	0.10	4
K3-090(1)	6782	553	498	49.8	0.90	0.10	72
K3-090(2)	6782	553	498	49.8	0.90	0.10	11
K3-085(1)	6782	553	470	47	0.85	0.10	207
K3-085(2)	6782	553	470	47	0.85	0.10	415
6 in. x 6 in. 21 in. Type K Cement (K4)							
K4-MOR1	5780	452	-	-	-	-	-

Specimen	MOR failure load, P (lb)	Experimental MOR (psi)	Max. applied stress, σ_{max} (psi)	Min. applied stress, σ_{min} (psi)	Actual S_{max} (σ_{max}/ MOR)	Actual R (σ_{min}/ σ_{max})	No. of load cycles to failure
K4-MOR2	5583	443	-	-	-	-	-
K4-095(1)	5780	452	429	42.9	0.95	0.10	23
K4-095(2)	5780	452	429	42.9	0.95	0.10	68
K4-090(1)	5780	452	407	40.7	0.90	0.10	61
K4-090(2)	5780	452	407	40.7	0.90	0.10	57
K4-085(1)	5780	452	384	38.4	0.85	0.10	446
K4-085(2)	5780	452	384	38.4	0.85	0.10	214
8 in. x 8 in. x 30 in. Expansive BCSA Concrete (C1)							
C1-MOR1	11240	500.8	-	-	-	-	-
C1-MOR2	10628	473.5	-	-	-	-	-
C1-095	10934	495.6	470.9	49.2	0.95	0.10	10
C1-090	10934	495.6	442.7	44.27	0.89	0.10	419
C1-085	10934	495.6	424.3	44.4	0.85	0.10	628
C1-080	10934	495.6	396.6	39.6	0.80	0.10	961
C1-075	10934	495.6	370.5	39.6	0.75	0.10	14712
6 in. x 6 in. x 21 in.-Type K (8-LWS)							
K-8LWS-MOR1	6754	544	-	-	-	-	-
K-8LWS-MOR2	6285	506	-	-	-	-	-
K-8LWS-095(1)	6754	544	516.6	51.6	0.95	0.10	2
K-8LWS-095(2)	6754	544	506.0	50.6	0.93	0.1	61
K-8LWS-090(1)	6754	544	486.5	48.6	0.89	0.1	153
K-8LWS-090(2)	6754	544	477.8	47.4	0.88	0.1	2668
K-8LWS-085(1)	6754	544	452.4	45.2	0.83	0.1	499
K-8LWS-085(2)	6754	544	459.1	45.9	0.84	0.1	9696
6 in. x 6 in. x 21 in.-Type K (10-LWS)							
K10LWSMOR1	6732	532	-	-	-	-	-
K10LWSMOR2	6560	510	-	-	-	-	-
K10LWS095(1)	6732	532	516.0	51.6	0.97	0.1	5730
K10LWS095(2)	6732	532	506.5	50.6	0.95	0.1	44
K10LWS090(1)	6732	532	480.2	48.0	0.90	0.1	12401
K10LWS090(2)	6732	532	477.5	47.7	0.90	0.1	12132
K10LWS085(1)	6732	532	458.0	45.8	0.86	0.1	3106
K10LWS085(2)	6732	532	445.9	44.6	0.84	0.1	9983
6 in. x 6 in. x 21 in.- Expansive BCSA Concrete (8-LWS)							
C8LWSMOR1	5954	475.5	-	-	-	-	-
C8LWSMOR2	5185	416.6	-	-	-	-	-
C8LWS095(1)	5954	474.5	446..4	44.64	0.94	0.1	132
C8LWS095(2)	5954	474.5	451.6	45.2	0.95	0.1	67
C8LWS090(1)	5954	474.5	435.7	48.4	0.92	0.1	78
C8LWS090(2)	5954	474.5	422.0	42.2	0.89	0.1	22

Specimen	MOR failure load, P (lb)	Experimental MOR (psi)	Max. applied stress, σ_{max} (psi)	Min. applied stress, σ_{min} (psi)	Actual S_{max} (σ_{max}/ MOR)	Actual R (σ_{min}/ σ_{max})	No. of load cycles to failure
C8LWS085(1)	5954	474.5	407.7	40.7	0.86	0.1	48
C8LWS085(2)	5954	474.5	399.6	39.9	0.84	0.1	329
6 in. x 6 in. x 21 in.- Expansive BCSA Concrete (10-LWS)							
C10LWSMOR1	6214	491.0	-	-	-	-	-
C10LWSMOR2	5866	464.5	-	-	-	-	-
C10LWS095(1)*	6214	491.0	466.7	46.6	0.95	0.1	56
C10LWS095(2)	6214	491.0	482.0	48.2	0.98	0.1	140
C10LWS090(1)	6214	491.0	451.3	45.1	0.92	0.1	5
C10LWS090(2)	6214	491.0	451.3	45.1	0.92	0.1	488
C10LWS085(1)	6214	491.0	415.4	41.5	0.85	0.1	254
C10LWS085(2)	6214	491.0	415.4	41.5	0.85	0.1	1182

**Failure did not occur at middle third of the beam.*

5.3.3.1 Conventional Concrete

Two sets of 6 in. x 6 in. x 21 in. specimens made with conventional portland cement concrete were tested under cyclic fatigue loading. For the first set (PC1), the N values at failure generally increased as the stress level decreased, except for the lowest stress level of S=0.75, which was followed by a decrease in the number of load cycles. For the second set (PC2), a noticeable variation in N values was observed among specimens tested with the same stress level. This scatter in the data resulted in a lower coefficient of determination (R^2) for the S-N curve of the PC mix, as shown in Figure 5.5. Although plotting separate curves for each set would produce different trends, the results were combined into a single graph since both sets represent the same type of concrete. It should also be noted that the concrete for each set is from different batches, which may introduce variation in the mix properties and contribute to variability in fatigue strength.

The results of Table 5.7 were used to plot the following S-N curves for the different specimen sets.

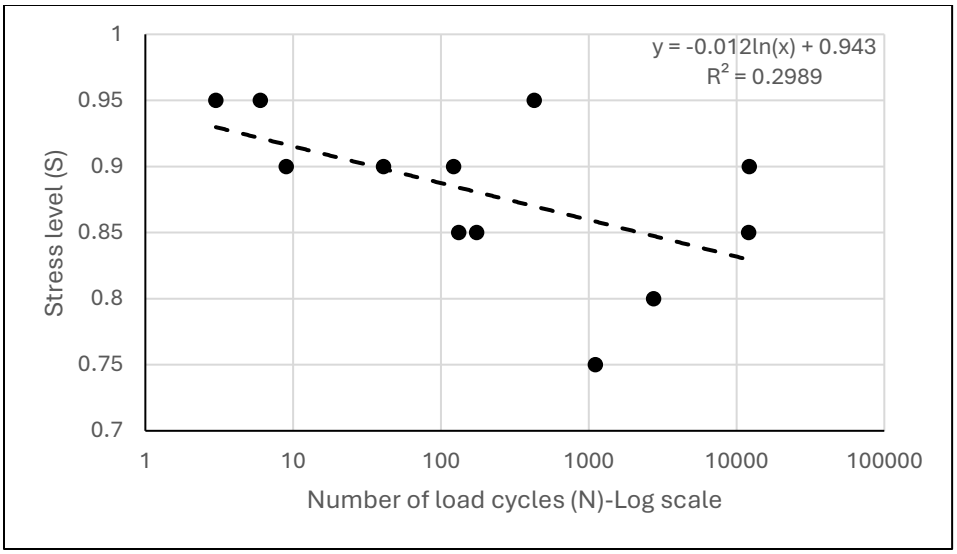


Figure 5.5: S-N curve for 6 in. x 6 in. conventional concrete (PC1 and PC2)

5.3.3.2 Expansive BCSA Concrete

Similar to the PC mix, the N value for the 6 in. x 6 in. x 21 in. expansive rapid setting cement concrete specimens generally increased as the applied stress level decreased. For the first set of specimens (C2) the N value progressively increases with lower stress levels; however, the N value for S=0.85 showed some inconsistency. Some such variability is expected since concrete is a heterogeneous material, therefore the range of N values may overlap, especially at higher stress levels where N values are small. Compared with Type K and conventional concrete, expansive BCSA cement concrete failed after a higher number of cycles. A difference between the results of the 6 in. x 6 in. and 8 in. x 8 in. specimens of the same material was also observed, which can be attributed to the size effect. The 8 in. x 8 in. concrete specimens exhibited a higher value of $R^{2,}$ indicating less scatter in the fatigue data. Meanwhile, the N value for S=0.75 of the 6 in. x 6 in. specimen is 117 cycles; however, for the same stress level, the N value of 8 in. x 8 in. specimens is 14712 cycles. This behavior can be partially explained by the heterogeneous nature of concrete. Larger specimens reduce the likelihood of premature local failure caused by

localized zones of weaker or poor-quality concrete or due to a relatively lower amount of shrinkage-induced micro-cracks. Due to a higher R^2 value (0.875) and reduced scatter in the S-N data, 8 in. x 8 in. specimens appear to better represent the fatigue behavior of the material. However, additional testing is recommended to further verify this observation and provide a more comprehensive assessment of the size effect. Figures 5.6 and 5.7 show the S-N curve for expansive BCSA mixtures with 6 in. x 6 in. and 8 in. x 8 in. dimensions, respectively.

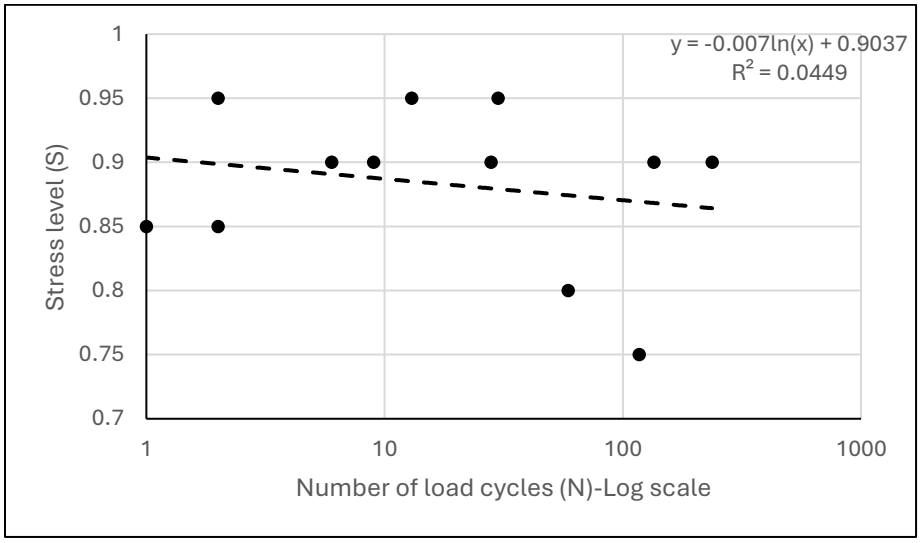


Figure 5.6: S-N curve for the 6 in. x 6 in. expansive BCSA concrete (C2 and C3)

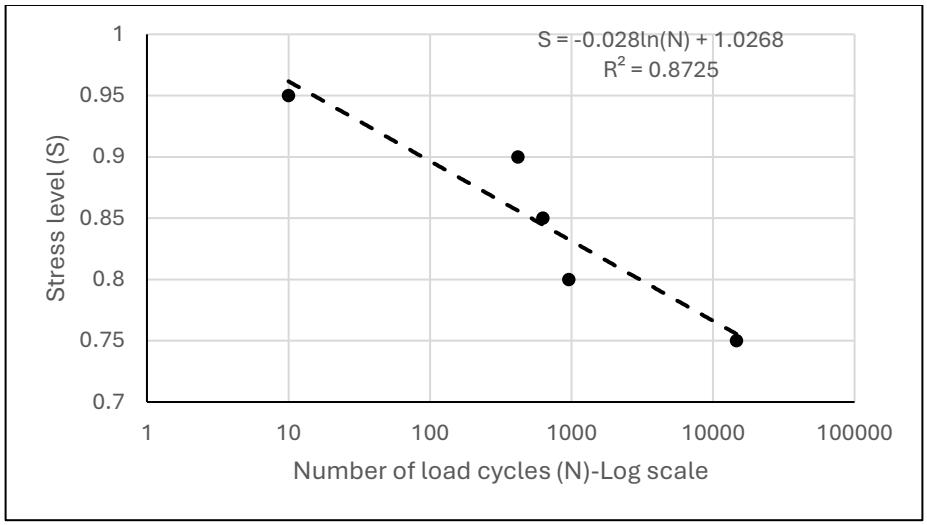


Figure 5.7: S-N curve for the 8 in. x 8 in. expansive BCSA cement concrete (C1)

5.3.3.3 Type K Cement Concrete

The Type K cement concrete mix 6 in. x 6 in. specimens yielded a more consistent N for each stress level, which produced a higher R^2 value of 0.64 compared to the PC and Expansive BCSA cement counterparts. In addition, the 8 in. x 8 in. Type K plus portland cement concrete specimens had the highest R^2 value (0.97) of all tested specimens for the different types of concrete mixes. This consistency indicates a consistent S-N behavior for the mix, which will better predict the actual fatigue behavior of the mix. The Batch K2 S-N data did not follow anticipated trends, which could be due to testing error or material heterogeneity, and their data were discarded from the S-N curve shown in Figure 5.8. The Type K with portland cement mixture outperformed both the Expansive BCSA cement and conventional concrete in terms of the number of load cycles before failure. After applying 10,000 cycles for specimen K1-0.80, the loading frequency was increased from 1.0 Hz to 3.0 Hz. This was done to accelerate the testing time.

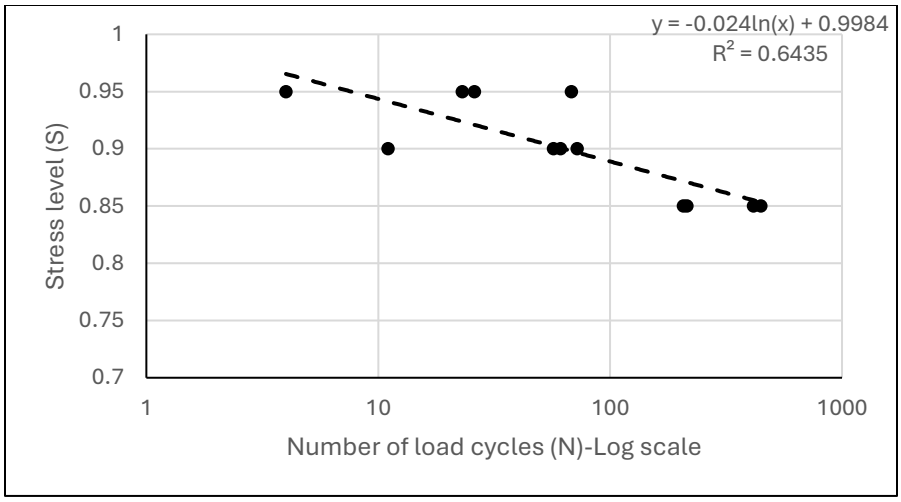


Figure 5.8: S-N curve for the 6 in. x 6 in. Type K cement concrete (K3 and K4)

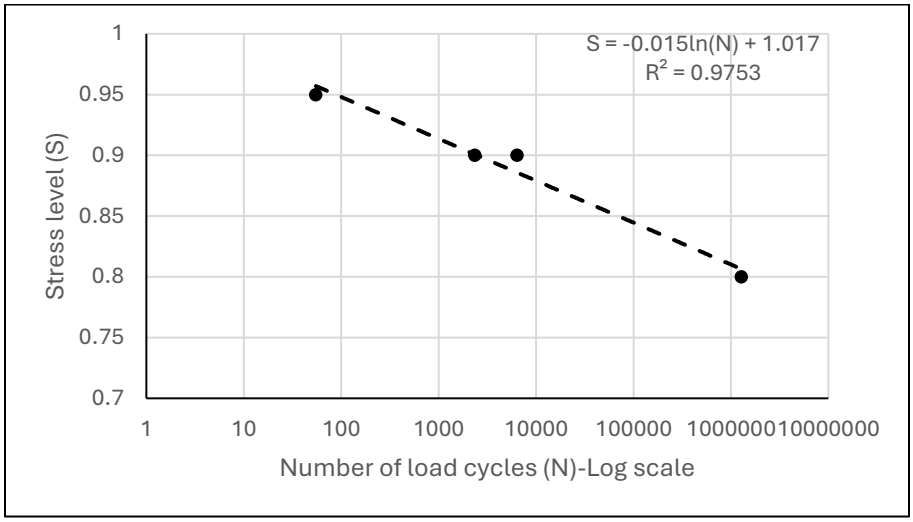


Figure 5.9: S-N curve for the 8 in. x 8 in. Type K cement concrete (K1)

5.3.3.4 CSA cement concrete mixes with LWS

Fatigue cracks typically initiate from the outer surface of the concrete specimen due to the presence of shrinkage-induced microcracks. Therefore, minimizing the shrinkage is essential to improve fatigue performance. One approach to reduce shrinkage is to use LWS as an internal curing agent. Incorporation of LWS provides additional water for cement hydration and reduces

volume change due to moisture loss. The resulting S-N curve for expansive BCSA with 8 LWS and 10 LWS are shown in Figures 5.10 and 5.11.

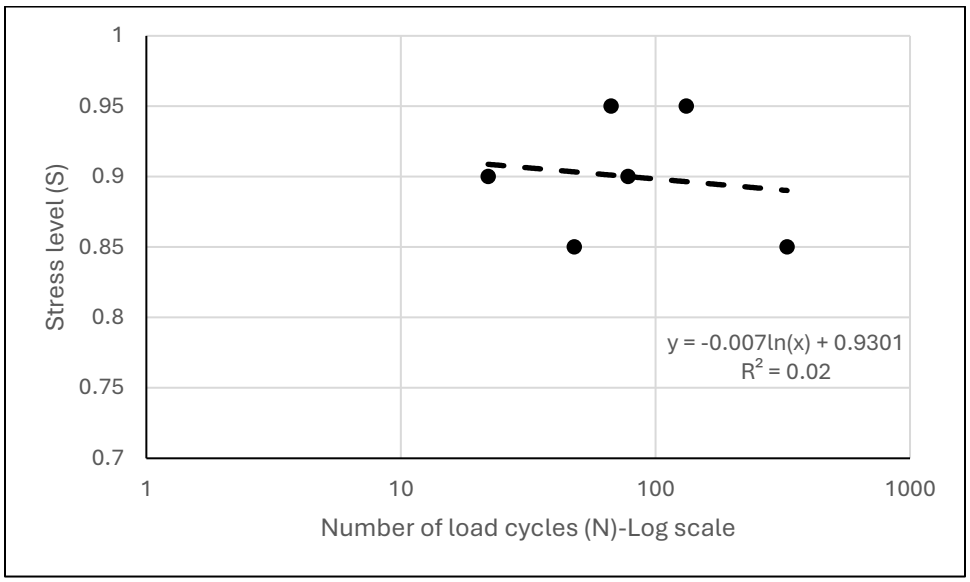


Figure 5.10: S-N curve for the 6 in. x 6 in. expansive BCSA concrete -8 LWS

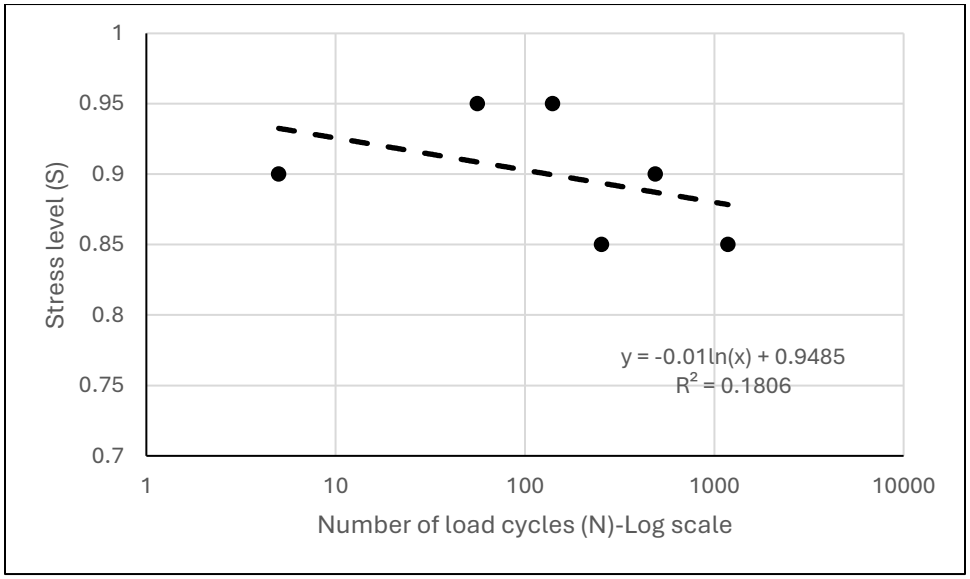


Figure 5.11: S-N curve for the 6 in. x 6 in. expansive BCSA concrete - 10 LWS

The fatigue test results for the mixes containing LWS indicate that the incorporation of LWS had minimal impact on the fatigue strength of the Expansive BCSA cement concrete. For the expansive BCSA cement concrete, the fatigue stress level (S) increased from 0.80 for the mix without LWS to 0.83 for the mix containing 8-LWS, indicating a minimal (3%) increase. With increasing the amount of LWS to 10 LWS, the S value becomes 0.80, indicating no change in fatigue strength from the no LWS case, therefore, internal curing did not change the fatigue behavior of expansive BCSA cement concrete.

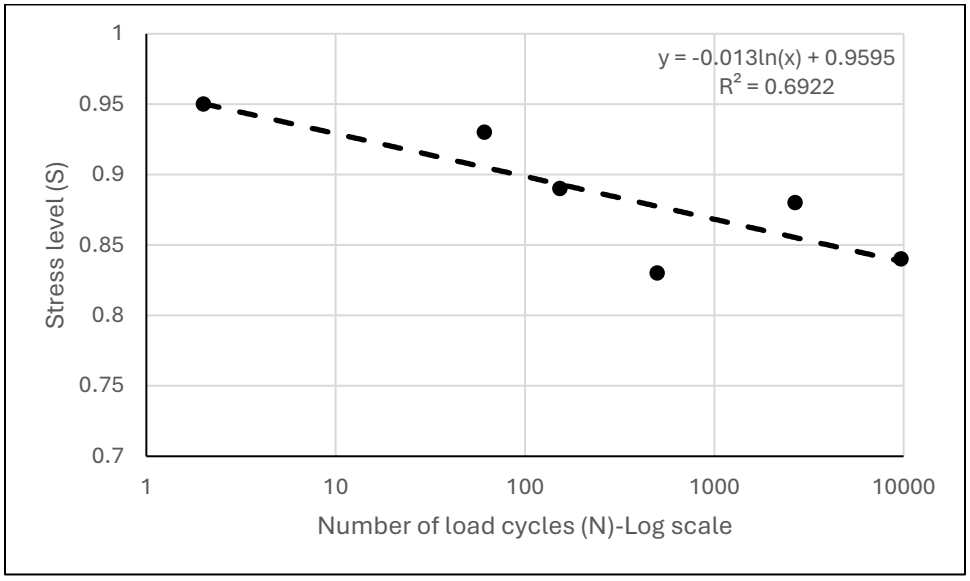


Figure 5.12: S-N curve for the 6 in. x 6 in. Type K cement concrete -8 LWS

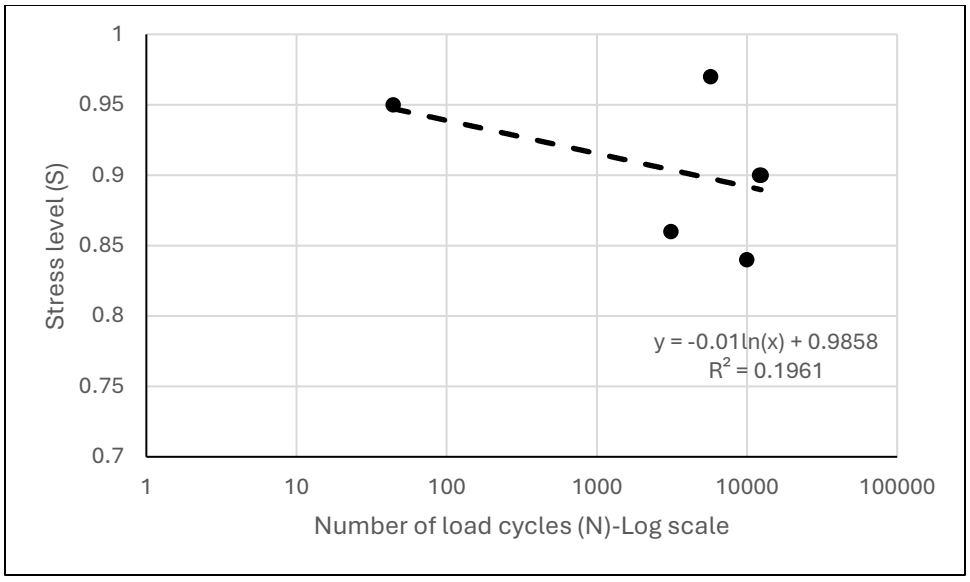


Figure 5.13: S-N curve for the 6 in. x 6 in. Type K cement concrete -10 LWS

For the Type K mix, the S value for the mix without LWS is 0.68 and increases to 0.77 and 0.84 with the addition of 8-LWS and 10-LWS, respectively, as shown in Figures 5.12 and 5.13. The improvement with addition of 8-LWS and 10 LWS corresponds to 13% and 23% increase in fatigue strength, respectively. Although the increase in fatigue strength due to LWS addition for both CSA cements can be observed, the percentage increase for the Type K cement concrete is higher compared to the Expansive BCSA mixes.

Figures 5.14(a) and 5.14(b) show the cross-section of the broken specimens of each type of CSA cement with and without LWS. The surface of the specimens made with Expansive BCSA cement with LWS is darker than the surface of the specimens without LWS, which could be linked to the influence of internal curing on the color of the specimens. However, color change is not significant for the mixes with Type K cement and portland cement as can be seen in Figure 5.15.



(a) (b)

Figure 5.14: Broken specimens of expansive BCSA cement (a) No LWS and (b) 8-LWS



(a) (b)

Figure 5.15: Broken Specimens of Type K cement concrete (a) No LWS and (b) 8-LWS

Since the fatigue test for the mixes with LWS was only conducted on one pair of specimens for each stress level, further tests are recommended to address the challenge of variability of the test due to the non-homogeneity of concrete.

Based on the previously defined concept of fatigue strength, the stress corresponding to 2 million non-reversible cyclic loads is known as fatigue strength. By substituting N=2,000,000 into the equation determined for each of S-N the curves, the corresponding fatigue strengths as a percentage of MOR were determined. The resulting values are summarized in Table 5.8.

Table 5.8. Fatigue strength of the 6 in. x 6 in. conventional and CSA cement concrete

Specimen	**Experimental Fatigue Strength (percentage of MOR)**	**R^2**
Conventional Concrete	0.77	0.299
Expansive BCSA Cement Concrete	0.80	0.045
Type K Cement concrete	0.65	0.643
Expansive BCSA Cement Concrete (C-8 LWS)	0.83	0.020
Expansive BCSA Cement Concrete (C-10 LWS)	0.80	0.180
Type K Cement with 8-LWS	0.77	0.692
Type K Cement (10-LWS)	0.84	0.196

Table 5.9. Fatigue strength of the 8 in. x 8 in. conventional and CSA cement concrete specimens (N=2×106)

Specimen	**Experimental fatigue life**	**R^2**
Expansive BCSA Cement Concrete	0.62	0.872
Type K Cement concrete	0.80	0.975

The fatigue strength of specimens varies with specimen size and concrete type. For the 6 in. x 6 in. specimens, expansive BCSA cement concrete exhibited the highest fatigue strength, followed by portland cement concrete, while Type K cement concrete showed the lowest fatigue strength. In contrast, for the 8 in. x 8 in. specimens, Type K cement concrete demonstrated the highest fatigue strength, followed by expansive BCSA Cement concrete, as shown in Table 5.9.

It can be observed that the 8 in. x 8 in. specimens of both CSA specimens produced more reliable fatigue strength values, as indicated by the higher R^2 on the corresponding S-N curves. This behavior may be attributed to the size effect, where larger specimens allows for a more uniform distribution of concrete constituents throughout the cross section and along the length. In addition, smaller specimens may experience greater early age shrinkage, which can lead to the formation of microcracks and can consequently influence the measured fatigue strength.

An important aspect for analyzing fatigue strength data was to compare the experimental data with the existing models. Four models, illustrated in Table 5.10, which are also previously discussed in the literature review, were used for predicting the fatigue strength. The results are compared with the experimental data, as shown in Table 5.11.

Table 5.10. Different fatigue models used for comparison

Model	**Equation**
Wholer	$S = a - b\ Log(N)$
Aas-Jacobsen	$S = a - b(1 - R)\ Log(N)$
Model Code	$S_{max} = 1 + \log N \cdot \frac{(Y-1)}{8}$
Eurocode	$S_{max} = 1 - \frac{(1-R)^{0.5}}{14} \log N$

The models were plotted to better observe their relative predictability, as shown in Figure 5.16. The higher the S value for a specific N value, the less conservative the model, since a higher S indicates a higher percentage of the material's strength can be utilized for a specific load cycle. In other words, the higher the fatigue strength of materials, the smaller cross-sectional dimensions are needed, making the structural design cost-efficient.

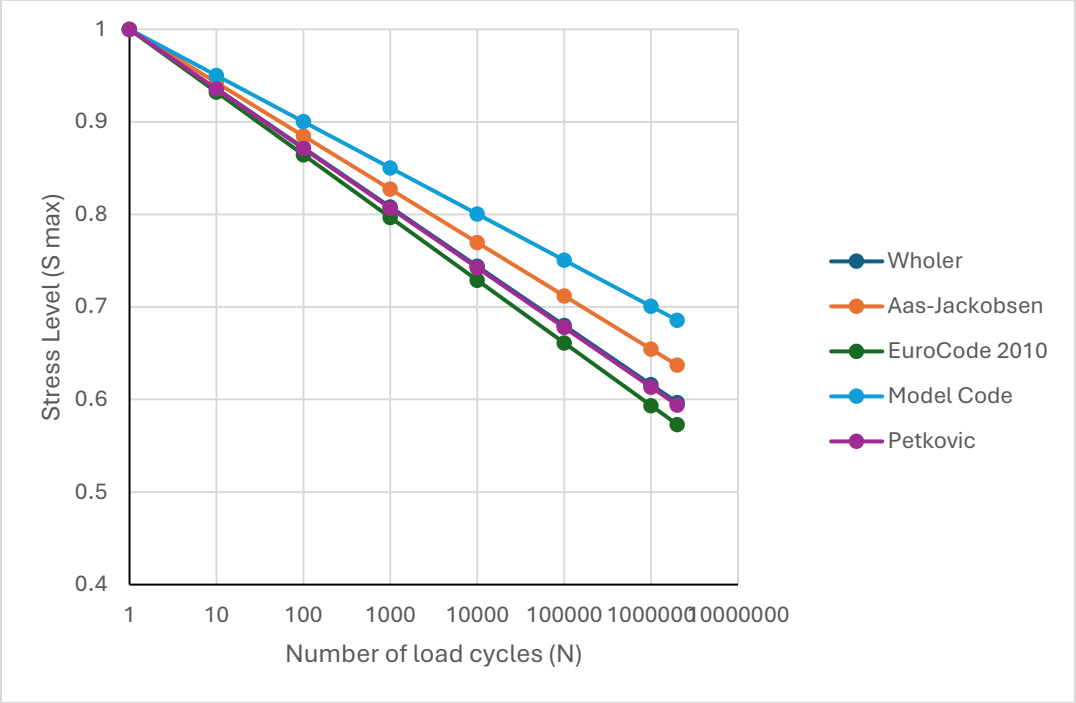


Figure 5.16: S vs. N curve for different concrete fatigue models

Table 5.11 evaluates the stress level from both the experimental results and fatigue models corresponding to different load cycles. The reason for selecting different values of N is that some models have a better prediction for a higher number of load cycles, while others have a better prediction for the lower load cycle values. To consider the overall performance of the models, a wide range of N values was used. The root mean square error (RMSE) value has been derived based on the corresponding experimental values. A lower RMSE value indicates smaller difference between experimental values and the models, indicating the model can predict the fatigue strength with better accuracy. The RMSE values for the PC and Type K plus portland cement are relatively smaller, which makes sense since the equations were developed for portland cement. However, RMSE values are higher for the expansive BCSA indicating that the existing models predict the fatigue behavior of expansive BCSA materials with lesser accuracy. This can further be evaluated by observing the S values in each column corresponding to a

specific N value and comparing them with the corresponding experimental values. For generating Table 5.11, the value of "a" in each model which corresponds to the y-intercept of the curve, was assumed as 1.0, and the "b" value, which represents the slope of the line, was used as 0.064, matching the common value used by the earlier researchers (Vicente, 2024).

Table 5.11. Experimental vs. analytical fatigue stress S_{max} comparison with RMSE

Specimen	N	10^1	10^2	10^3	10^4	10^5	10^6	$2{\cdot}10^6$	RMSE
PC (Portland Cement) (6 in. x 6 in.)	Exp	0.91	0.88	0. 86	0.83	0.80	0.78	0.77	-
	Wholer	0.94	0.87	0.81	0.74	0.68	0.62	0.60	0.071
	Aas-Jackobsen	0.94	0.88	0.83	0.77	0.71	0.65	0.64	0.047
	Model Code	0.94	0.88	0.82	0.77	0.71	0.65	0.63	0.048
	Eurocode	0.93	0.86	0.80	0.73	0.66	0.59	0.57	0.090
Expansive BCSA Cement (6 in. x 6 in.)	Exp	0.89	0.87	0.85	0.84	0.82	0.80	0.80	-
	Wholer	0.94	0.87	0.81	0.74	0.68	0.62	0.60	0.085
	Aas-Jackobsen	0.94	0.88	0.83	0.77	0.71	0.65	0.64	0.060
	Model Code	0.94	0.88	0.82	0.77	0.71	0.65	0.63	0.063
	Eurocode	0.93	0.86	0.80	0.73	0.66	0.59	0.57	0.104
Type K Cement (6 in. x 6 in.)	Exp	0.94	0.89	0.83	0.77	0.72	0.67	0.65	-
	Wholer	0.94	0.87	0.81	0.74	0.68	0.62	0.60	0.03
	Aas-Jackobsen	0.94	0.88	0.83	0.77	0.71	0.65	0.64	0.03
	Model Code	0.94	0.88	0.82	0.77	0.71	0.65	0.63	0.029
	Eurocode	0.93	0.86	0.80	0.73	0.66	0.59	0.57	0.051
Expansive BCSA Cement– 8 LWS (6 in. x 6 in.)	Exp	0.91	0.90	0.88	0.86	0.85	0.83	0.83	-
	Wholer	0.94	0.87	0.81	0.74	0.68	0.62	0.60	0.165
	Aas-Jackobsen	0.94	0.88	0.83	0.77	0.71	0.65	0.64	0.141
	Model Code	0.94	0.88	0.82	0.77	0.71	0.65	0.63	0.144

Specimen	N	10^1	10^2	10^3	10^4	10^5	10^6	$2 \cdot 10^6$	RMSE
	Eurocode	0.93	0.86	0.80	0.73	0.66	0.59	0.57	0.186
Expansive BCSA Cement– 10 LWS (6 in. x 6 in.)	Exp	0.92	0.90	0.88	0.86	0.83	0.81	0.80	-
	Wholer	0.94	0.87	0.81	0.74	0.68	0.62	0.60	0.156
	Aas-Jackobsen	0.94	0.88	0.83	0.77	0.71	0.65	0.64	0.132
	Model Code	0.94	0.88	0.82	0.77	0.71	0.65	0.63	0.135
	Eurocode	0.93	0.86	0.80	0.73	0.66	0.59	0.57	0.176
Type K Cement 8 LWS (6 in. x 6 in.)	Exp	0.93	0.90	0.87	0.84	0.81	0.78	0.77	-
	Wholer	0.94	0.87	0.81	0.74	0.68	0.62	0.60	0.111
	Aas-Jackobsen	0.94	0.88	0.83	0.77	0.71	0.65	0.64	0.085
	Model Code	0.94	0.88	0.82	0.77	0.71	0.65	0.63	0.088
	Eurocode	0.93	0.86	0.80	0.73	0.66	0.59	0.57	0.129
Type K Cement 10 LWS (6 in. x 6 in.)	Exp	0.96	0.94	0.92	0.89	0.87	0.84	0.84	-
	Wholer	0.94	0.87	0.81	0.74	0.68	0.62	0.60	0.176
	Aas-Jackobsen	0.94	0.88	0.83	0.77	0.71	0.65	0.64	0.151
	Model Code	0.94	0.88	0.82	0.77	0.71	0.65	0.63	0.153
	Exp	0.93	0.86	0.80	0.73	0.66	0.59	0.57	0.196

For a better comparison of each model's predictability, the RMSE values of each model and each material type in comparison to the experimentally derived values are plotted in the bar chart shown in Figure 5.17.

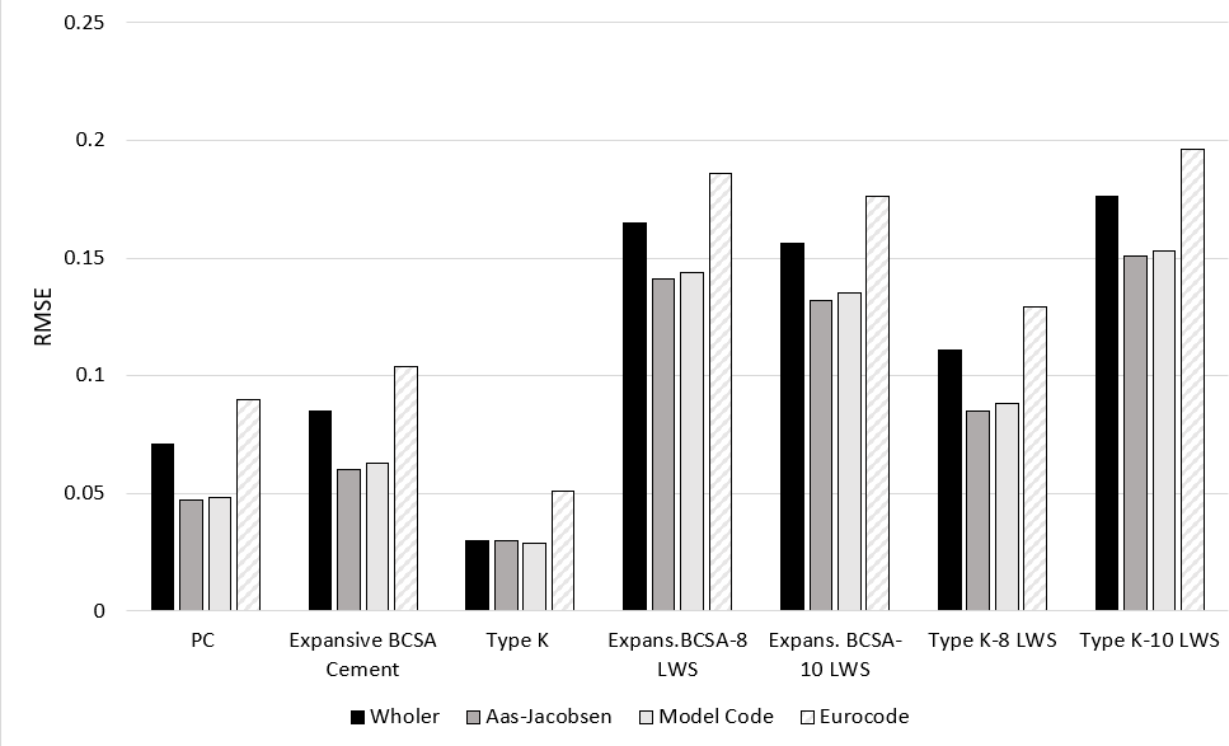


Figure 5.17: Comparison of fatigue models based on RMSE for different concrete types

The RMSE values are lower for the PC and Type K concrete mixes, which could be attributed to fact the models were developed for conventional concrete with portland cement as binder. However, the value of RMSE described in Figure 5.18 increases for all mixes including LWS. Similarly, the RMSE of the specimens with LWS compared to the mix without LWS is presented in Figure 5.18.

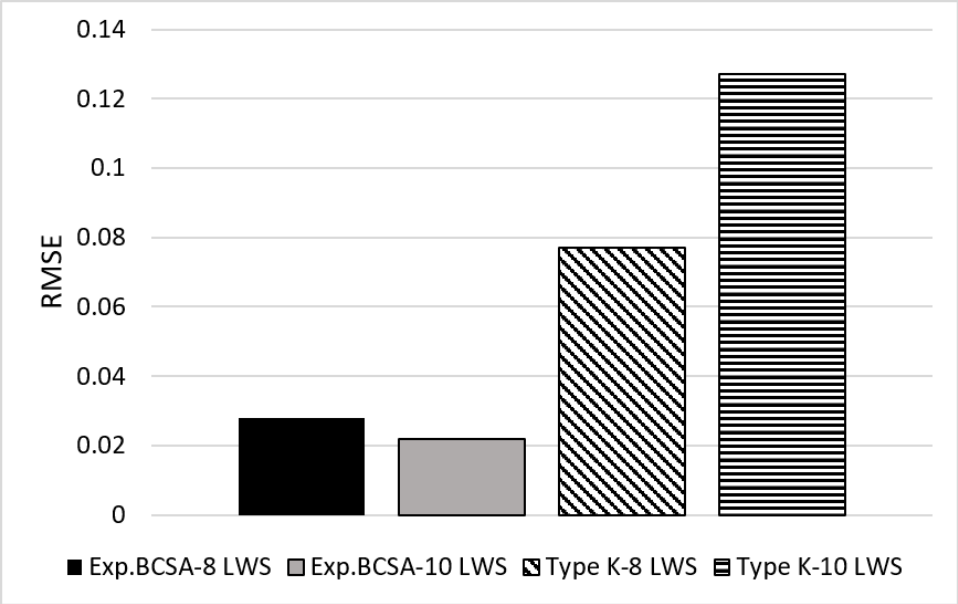


Figure 5.18: RMSE values for expansive BCSA and Type K specimens with LWS

5.4 Conclusions and Recommendations

This study evaluated the fatigue strength of different types of concrete subjected to cyclic loading. Two specimen sizes, 6 in. x 6 in. x 21 in. and 8 in. x 8 in. x 30 in. were tested to investigate the influence of specimen size on fatigue strength. A loading frequency of 1 Hz was selected for the majority of specimens to minimize the effects of vibration and dynamic loading. Previous studies have shown that shrinkage-induced micro-cracks play an important role in the initiation of fatigue failure. Therefore, expansive BCSA and Type K cement and LWS were used to minimize crack formation and enhance the fatigue strength. The fatigue test results were used to develop S-N curves for all concrete types, which were then used to estimate the fatigue stress corresponding to a specific N value. The experimental results were also compared with predictions from existing fatigue models. Based on the analysis of the results, the following outcomes are concluded:

- As discussed in the literature review, the endurance limit for conventional concrete is typically reported between 50%-55%. Using S=0.55 for the S-N curve equation of conventional concrete yields $N=1.67\cdot 10^{14}$. This value is significantly higher than the number of cycles for which a pavement is designed and therefore satisfies the definition of endurance limit.
- Both Type K and expansive BCSA cement concrete continue to gain strength even beyond 28 days. Therefore, to accurately determine the fatigue loading limits, an MOR test should be performed before each fatigue test.
- The R^2 value determined from fitting the S-N curves of the 6 in. x 6 in. specimens was lower compared to that from 8 in. x 8 in. specimens, indicating greater scatter in the fatigue data for the smaller specimens. This suggests that the reliability and precision of the fatigue test results may be improved by using large specimens. Overall, the R^2 value for the Type K cement concrete was higher compared to the PC and expansive BCSA specimens.
- Test results from 6 in. x 6 in. specimens indicate that the number of load cycles to failure increases with increasing loading frequency.
- The addition of LWS significantly enhanced the fatigue strength of Type K cement concrete. For expansive BCSA cement, the incorporation of 8 LWS increased the fatigue strength by 4%, while increasing the LWS to 10 LWS resulted in no additional improvement compared to the mix without LWS. In contrast, for the Type K plus portland cement concrete, the addition of 8 LWS increased the fatigue strength by 18.4% and a further increase to 10 LWS improved the fatigue strength by 29% with respect to the Type K mix without LWS. The results indicate that 8 LWS provided the maximum fatigue strength for the expansive BCSA concrete and for the Type K plus portland cement mix, the 10 LWS replacement produced the maximum fatigue strength.

- The fatigue strength obtained from the 8 in. x 8 in. specimens appears to provide a more realistic and reliable estimate, as indicated by the higher R^2 value and reduced scatter in the fatigue data compared to the 6 in. x 6 in. specimens. The 6 in. x 6 in. specimens of expansive BCSA yielded a fatigue strength of 0.8 with R^2=0.045 whereas fatigue strength is 0.62 with R^2=0.872 for 8 in. x 8 in. specimens of the same mixture. For Type K cement concrete the 6 in. x 6 in. specimens yielded a fatigue strength of 0.65 with R^2=0.643 and this value is 0.80 with R^2=0.975 for 8 in. x 8 in. specimens.
- Additional fatigue testing with saturated condition of specimens is recommended.

5.5 References

1. Rice, E. K. (2012). "Shrinkage compensating concrete: Past, present and future—Part I." *ACI Convention*, Toronto, ON, Canada.
2. Shi, X. P., Fwa, T. F., and Tan, S. A. (1993). "Flexural fatigue strength of plain concrete." *ACI Materials Journal*, 90(5), 435–440. https://doi.org/10.14359/3872
3. ASTM C192/C192M-19. (2020). *Standard practice for making and curing concrete test specimens in the laboratory*. ASTM International, West Conshohocken, PA.
4. ASTM C78/C78M-22. (2022). *Standard test method for flexural strength of concrete (using simple beam with third-point loading)*. ASTM International, West Conshohocken, PA.
5. ASTM C845/C845M-18. (2018). *Standard specification for expansive hydraulic cement*. ASTM International, West Conshohocken, PA. https://doi.org/10.1520/C0845_C0845M-18
6. Lloyd, J. P., Lott, J. L., and Kesler, C. E. (1968). *Fatigue of concrete*. Engineering Experiment Station, University of Illinois, Urbana, IL.
7. Oklahoma Department of Transportation (ODOT). (2019). *Standard specifications for highway construction*. Oklahoma Department of Transportation, Oklahoma City, OK.
8. Rama Krishnan, V., Wu, G. Y., and Hosalli, G. (1989). "Flexural fatigue strength, endurance limit, and impact strength of fiber reinforced concretes." *Transportation Research Record*, No. 1226.
9. Sohel, K. M. A., Al-Hinai, M. H. S., Alnuaimi, A., Al-Shahri, M., and El-Gamal, S. (2022). "Prediction of flexural fatigue life and failure probability of normal weight concrete." *Materiales de Construcción*, 72(347). https://doi.org/10.3989/mc.2022.03521

10. Tanksley, S. D. (2018). *Internal curing of calcium sulfoaluminate cement concrete using lightweight aggregate*. Master's thesis, University of Oklahoma, Norman, OK.
11. "The use of calcium sulfoaluminate rapid setting cement for underground construction." (2013). CTS Cement Manufacturing Corp., Cypress, CA.
12. Thomas, R. J., Maguire, M., Sorensen, A. D., and Quezada, I. (2018). "Calcium sulfoaluminate cement benefits and applications." *Concrete International*, 40(1), 37–42.
13. Vicente, M. A., Mena-Alonso, Á., González, D. C., and Mínguez, J. (2025). "A new approach to concrete fatigue S–N curves considering load application rate." *Proceedings of the 12th International Conference on Fracture Mechanics of Concrete and Concrete Structures (FraMCoS-12)*, Vienna, Austria.